FREQUENCY STABILIZATION OF GaAlAs LASER USING A DOPPLER-FREE ATOMIC SPECTRUM

by

Hirokazu HORI

October 1983

Kyoto University

Kyoto, Japan

FREQUENCY STABILIZATION OF GaAlAs LASER USING A DOPPLER-FREE ATOMIC SPECTRUM

by

Hirokazu HORI

October 1983

Kyoto University

Kyoto, Japan

ERRATA

PAGE	LINE	ERROR	SHOULD READ
12	17	limitted	limited
14	17	meterology	metrology
23	7	wheather	whether
23	14	succesfully	successfully
25	1	is appeared	appears
27	8	an saturated	a saturated
30	1	unabsorbong	unabsorbing
30	14	factor	factor of
34	9	moduration	modulation
35	12	absorptipon	absorption
39	15	achived	achieved
40	25	spaectrum	spectrum
42	24	for an	for
58	16	Loretzian	Lorentzian
67	4	Loretzian	Lorentzian
84	21	are appeared	appeared
102	Fig. III-3	FREQUENCY	WAVELENGTH
110	25	1×10^{-3} cm^{-3}	1×10^{10} cm^{-3}
136	20	sacrifice	sacrifices
137	4	use	uses
159	Eq. (IV.36)	N-1	M-1

ACKNOWLEDGEMENT

The author would like to express his sincere appreciation to Professor Toru Ogawa for his continuous guidance, many valuable discussions and stimulating suggestions throughout the present work, and for his careful reading of the manuscript. The author is deeply grateful to Dr. Tsutomu Yabuzaki for his helpful discussions and enlightening in all phases of this work, and for his critical reading of the manuscript.

The author also wishes to express his gratitude to Professor Susumu Kato and Professor Iwane Kimura for their valuable comments and suggestions.

The author is deeply indebted to Mr. Masao Kitano for his constructive discussions and experimental help and for providing a fine word processor program for printing the dissertation. He also wishes to acknowledge the valuable discussions and suggestions of Mr. Minoru Tsutsui and other staffs of the Radio Atmospheric Science Center and Professor Kimura's group.

The author wishes to acknowledge the contribution of Mr. Akira Ibaragi in early stages of the present work. Some parts of the work were performed by the help of Messrs. Yoshinobu Kitayama and Junji Monden. A number of valuable discussions with Dr. Takeshi Manabe and Dr. Takashi Sato are also acknowledged with many thanks.

It is pleasure to indebt to Dr. Takeki Sakurai for his encouragement in this work.

ABSTRACT

This thesis is concerned with high frequency-stabilization of a GaAlAs laser using a Doppler-free saturated absorption spectrum of the Cs-D_2 line at 852.1 nm.

The semiconductor lasers have been developed extensively in recent years, and double-heterostructure type GaAlAs lasers operating at room temperature on a single mode in a spectral range from infrared to visible are now commercially available. Because of small size, low electric power for operation, and easy operation on a single mode, the semiconductor lasers are now used in wide variety of practical applications.

As a reflection of high frequency-tunability, the frequency stability of a semiconductor laser is rather poor in free-running condition. It is strongly desired to stabilize the laser frequency for its applications to optical telecommunications, precision measurements and high resolution laser spectroscopy.

For He-Ne lasers or dye lasers, ultrahigh frequency-stability has been achieved by utilizing the saturated absorption technique, which enable us to observe Doppler-free spectra of atoms or molecules. For example, the frequency-stability better than 10^{-13} has been obtained in He-Ne lasers whose frequencies are locked at the saturated absorption spectra of CH_4 and I_2. It is obvious that the Doppler-free spectrum should be used in the frequency stabilization of the semiconductor laser. However,

this had not been performed until this work. In most of works reported so far, a Fabry-Perot cavity or a Doppler-broadened absorption line of atoms or molecules has been used as a frequency reference.

The first half of this thesis is devoted to the first observation of the saturated absorption spectra of the Cs-D_2 line. This is the first experiment to use a semiconductor laser in the saturated absorption spectroscopy. In the case of alkali-metal vapor, it is possible to observe the saturated absorption spectra by using a GaAlAs laser with output power less than 1 mW. This is because the laser excitation causes the hyperfine pumping in the ground state of atom, which enhances considerably the saturation of absorption.

In this experiment, a temperature-controlled laser system is constructed, which is suitable for the high resolution spectroscopy. By stabilizing the diode temperature within 10^{-3} degree, the fluctuation of the laser frequency can be reduced to be less than 5 MHz. Furthermore, the center frequency can be tuned precisely a wide frequency range by changing the stabilized temperature.

The Doppler-free spectra, i. e. Lamb dips and crossover resonances, are clearly obtained on the Doppler-broadened absorption lines from both of the hyperfine levels with F = 3 and 4 in the ground state of Cs. The spectral widths of the observed Doppler-free spectra are about 20 $\sim$ 30 MHz (HWHM), which are much smaller than the Doppler-broadened width 185 MHz (HWHM). The

widths, however, are much broader than the natural linewidth 2.6 MHz (HWHM) of the D_2 line due to the power broadening, misalignment of the laser beams and the spectral width of the laser. The relative positions of the observed Doppler-free spectra are in good agreement with these expected from theoretical values of the hyperfine separation in the $6^2P_{3/2}$ state of Cs.

An experimental evidence of the hyperfine pumping is shown by monitoring the velocity distribution of atoms in both hyperfine levels in the ground state, by using two GaAlAs lasers simultaneously. Furthermore, the spectra completely free from Doppler-broadened background are observed. These results show that the temperature stabilized GaAlAs laser can be a powerful tool in the high resolution laser spectroscopy.

The later part of this thesis is devoted to the frequency stabilization of the GaAlAs laser by using one of the Doppler-free spectra of the Cs-D_2 line. Under stabilization of the diode temperature, the laser frequency is locked to the crossover resonance by feeding back the error signal (the first derivative of the Doppler-free spectra) to the injection current. The short-term frequency-fluctuation is suppressed to be less than 10 kHz, and the long-term frequency-fluctuation observed is 37 kHz or less for the time interval of 3000 s. The frequency stability of the stabilized GaAlAs laser is analyzed in terms of the Allan variance, and the Allan variance is found to be less than 1.0×10^{-11} for the averaging time between 0.1 s and 1000 s,

and the minimum value is 3.0×10^{-12} at the averaging time 1.3 s, which is the highest frequency-stability of semiconductor lasers reported so far.

For further improvement of the long-term stability, an improved temperature-control system is constructed, in which the double-loop temperature-control and the proportional-integral-differential servocontrol are carried out. The results of the preliminary experiment show that the fluctuation of the laser frequency can be reduced within 1 MHz.

Using the scheme described above, it is possible to make a compact and portable laser system whose frequency is highly stabilized. Actually, a compact optical system is constructed using small optical components which are mounted on a platform with size of $20 \times 10 \times 5$ cm^3.

Such a compact frequency-stabilized GaAlAs laser system is expected to be very useful in practical applications. Since the wavelength of semiconductor laser has been extended down to about 700 nm, it is now possible to stabilize the laser frequency to another atomic or molecular absorption lines, such as Rb-D line, by using techniques developed in this thesis.

CONTENTS

CHAPTER I

GENERAL INTRODUCTION

I-1 Introduction

This thesis is concerned with the frequency stabilization of semiconductor laser using a Doppler-free atomic spectrum obtained by the saturated absorption spectroscopy.

Semiconductor lasers have been developed extensively in recent years, and now double-heterostructure type single-mode cw lasers operating at room temperature are commercially available. Their spectral range covers from infrared to visible, and further wide-range oscillation is now under research by using various semiconductor materials. The semiconductor lasers have many advantages, such as small size, low electric power for operation and easy operation on a single longitudinal mode. Because of such advantages, the semiconductor lasers are used in wide variety of practical applications. They also have very high frequency-tunability, and continuous frequency-scanning is possible with resolution of better than 100 MHz over 10 GHz easily by controlling diode temperature and injection current. More than 10 mW is now available as their output power. Therefore the semiconductor lasers are also very attractive tools

for the high resolution laser spectroscopy.

As a reflection of high frequency-tunability, the frequency-stability of the semiconductor laser is rather poor in free-running condition. The oscillation frequency is influenced by small fluctuations of the injection current and the diode temperature. The frequency stabilization is strongly needed for practical applications such as the precision measurements, laser spectroscopy, FM type optical telecommunications.

In the frequency stabilization of lasers, a Doppler-free atomic or molecular spectrum is one of the best frequency-reference to which the laser frequency is locked. The most useful way to get the Doppler-free spectrum is the saturated absorption spectroscopy. This thesis deals with the frequency-stabilization of a GaAlAs laser using one of the Doppler-free saturated absorption spectra of the Cs-D_2 line at 852.1 nm. In this work, the saturated absorption spectra of Cs have been observed for the first time by using a semiconductor laser.[1] The laser power $\sim$1 mW is enough because the optical pumping between the ground hyperfine levels of Cs reduces significantly the light power required for the saturation spectroscopy. The observed width of the Doppler-free spectra was about 20 $\sim$ 30 MHz (HWHM), and by locking the laser frequency to one of the Doppler-free spectra, the frequency stability of the GaAlAs laser better than 10^{-11} was obtained.[2] It must be emphasized that a small laser system whose frequency is highly stabilized can be constructed, and so it has high potentiality for the practical

applications. Applications of the GaAlAs laser for the high resolution laser spectroscopy is also investigated in this work, in which a continuous scanning of the laser frequency is carried out by controlling the diode temperature with high resolution.

As an introduction of this thesis, a brief review is presented in Sec. I-2 on the frequency-stability and the frequency-stabilization of the semiconductor lasers. Where a brief survey on the potentiality of the semiconductor laser in the laser spectroscopy is also presented. In Sec. I-3, a brief review is given on the saturated absorption spectroscopy which is used to obtain a sharp Doppler-free spectrum and on the optical pumping of atoms which plays an important role in the saturated absorption spectroscopy of alkali-metal atoms. A brief review on the frequency stabilization of gaseous laser and dye laser is also given for a comparison with that of the semiconductor laser. Finally, in Sec. I-4, the outline of this thesis is described.

I-2 Frequency Stabilization of Semiconductor Laser

I-2-1 Properties and Frequency Stability of Semiconductor Laser

Since the first operation of GaAs laser in 1962,[3] the semiconductor lasers have been extensively improved according to development of semiconductor materials and diode structures. In

1970, continuous wave operation became possible at room temperature by employing double heterostructure.[4] Since then the semiconductor lasers have been used in wide variety of practical applications. Nowadays, as for cw injection lasers, GaAlAs lasers cover the spectral range between 700 nm and 950 nm,[5] InGaAsP lasers cover between 1.1 μm and 1.7 μm,[6] and PbSnSe and PbSnTe lasers operating at the liquid-nitrogen temperature cover between 5 μm and 30 μm.[7),8] With regard to the double-heterostructure type lasers, there are many types of practical diode structure, which are slightly different to each other in electrical and spectral characteristics. Output power of semiconductor laser has been increased, and a GaAlAs laser with the maximum output power more than 10 mW is now commercially available.[9] Lifetime of GaAlAs laser has also been significantly prolonged, and $10^5 \sim 10^7$ hour operation is expected in low output condition.[10]

Because of high gain in active layer, semiconductor laser can easily operate on a single longitudinal mode, however, its spectral width is rather broad in comparison with other types of single-mode lasers such as gaseous lasers and dye lasers. Such rather broad spectral width is mainly due to large loss of laser cavity and to high temperature of active layer where thermal noise is difficult to avoid.[11)-14] Typical spectral width of a GaAlAs laser was carefully measured by Fleming et al..[15] They reported that the spectral width is about 114 MHz (FWHM) at 1 mW output per facet and the spectral broadening is inversely

proportional to the output power. Their results were supported theoretically by Henry[16] from consideration of carrier-density modulation due to spontaneous emission.

Semiconductor lasers have high frequency-tunability. Generally, the oscillation frequency shifts toward low frequency side according to increase of the diode temperature and to increase of the injection current, repeating continuous change and mode hopping along a change of the gain maximum. In the continuously changing region, the laser frequency varies due to changes of refractive index and length of the laser cavity caused by heat.[17] The refractive index of the laser cavity varies owing to a change of carrier density which depends on both changes of the injection current and the diode temperature. In the case of GaAlAs laser, the rates of change in the continuously changing region are typically several 1 GHz/mA and several 10 GHz/°C at wavelength 800 nm for a static changes of the injection current and the diode temperature respectively.[18]-[20] Continuously tunable region spreads over more than 10 GHz in the case when either of the injection current or the diode temperature are changed, and the frequency gap of mode hopping is more than 10 GHz. It is possible to get wider tunable region by choosing an adequate combination of the injection current and the diode temperature.

In the case of GaAlAs laser, a frequency modulation with extremely high frequency is possible by modulating directly the injection current. The direct frequency-modulation

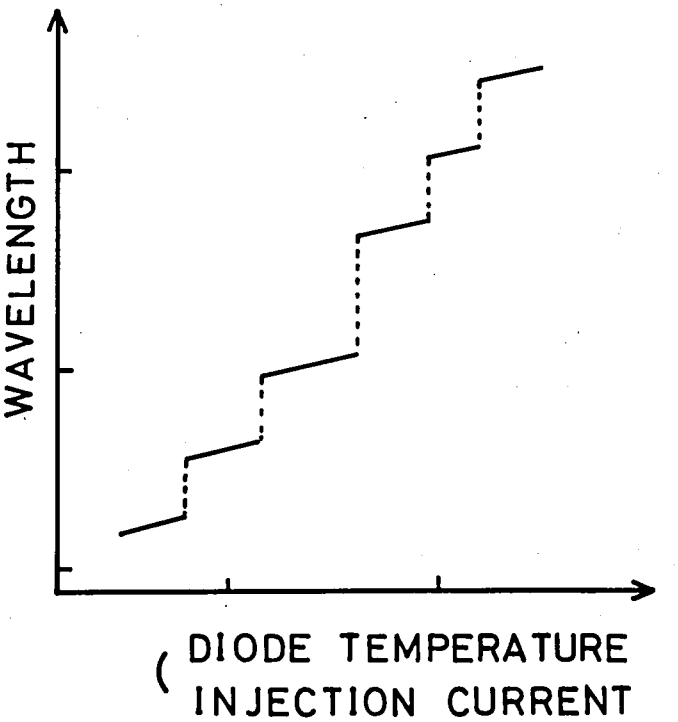

Fig. I-1 Typical oscillation characteristic of a semiconductor laser. In the case of GaAlAs laser the rates of frequency change in the continuously changing region are several 1 GHz/mA and several 10 GHz/°C at wavelength 800 nm.

characteristic was recently measured by Kobayashi et al.,[19] and the result shows that 0.1 ∿ 3 GHz/mA frequency deviation can be achieved with the modulation frequency up to 5 GHz.

As a reflection of high frequency-tunability, the frequency stability of semiconductor laser is rather poor in free-running condition. The oscillation frequency fluctuates due to small changes of the injection current and the diode temperature. For example, consider the case of GaAlAs laser operating at room temperature with injection current about 10 mA. It may be expected for an ordinary regulated current-source to have stability of 10^{-4}. In such a case, the fluctuation of the laser frequency is estimated to be about 1 MHz due to the fluctuation of the injection current. On the other hand, it is difficult to suppress the fluctuation of the diode temperature within 0.1 °C only by an air conditioner, which causes at least 1 GHz change of the laser frequency. Since the variation of room temperature is relatively slow, it determines mainly the long-term frequency-stability. While, the short-term frequency-stability is about 10^{-8} in free-running condition,[21] which is mainly determined by the fluctuation of the injection current.

I-2-2 Frequency Stabilization of Semiconductor Lasers

In recent years, the frequency stabilization of a cw semiconductor laser has been attempted by using several methods with aim of their applications to precision measurements, high

resolution spectroscopy, optical telecommunication[22] and so on. General way of the frequency stabilization is that, the oscillation frequency is locked to an external frequency-reference by controlling the operation conditions such as the diode temperature and the injection current.

As an external frequency-reference a Fabry-Perot interferometer has been mainly used so far. In 1970, Bykovskii et al.[23] locked a liquid-N_2-cooled GaAs laser to a center of transmission fringe of a Fabry-Perot cavity by controlling the injection current, and they obtained a few MHz relative stability for 5 ∿ 10 min. In 1975, Picqué et al.[24] locked a GaAs laser operating at 80 °K to a Fabry-Prot cavity by controlling the injection current under control of the diode temperature by using cooled He-gas stream. Only by temperature control, they obtained 30 MHz frequency-stability. By frequency locking, they obtained the relative frequency-stability of 270 kHz with absolute frequency-drift of 3.6 MHz/min, which was measured by utilizing D_2 absorption line of Cs vapor at 852.1 nm. In 1980, Favre et al.[25] locked a GaAlAs laser operating at room temperature to a resonance frequency of a Fabry-Perot cavity by controlling the injection current under the control of the diode temperature by using a thermoelectric cooler. They obtained mean frequency drift less than 1 MHz for 20 min and short-term frequency-jitter of 1.5 MHz. In 1981, Kikuchi et al.[26] locked a GaAlAs laser operating at room temperature to a side of transmission fringe of a Fabry-Perot cavity by controlling the diode temperature using a

thermoelectric cooler. They obtained 1 MHz relative frequency-stability which was maintained for 2 hours.

The method of the frequency stabilization by using Fabry-Perot cavity has an advantage that the laser frequency can be locked at any value desired within the tunable range of the laser, and hence a stabilized frequency-scanning may be possible. Frequency-modulation in the servocontrol is avoidable by modulating the Fabry-Perot cavity instead. However, the resonance frequency of Fabry-Perot cavity is not absolute and may fluctuate due to thermal expansion of cavity length, external mechanical vibrations and acoustic noise. To improve this, Tsuchida et al.[21] stabilized the length of the Fabry-Perot cavity by using an iodine-stabilized He-Ne laser at 633 nm, and then they locked a GaAlAs laser at a resonance frequency of the stabilized cavity by controlling the diode temperature by using a thermoelectric cooler. They obtained the frequency stability in terms of Allan variance between 2.1×10^{-9} and 9.6×10^{-9} at the averaging time τ_{av} between 10 ms and 500 s. Because of slow response of the diode temperature, only the long-term stability was improved. To improve short-term stability, in 1981, they locked a GaAlAs laser to the stabilized Fabry-Perot cavity by controlling the injection current, in an underground tunnel where the room temperature is regulated within 0.1 °C/day.[27] They obtained the Allan variance between 2.0×10^{-11} and 2.1×10^{-9} at τ_{av} between 10 ms and 500 s, which was almost determined by the stability of the He-Ne laser controlling the Fabry-Perot cavity.

In 1982, Tsuchida et al.[28] improved futher short-term stability of a GaAlAs laser by locking the laser frequency to an uncontrolled heavy Fabry-Perot cavity, which does not fluctuate in a short time-interval. They obtained the minimum Allan variance of 2.1×10^{-12} at τ_{av} = 90 ms. It should be noted that, Dandridge et al.[29] and Cobb et al.[30] have been studied on the techniques to reduce optical phase-noise by using a Fabry-Perot cavity.

When an atomic or molecular absorption line exists within tunable range of a semiconductor laser, it must be better to use it as an absolute frequency-reference. Although the frequency is fixed and not tunable, such absolute frequency-reference is stable against external perturbations. By locking the laser to the center of the absorption line, extremely high frequency-stability can be obtained with high reproducibility. Since the tunable range of the semiconductor laser is very wide, there are much chance of coincidence of the laser frequency with an atomic or molecular absorption line. In 1980, using the methane absorption line in the ν_4 band at the wavelength about 7.7 μm, Ohi[31] stabilized a PbSnTe laser operating at the liquid N_2 temperature by controlling the injection current, and obtained the minimum Allan variance of 4.3×10^{-11} at τ_{av} = 15 s. In 1982, using one of the absorption lines of water vapor in the (2,1,1) vibration-rotation band at 820 nm, Tsuchida et al.[32] stabilized a GaAlAs laser by controlling the injection current under condition of stable room-temperature of 0.1 °C/day. They

obtained the Allan variance between 1.1×10^{-11} and 1.9×10^{-9} at τ_{av} between 10 ms and 500 s. Tsuchida et al.,[33] in 1982, stabilized a GaAlAs laser using an absorption spectrum of ^{85}Rb-D_2 line at 780.0 nm with spectral width 500 MHz. They have locked the laser frequency by controlling the injection current under condition of stable room-temperature, and they obtained the Allan variance between 1.4×10^{-12} and 3.0×10^{-10} at τ_{av} between 10 ms and 500 s. Also in 1982, Yamaguchi et al.[34] reported on the frequency stabilization of a GaAlAs laser by using one of the optogalvanic spectra of Ar at 840.8 nm. They locked the laser frequency by controlling the injection current under the diode temperature controlled by a thermoelectric cooler. They have obtained the short-term frequency-stability of 200 kHz and estimated the minimum Allan variance of 4×10^{-11} at τ_{av} = 20 s. In 1982, Yamaguchi et al.[35] observed also the first overtone vibration-rotation lines of HF at 1.3 μm by using an InGaAsP laser operating at room temperature. They controlled the diode temperature by using a cryostat controlled with the stability of ∿0.001 °C within the range between -40 and 30 °C. After locking the laser frequency to one of the R-band lines, they have obtained the Allan variance between 2.0×10^{-10} and 7.9×10^{-11} at τ_{av} between 1 s and 240 s.

In all the works mentioned above, the frequency-locking was made by using absorption lines, which were rather broad due to thermal motion of atoms or molecules, i. e. Doppler-broadening. It must be better to use a Doppler-free spectrum of atoms or

molecules. In 1981, Yabuzaki et al.[1] observed the saturated absorption spectra of the Cs-D_2 line at 852.1 nm, for the first time, by using a GaAlAs laser. The observed width of the Doppler-free spectra was about 20 $\sim$ 30 MHz (HWHM). They tried to lock the laser frequency to one of the Doppler-free spectra and obtained the minimum Allan variance about 1.6×10^{-10} at τ_{av} between 15 s and 240 s. In 1982, Hori et al.[2] improved above system of the frequency-locking, and they obtained the short-term stability about 10 kHz, and the Allan variance σ between 3.0×10^{-12} and 1.0×10^{-11} at τ_{av} between 0.1 s and 1000 s. This thesis deals with above experiments of the frequency stabilization of a GaAlAs laser.

I-2-3 Frequency Stabilization Using Doppler-Free Spectrum

As is mentioned in Sec. I-2-2, the absorption line of gaseous atoms or molecules is used as an absolute frequency-reference in the frequency-locking of a semiconductor laser. The spectral sharpness in these cases is usually limitted by Doppler-broadening due to thermal motion of atoms or molecules. Typical width of Doppler-broadened absorption spectrum is several hundred megahertz or more, and it affects on the final frequency-stability of the laser locked to the spectrum. It should be better to get higher stability to use a narrow Doppler-free spectrum of atoms or molecules. The most convenient way to obtain the Doppler-free spectrum is the saturated absorption

spectroscopy,[36),37)] by which a Doppler-free spectrum of width below 100 MHz is observed with relatively high signal-to-noise ratio. If one locks the laser frequency to the saturated absorption spectrum, an extremely high frequency-stability can be obtained. In fact, the frequency-stability better than 10^{-13} has been obtained in He-Ne lasers locked to the saturated absorption spectra of CH_4 and I_2, and they are now used as the secondary frequency-standard. It is obvious that the Doppler-free atomic or molecular spectrum is much better to be used in frequency stabilization of the semiconductor lasers. However, this had not been performed until our recent works described in this thesis.

Recently, we could observe for the first time the saturated absorption spectra of the Cs-D_2 line at 852.1 nm using a GaAlAs laser operating at a room temperature and tried to stabilize the laser frequency by using one of the Doppler-free spectra.[1)] The sharpness of the observed Doppler-free spectra was about 20 $\sim$ 30 MHz (HWHM), and an extremely high frequency-stability of the GaAlAs laser is expected to achieve by locking the laser frequency to one of the sprctra. To lock the laser frequency to such narrow spectrum, it is very important to reduce a fluctuation of the diode temperature, before locking the laser frequency, at least within 1×10^{-3} °C which gives the fluctuation of laser frequency of about 10 MHz. Namely, it is desired that the laser frequency is beforehand within the Doppler-free spectrum, at the center of which the laser frequency is stabilized. We tried to control the diode temperature by using a

thermoelectric cooler and a temperature-measuring system with high sensitivity. Only by the temperature control, we could reduce the frequency fluctuation of the GaAlAs laser within 5 MHz, which corresponded to the temperature stability 3×10^{-4} °C. Under the control of the diode temperature, the laser frequency was locked to one of the Doppler-free spectra of the Cs-D_2 line by controlling the injection current. The experimental results showed that the short-term frequency-stability was less than 10 kHz and the Allan variance was between 3.0×10^{-12} and 1.0×10^{-11} at τ_{av} between 0.1 s and 1000 s.[2)]

Since the Doppler-free spectra of the Cs-D_2 line could be obtained with sufficient signal-to-noise ratio by using a simple optical system and a small Cs cell at room temperature, we can construct a compact system of the highly-stabilized GaAlAs laser. Such system has high potentiality to be used as a convenient standard of wavelength or optical frequency and in optical telecommunications, meterology, precision measurements and laser spectroscopy.

I-2-4 Potentiality of Semiconductor Laser in Laser Spectroscopy

As mentioned already, a semiconductor laser can easily operate on a single mode with very high frequency-tunability, and is one of the most useful monochromatic light source in the infrared region. The spectral width of the semiconductor lasers is rather broad, so far, typically of the order of 10 MHz or

more, however, this may be improved by utilizing spectral narrowing effects due to optical feedback.[38),39)]

The oscillation frequency can easily be swept by varying the diode temperature and injection current, and the continuous scanning is possible over 10 GHz or more. In most high-resolution spectroscopy, a frequency stability about 1 MHz is enough because the natural linewidth of atomic or molecular absorption spectrum is of the order of 1 MHz. To obtain such stability, about 10^{-4} degree and 0.1 μA controls are needed for the diode temperature and injection current respectively. It is not so difficult to achieve this because of the small size and low electric power operation of the semiconductor laser. In the case of a GaAlAs laser operating at room temperature, the frequency stability about 1 MHz can be achieved without sacrificing high frequency-tunability by utilizing the system of temperature control developed in this work. A high resolution frequency-scanning is possible by varying the stabilized diode-temperature and using a Fabry-Perot resonator as a frequency marker.

There are not so many reports on the high resolution spectroscopy by utilizing the semiconductor lasers, so far, and several atomic and molecular absorption lines of Cs, Rb, Ar, CH_4, HF, and H_2O have been reported in connection with the frequency stabilization (Sec. I-2-2). In the case of the Cs-D_2 line, the first observation of its saturated absorption spectra has been performed in this work. By using atomic beams, the optical

pumping of Cs and Rb has been investigated for improvement of the atomic clock.

Since the wavelength of the semiconductor laser is extending down to 700 nm, it is expected to apply the semiconductor lasers to wide variety of the laser spectroscopy. Furthermore, an application of the GaAlAs laser to FM laser-spectroscopy[40] may be possible because a frequency-modulation with high-frequency can be achived by modulating directly the injection current. It is also interesting to use a combination of two or more semiconductor lasers in the laser spectroscopy. One of such experiment is carried out in this work, in which a Doppler-free spectrum completely free from Doppler-broadened background can be obtained. Such experiment using many single-mode and frequency-tunable lasers is not so difficult for easy operation of the semiconductor lasers.

I-3 Saturated Absorption Spectroscopy and Optical Pumping

I-3-1 Atomic Absorption Spectrum as Frequency Reference

An advance in physics and technology is often closely connected with the precision measurements of some physical quantities with extremely high resolution above ordinary experiences. In the field where the measurement of time, frequency, length and velocity are concerned, the laser with known wavelength is a very useful tool. A continuous wave laser

conventionally consists of a laser material and an optical resonator and operates on the cavity modes. The oscillation frequency, in free-running condition, may fluctuate and drift across gain profile according to a change of cavity spacing and to other perturbations. In ordinary sense, the laser frequency, especially of gaseous laser, is rather stable but it cannot meet a requisition of modern physics and technology. For further high resolution measurements, many attempts have been performed to stabilize the laser frequency.

Usual method used in the frequency stabilization of lasers is to prepare an absolute frequency-reference and to lock the laser frequency to it by controlling the oscillation parameters such as cavity length. Since the frequency stability expected to achieve depends on the spectral stability and sharpness of the frequency reference, it is required for the frequency reference to be a very narrow spectrum, to be free from external perturbations and to be observed with high signal-to-noise ratio.

One of the best frequency reference is the transition frequency between energy levels of unperturbed atoms or molecules. The transition frequency ν_{ij} and the energy difference between levels with energy E_i and E_j ($E_i > E_j$) are related by Planck constant h as

$$\nu_{ij} = \frac{E_i - E_j}{h}, \qquad \text{(I.1)}$$

and it can be regarded as constant. When one of the transition frequency of atoms or molecules is in the tuning range of the laser, one can refer it by observing the resonant light absorption of atomic or molecular vapor. When an atom or molecule is at rest, the absorption spectum has a narrow natural width which is inversely proportional to the lifetime of the upper energy level. Typically the lifetime is of the order of 10^{-8} s, and the natural spectral width is about 10 MHz. However in vapor each atom or molecule moves with thermal velocity and comes into resonance with the light frequency-shifted due to Doppler effect. According to the velocity distribution, the absorption spectrum of atomic or molecular vapor is inhomogeneously broadened, which refers to Doppler-broadening. Typically the Doppler-broadening is more than 100 MHz at ordinary temperature, and such broadened absorption spectrum cannot be a good frequency-reference.

Many techniques have been studied to eliminate Doppler-broadening of the absorption lines,[41] and we can now utilize the techniques of the saturated absorption spectroscopy,[36),37)] the two-photon absorption spectroscopy,[42] the atomic-beam spectroscopy,[43] the optical double-resonance technique,[44] and so on. Especially, the saturated absorption spectroscopy is the most powerful technique for the frequency stabilization of lasers. It provides Doppler-free spectrum with high signal-to-noise ratio by using a simple setup. The saturated absorption technique has already been used in the frequency stabilization of

gaseous lasers, and an extraordinary high frequency-stability better than 10^{-13} has been obtained. The saturated absorption spectroscopy is also a very useful technique to measure microscopic structures of atomic or molecular energy levels. It is the typical method in the laser spectroscopy utilizing all of the spectral sharpness, the spacial coherence and the high intensity of laser. Further significant feature arises, when the optical pumping is combined with the saturated absorption technique. We present in following sections, a brief review on the saturated absorption spectroscopy and the optical pumping, which is helpful for understanding of this thesis.

I-3-2 Doppler-Free Saturated Absorption Spectroscopy

(a) Lamb dip

A conceptual setup for the saturated absorption spectroscopy consists of an absorption cell and two counter-propagating laser beams, see Fig. I-2. Both beams travelling in the +z and -z direction are quasi-monochromatic with frequency ω and wavenumber k and overlap to each other completely in the cell. Atomic vapor is enclosed into the cell with very low pressure. For simplicity, we consider at first that only two energy levels of atom are concerned with resonant transition.

An atom shows naturally a narrow absorption spectrum and comes into resonance with the laser frequency within narrow

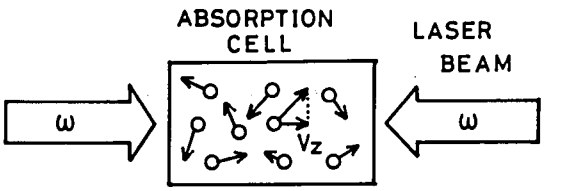

Fig. I-2 Conceptual optical alignment of the saturated absorption spectroscopy. Two counter-propagating laser beams are tuned to the same frequency.

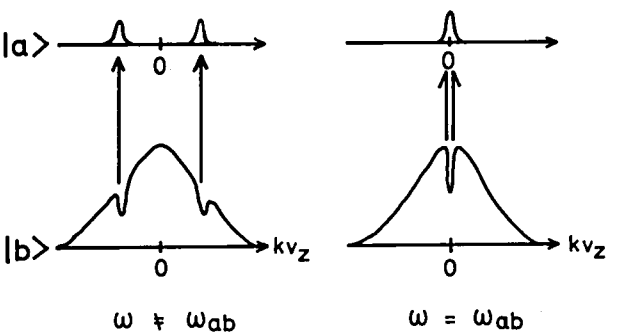

Fig. I-3 Velocity distribution of two-level atoms. Two counter-propagating laser beams burn two holes in the velocity distribution of atoms in the lower level |b>. When the laser frequency is tuned at the center of the atomic transition frequency, the two holes are overlapped to each other.

vicinity of the transition frequency ω_{ab}. In vapor, an atom thermally moves with velocity v_z along z axis, and the laser frequency is Doppler-shifted of the amount of kv_z in the rest frame of atom. So in this case, the resonant light absorption occurs under one of the following conditions.

$$\omega_{ab} = \omega + kv_z, \tag{I.2a}$$

$$\omega_{ab} = \omega - kv_z. \tag{I.2b}$$

Let us consider how the laser beams are absorbed when the laser frequency ω is swept. In the case $\omega \neq \omega_{ab}$, atoms on resonance belong to two different velocity groups. Namely, two laser beams interact to the atoms independently. So, except the position $\omega \simeq \omega_{ab}$, the absorption spectrum is coincident with the ordinary Doppler-broadened spectrum obtained for a single laser beam.

The atoms on resonance are pumped by an intense light field to upper level against the relaxation, and some amount of atoms are in the upper level steadily. As a result a hole is burned in the velocity distribution of atoms in the ground level, which decreases the population difference between two energy levels. The hole burning saturates the light absorption, because the light absorption is proportional to the population difference. In the case that $\omega = \omega_{ab}$, the two resonance conditions in Eq. (I.2) are simultaneously satisfied by atoms with $v_z = 0$, and the two laser beams pump atoms in narrow portion at the center of the velocity distribution. Namely, the overlapping of the hole burning occurs, which results in the enhancement of saturation

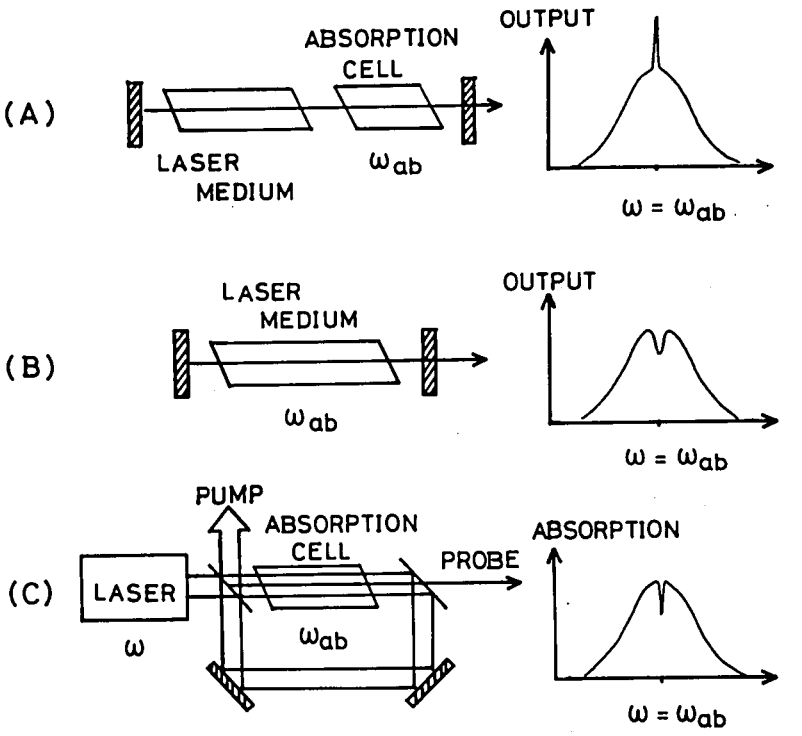

Fig. I-4 Three typical setups for the saturated absorption spectroscopy. The absorption cell is placed into the laser cavity (A), (B), and out of the laser cavity (C). The Doppler-free spectra so-called inverted Lamb-dip (A) and Lamb dip (B), (C) appear at $\omega = \omega_{ab}$.

(Fig. I-3). Consequently, a narrow dip can be observed at the center of the Doppler-broadened absorption spectrum. As described later, the width of the dip is determined by atomic homogeneous linewidth. The Doppler-free narrow dip is called "Lamb dip".[45),46)]

There are two typical ways of the saturated absorption experiment in practice, depending on wheather an absorption cell is placed into or out of the laser cavity. In the former, a narrow peak appears in the laser-gain profile[36)] (Fig. I-4A). When the absorption medium is the laser medium itself, a dip of laser gain appears at the center of the gain profile[45)] (Fig. I-4B). Lamb dip originally refers to such dip in the laser gain, and sometimes the narrow peak of the gain profile is called as "inverted" Lamb-dip. The inverted Lamb-dip has been succesfully used in the frequency stabilization of gaseous lasers. When the absorption cell is placed out of laser cavity, the laser beam is split into two beams and applied into the absorption cell from the opposite direction to each other (Fig. I-4C). Usually one laser beam is relatively intense and used as a pump beam which produces hole burning, and the other laser beam is weak and used as a probe beam. An intensity change of the weak probe beam is detected after transmitted through the cell as sweeping the laser frequency. The absorption signal of the probe beam is strongly saturated at the center of the Doppler-broadened absorption line owing to the hole burning of the pump beam, and a narrow Doppler-free spectrum, i. e. a dip in the absorption signal of the probe

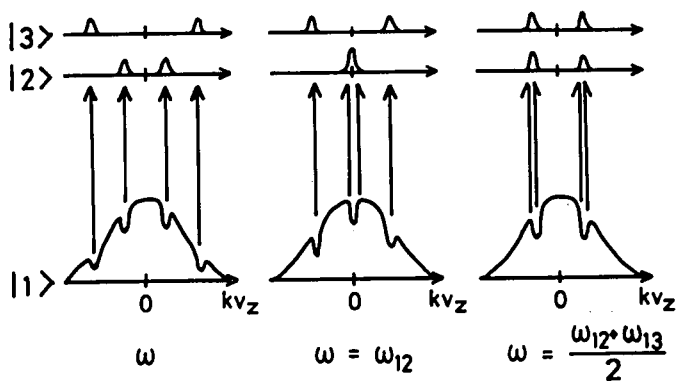

Fig. I-5 Velocity distribution of three-level atoms. Two counter-propagating laser beams burn four holes in the velocity distribution of atoms in the lower level $|1\rangle$, and two of the holes are overlapped to each other at $\omega = \omega_{12}$ and $\omega = \omega_{13}$ (Lamb dip), and also at $\omega = (\omega_{12}+\omega_{13})/2$ (crossover resonance).

beam, is appeared on the Doppler-broadened background. This narrow spectrum is also called Lamb dip. In this thesis, we are concerned with this type of the saturated absorption spectra of the Cs-D_2 line.

(b) Crossover resonance

When there are two closely spaced energy levels, such as hyperfine levels in the excited state or ground state, another type of the Doppler-free spectrum so-called "crossover resonance"[47] can be observed at the arithmetic mean frequency of two transitions in addition to two Lamb dips. Consider the case of atom with three energy levels, two levels being in the excited state. In this case, two optical transitions are possible from the ground state, and let us write ω_{21} and ω_{31} as the transition frequencies. Similarly to Eq. (I.2), the resonant light absorption occurs when one of the following conditions is satisfied.

$$\omega_{12} = \omega + kv_z, \tag{I.3a}$$

$$\omega_{12} = \omega - kv_z, \tag{I.3b}$$

$$\omega_{13} = \omega + kv_z, \tag{I.3c}$$

$$\omega_{13} = \omega - kv_z. \tag{I.3d}$$

When the laser frequency ω is in the Doppler-broadened absorption lines, hole burnings are produced by two counter-propagating beams at four different velocities v_z according to the resonance

conditions in Eqs. (I.3). As in the case of two-level atom, two Lamb dips can be observed at $\omega \simeq \omega_{12}$ and $\omega \simeq \omega_{13}$. When the laser frequency is tuned at $(\omega_{21}+\omega_{31})/2$, two pairs of the resonance conditions, Eqs. (I.3a) and (I.3d), and Eqs. (I.3b) and (I.3c), are simultaneously satisfied by atoms with $v_z = (\omega_{21}+\omega_{31})/2k$. In this case, one laser beam pumps atoms to one upper level and the other beam pumps simultaneously to the other upper level (Fig. I-5). The overlapping of the hole burnings produced by two laser beams enhances the saturation of absorption, and the third narrow dip of absorption appears on the Doppler-broadened background. This Doppler-free spectrum is the crossover resonance where two atomic transitions are simultaneously concerned with the spectrum. When many energy levels are closely spaced, and Doppler-broadened absorption lines are overlapping, Lamb dips appear at the centers of the transitions, and crossover resonances are observed at the arithmetic mean of possible pairs of the transitions.

The linewidth of the saturated absorption spectrum is larger than the homogeneous linewidth owing to power broadening,[45] but is typically about 10 MHz under low vapor pressure and without collisions. Such a narrow spectrum is a good absolute frequency-reference in the frequency stabilization of lasers. We can also determine the microscopic structure of atomic or molecular energy levels which overlap due to Doppler-broadening. By using the saturated absorption technique, the first-order Doppler-effect can completely be eliminated. The second-order Doppler-effect

appears to be a narrow asymmetric broadening and a shift of the saturated absorption spectra.

The Doppler-free spectra considered above are essentially due to the two-level saturation effect where relatively intense laser power is required to pump atoms stationary into upper level against to the fast relaxation. In order to observe the Doppler-free spectra of atoms succesfully, $\sim$10 mW is at least required for the laser power. When an saturated absorption cell is used out of laser cavity, such output power is not always available, especially by semiconductor lasers. However, it is noted that, when the optical pumping in the atomic ground state takes place,[48] the saturated absorption spectroscopy is possible by using much weaker laser beams. We discuss on the optical pumping in the following section.

It should be noted that, the hole burning in the ground state saturates not only the light absorption but also the anomalous dispersion which is also proportional to the population difference between upper and ground levels.[49] Especially when the circularly polarized laser beam is used as a pump beam, the hole burning produces an asymmetrical saturation of anomalous dispersion for right- and left-circular polarization. This results in the circular birefringence and dichroism. A linear polarized probe beam, which is superposition of two circular polarizations, is sensitive to detect the hole burning if one use the phenomenon called "optical rotatory power" or "optically induced Faraday rotation".[50] Namely, the plane of probe

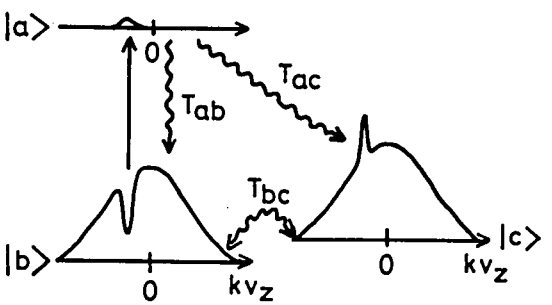

Fig. I-6 Velocity distribution of three-level atoms when the velocity-selective optical pumping takes place.

polarization rotates due to the anisotropy in refractive indices for the circular polarization. By using this phenomenon, we can observe a Doppler-free spectrum as the polarization change in the probe beam, and the method is called polarization spectroscopy.[51] Since the anomalous dispersion has antisymmetrical frequency-dependence around the resonance frequency, from the polarization spectrum we can identify whether the laser frequency is detuned at higher or lower frequency side of the resonance. The polarization spectrum has been utilized in the frequency stabilization of a gaseous laser. No frequency modulation is required for the servocontrol of the laser frequency.

I-3-3 Velocity-Selective Optical Pumping in Saturation Spectroscopy

It is well known that a weak light intensity is enough to observe saturation of atomic absorption if the optical pumping[52)-54)] takes place between sublevels in the atomic ground state. In the saturated absorption spectroscopy, the velocity-selective optical pumping[55)] makes it possible to observe Doppler-free spectrum by using a laser with weak output power less than 1 mW.

In order to understand the principle of the optical pumping, let us consider a three-level atomic model shown in Fig. I-6, where two energy levels $|a\rangle$ and $|b\rangle$, which are coupled through

resonant light absorption, are accompanied with a nonabsorbong level $|c\rangle$ near the ground level $|b\rangle$. Atoms on resonance to the light frequency are excited from $|b\rangle$ to upper level $|a\rangle$ and quickly decay back to $|b\rangle$ and also to the nonabsorbing level $|c\rangle$. In an above pumping cycle, the light field transfers some amount of resonant atoms effectively from $|b\rangle$ to $|c\rangle$. Since the relaxation from $|c\rangle$ to $|b\rangle$ is generally very slow, a large amount of atoms are pumped from $|b\rangle$ to $|c\rangle$ after many cycles of the pumping. Namely, relatively weak light intensity is enough for above optical pumping because the relaxation time T_{bc} between $|b\rangle$ and $|c\rangle$ is much larger than those from the upper level $|a\rangle$, T_{ab} and T_{ac}. A simple calculation for the three-level system shows that the saturation threshold of the light intensity is reduced by a factor T_{ac}/T_{bc} in comparison with the two-level system.[56] In the case of the D-line of alkali-metal atoms, the relaxation time of the excited state is about 10^{-8} s, and that among Zeeman sublevels or hyperfine levels in the ground state is typically of the order of 10^{-4} s. So the factor T_{ac}/T_{bc} becomes $\sim 10^4$. This enables us to observe many nonlinear phenomena even at extremely weak light intensities. In fact, self focusing of the laser beam has been observed at the light power of several 10 μW,[57] when the light beam is circularly polarized. Note that, the optical pumping takes place even when $|c\rangle$ is not nonabsorbing level if the absorption rate is less than that for the level $|b\rangle$.

The hyperfine levels in the ground state of alkali-metal atoms are separated of the order of 1 GHz due to coupling of

electron angular momentum with nuclear spin. If the hyperfine separation is larger than line broadening such as Doppler-broadening, the absorption lines from hyperfine levels in the ground state are also separated (Fig. I-7). A pumping light with narrow spectrum excites atoms selectively from one of the hyperfine level in the ground state and causes the optical pumping, so-called "hyperfine pumping".[53] As an example, consider the case of the D_2 absorption line of Cs.[58] The ground state of Cs consists of two hyperfine levels with the frequency separation 9 GHz, and absorption lines from these levels are well separated in a vacuum Cs cell at room temperature. Therefore, by applying quasi-monochromatic laser beam, the hyperfine pumping is caused velocity-selectively, which makes it possible to observe the saturated absorption spectra by using a semiconductor laser with output power less than 1 mW.

It should be noted that, the velocity-selective hyperfine pumping can be applied to the laser spectroscopy with high resolution, when the frequencies of the pump and probe beams can be tuned independently. Such an application is presented in this thesis, where a Doppler-free absorption signal of the Cs-D_2 line is observed with no Doppler-broadened background. It is also noted that, the hyperfine pumping of alkali-metal atoms is applicable to the microwave frequency standards. In fact, the hyperfine pumping in the ground state of ^{87}Rb has been used for this purpose.[59] For the Cs beam atomic clock,[60),61] it has been reported that the frequency stability is improved by

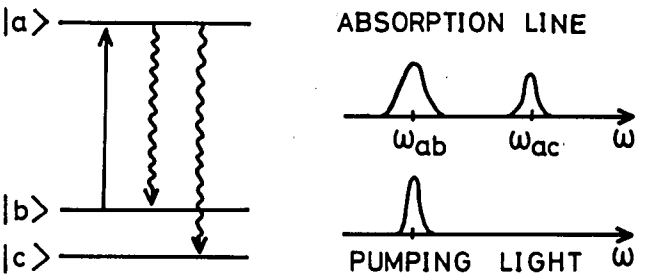

Fig. I-7 Energy diagram of atom showing the hyperfine pumping. The atoms in the level |b> are selectively excited by the light with narrow spectral width due to the conservation rule of energy.

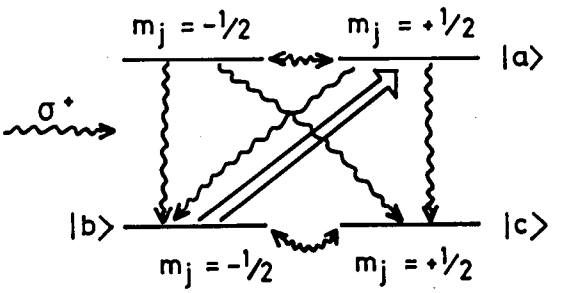

Fig. I-8 Energy diagram of atom showing the Zeeman optical pumping. The atoms in the level b> are selectively excited to the level |a> by the σ^+ circularly polarized light due to the conservation rule of angular momentum.

applying the hyperfine pumping in place of a hexapole state-selector magnet.[62),63)]

As to Zeeman sublevels in the atomic ground state, an adequately polarized pumping light is capable of selective excitation from one of the ground sublevels, even though the sublevels are degenerate in the absence of a magnetic field. For a simplicity, let us assume that both of ground and upper states have total angular momentum of $J = 1/2$ and so consist of two Zeeman sublevels with the magnetic quantum number $m_J = \pm 1/2$ (Fig. I-8). They correspond to the ground state $S_{1/2}$ and the first excited state $P_{1/2}$ of alkali-metal atoms, if the hyperfine coupling is ignored. When pumping light is σ^+ circularly polarized, the selection rule of the angular momentum allows only the transition from the level with $m_J = -1/2$ in the $S_{1/2}$ state to the level with $m_J = 1/2$ in the $P_{1/2}$ state. The excited atoms quickly decay to both ground sublevels, and the Zeeman optical pumping is performed in the ground state.

For the states with larger value of J, the optical pumping scheme is a little more complicated. In such a case, the optical pumping produces unequal population distribution among the Zeeman sublevels in the ground state, so that multipole moment such as electric quadrupole moment (alignment) is produced in addition to the magnetic dipole moment (orientation).[53)] By combining with the radiowave resonance, the Zeeman optical pumping has been widely used both in the fundamental studies of atoms or molecules and in practical applications such as optical pumping

magnetometer.[64),65)]

When a quasi-monochromatic laser beam is used as the pumping light, the Zeeman optical pumping is caused by both of spectral-selective and velocity-selective excitation. As the result, many important features arises. Although we are not concerned in this thesis, it should be noted that the Zeeman optical pumping can be applied to the polarization spectroscopy in the frequency stabilization of semiconductor lasers, where no frequency moduration is essentially required in the servocontrol loop of the laser frequency.

I-3-4 Frequency Stabilization of Lasers

Here, we present a brief review on the frequency stabilization of gaseous lasers and dye lasers for comparison with that of semiconductor lasers.

In the case of the gaseous laser, which generally consists of a discharge tube and an optical cavity, the laser gain profile is given by a Doppler-broadened spectrum. The laser frequency drifts across the gain profile according to a change of cavity spacing due to mechanical vibration and thermal expansion. Typical width of the gain profile and the cavity mode spacing are about 100 MHz in visible, so that the frequency stability is of the order of 10^{-6} in free-running condition. The short-term stability is also under influence of discharge noise.

In the frequency stabilization of gaseous lasers, the

saturated absorption technique has mainly been used. In the first stage, a Lamb dip appearing at the center of the gain profile was used in the frequency locking of He-Ne laser, and the frequency stability obtained was $\sim 10^{-9}$. Remarkable improvement has been made by locking the laser frequency to an inverted Lamb-dip, which appears on the gain profile when a saturated absorption cell is inserted into the laser cavity. As a frequency reference for the frequency locking, molecular absorption line is mainly used because its resonance frequency is less affected by an external perturbation such as magnetic field and pressure shift.

Although many molecular absorptipon lines exist from visible to infrared, a few of them coincide with the gaseous laser line. Typical examples are He-Ne lasers locked to CH_4 vibration-rotation spectrum at 3.39 μm[36),66)] and to I_2 hyperfine transitions at 612 nm[67)-69)] and 633 nm.[70),71)] In the former, one of the pressure shifted laser line of Ne happens to be centered by the CH_4 absorption spectrum. By locking the laser frequency to the inverted Lamb-dip with ∿100 kHz width, the frequency stability of $10^{-14} \sim 10^{-15}$ has been obtained, which competes with the stability of the Cs beam frequency-standard. In the later, the width of the inverted Lamb-dip is a few MHz which includes pressure broadening and power broadening, and the frequency stability of the order of 10^{-13} has been obtained. The absolute wavelength of these stabilized lasers was determined by using Kr^{86} standard at 605.7 nm,[66)] and its international

intercomparison was performed in the case of the I_2-stabilized lasers.[72] These lasers with extremely high frequency-stability have been used in measurement of physical quantities, such as the light velocity,[73] and in a test of physical concept, such as the isotropy of space.[74]

Beside these, the CO_2 laser at 10 μm has been also stabilized at inverted Lamb-dip by using CO_2 and SF_6 absorption line,[75] and Ar^+ laser at 515 nm has been stabilized at a Lamb dip of external I_2 absorption cell.[76] In the case of these lasers, the frequency-stability of $10^{-12} \sim 10^{-14}$ have been reported.

In a high resolution spectroscopy, the frequency scanning of the stabilized laser is sometimes required. For this purpose, a method called offset-locking has been developed,[77] in which one laser is stabilized to another stabilized one by using the beat frequency between these lasers.

In above technique of the frequency stabilization, the first or third derivative of the spectrum obtained by means of lock-in detection is usually used in the servocontrol of the laser cavity. By using the third derivative, the Doppler-broadened background can be eliminated from the saturated absorption spectrum. However the laser frequency must be slightly modulated, which is sometimes undesirable in its applications to the spectroscopy. To avoid this, the frequency stabilization of He-Ne laser at 3.39 μm has been performed by using the polarization spectroscopy of CH_4 intracavity absorption cell.[78]

Since the spectrum obtained by the polarization spectroscopy has a dispersion shape, the frequency stabilization can be made without laser frequency modulation. By this method, the frequency stability $\sim 10^{-12}$ has been obtained. Instead of modulating the laser frequency, it is possible to modulate the molecular absorption frequency by using the stark shift.[79)]

The frequency stabilization described above aims at the wavelength- or frequency-standard for the precision measurements. Although the fundamental scheme of the frequency stabilization is simple, the practical system requires special materials. In ordinary use for the laser spectroscopy, the frequency-stability of 10^{-9} is likely enough because the natural linewidth of the absorption spectrum is typically of the order of 1 MHz. For such purposes, a frequency-stabilization of a commercially available He-Ne laser by using a Zeeman split spectrum has been studied.[80)]

In the case of cw dye laser, which consists of a thin stream of dye solution and an optical cavity with some frequency-selective optical elements, the dye stream is excited by a pump laser such as Ar^+ laser, and the gain profile is given by a broad and continuous band-spectrum. The dye laser oscillates on a single or multi cavity-mode at the frequency giving a peak of total transmission of the intracavity frequency-selective elements, such as tunable etalons and birefringent filter. The dye laser has very high frequency-tunability and is one of the most important light source in the laser spectroscopy. Similarly

to the semiconductor laser, the frequency stability of dye laser is poor in free-running condition, which is a reflection of high frequency-tunability. The frequency stability of dye laser depends on fluctuations of dye stream, cavity spacing, pump laser power, frequency-selective elements, and all of their alignment. For example, a fast fluctuation of optical thickness of the dye stream may result in about 500 kHz frequency-fluctuation.[81)]

The frequency stabilization of dye laser has been studied in aim at an ultrahigh-resolution spectroscopy. To scan precisely the frequency, the technique of frequency-offset-locking mentioned already has been used.[81),82)] In this method, the laser frequency is locked to the resonance of an external optical resonator, which is stabilized by using a He-Ne laser. The frequency of the He-Ne laser is offset-locked to a I_2- or CH_4-stabilized He-Ne laser. In this case, the frequency-stability of the dye laser was found to be approximately given by that of the He-Ne reference laser. This was applied to a high resolution spectroscopy of Ca atomic beam and to a determination of the Rydberg constant with high accuracy.[83)]

Recently a dye laser spectrometer for ultrahigh spectral resolution was proposed,[81)] in which an I_2-stabilized He-Ne laser was used to provide a reference frequency. The dye laser frequency was controlled by using an intracavity ADP phase modulator with fast servo electronics and piezo-electric cavity-transducer. The result was that the linewidth of the stabilized dye laser, i. e. the short-term frequency-fluctuation, was

reduced to 1.8 kHz, and continuous tuning over 900 MHz could be obtained with 1 kHz step resolution. This system was utilized to investigate two-photon optical Ramsey fringes in Rb atomic beam and the fringe of 17 kHz width was firstly observed.[84)]

The technique described above is important in the studies to test the foundation in physics with ultrahigh resolution. However, the system is extremely complicated and requires very special materials and circumstances.

In addition to above special technique, the dye laser frequency has been stabilized by much simple methods utilizing a lens effect in a discharge tube,[85)] a vapor prism[86)] and a Faraday filter.[87)] To obtain a single-mode oscillation of dye laser, many frequency-selective elements in the laser cavity are required. By using a Faraday filter, a single-mode oscillation and the frequency stabilization are simultaneously achived without any other frequency-selective elements, and the frequency-locking to Na D-lines[56),88)] and to several lines of Ne[89)] has been reported.

In the frequency stabilization of semiconductor laser, a high frequency-stability can be achieved by using a relatively simple system. In comparison with gaseous laser, the semiconductor laser covers very wide frequency region, so there are much chance of coincidence with atomic or molecular absorption lines. The frequency locking to a Doppler-free atomic or molecular spectrum can easily be performed by controlling diode temperature and injection current. In the case of

semiconductor laser, an ultrahigh frequency-stability, such obtained for the He-Ne/CH_4 laser system, is difficult to obtain for the present, because of relatively wide spectral width ($\sim$10 MHz). However, it may be possible to achieve frequency stability of the semiconductor laser $\sim 10^{-13}$, which is comparable with that of ordinary I_2-stabilized He-Ne laser. It should be noted that a spectral-narrowing effect of semiconductor laser has been reported in which optical-feedback effect is utilized. The semiconductor laser is very small, and a small optical system can be used for the frequency locking. As is shown in this work, a compact and portable laser system with very high frequency-stability ($\sim 10^{-12}$) can be constructed, which is also very stable against mechanical vibrations and acoustic noise and requires no special circumstance for stable operation. Such a system has high potentiality for practical applications and can also be used as a rocket-borne laser system.

In comparison with dye laser, the semiconductor laser operates on a single mode much easily, i. e. without any additional spectral-selective element, and is highly frequency-tunable only by controlling diode temperature and injection current. So, it may not be so difficult to obtain stabilized frequency-scanning of the semiconductor laser by using a similar method of frequency-offset locking used in the stabilized dye laser. In this method, a semiconductor laser locked to a Doppler-free atomic or molecular spaectrum can be used as a reference laser to stabilize an external Fabry-Perot resonator.

Furthermore, such stabilized optical resonator may also be useful for frequency stabilization of dye laser and other lasers.

I-4 Outline of This Thesis

In the present thesis, we firstly study on the theory of the saturated absorption spectroscopy for some simplified cases which arise in the Cs-D_2 line (Chapter II). Secondly, we study on the saturated absorption spectra of Cs-D_2 line by using a GaAlAs semiconductor laser, and discuss about the observed Doppler-free spectra. We also present a method of the temperature stabilization of GaAlAs laser which is the first stage of the frequency stabilization. We also present an application of the temperature stabilized GaAlAs laser to a high resolution laser spectroscopy (Chapter III). We study on the frequency stabilization of the GaAlAs laser using one of the Doppler-free spectra of the Cs-D_2 line and report the experimental results of frequency locking. We also study on the construction of an improved and compact system of the frequency stabilized GaAlAs laser (Chapter IV). We will describe in more detail on the study discussed in each chapter.

In chapter II, we present a theoretical treatment of the saturated absorption spectroscopy where an interaction between atom and laser beam is discussed by using a semiclassical theory. We firstly show that an atom can be treated by using a simplified two- or three-level system whose behavior can be

discussed by using a rate equation. We next discuss on the absorption spectrum of atoms in vapor and on the saturation of the absorption. We also show that the process of the optical pumping can strongly enhance the saturation effect. Under those foundations, the shape of the saturated absorption spectrum is theoretically calculated. We give representations of the width and depth of the Doppler-free spectra in terms of the saturation parameter. These results can be used to analyze the observed saturated absorption spectra of the Cs-D_2 line.

In chapter III, we experimentally study on the saturated absorption spectra of the Cs-D_2 line by using a GaAlAs laser. We firstly give a theoretical consideration to the practical case of the cesium atom and discuss on the atomic parameters concerning with the D_2 absorption line and its Doppler-free spectra. Using the results of Chap. II, it is shown that the saturation threshold can be reduced by the hyperfine pumping, i. e. a weak output power of a semiconductor laser is enough for an observation of the saturated absorption spectra of the Cs-D_2 line. The temperature control of the GaAlAs laser is studied as the first stage of the frequency stabilization. It is shown that the frequency fluctuation of such a semiconductor laser can be reduced down to a few MHz only by the temperature control. Since the frequency stabilization is done without any loss of high frequency-tunability in this case, the system can be used for an usual high resolution spectroscopy. We next report the experimental result of observed Doppler-free spectra of the Cs-

D_2 line. We carried out also an experiment in which we observe directly the process of the hyperfine pumping by using two GaAlAs lasers. In the last section of chapter III, we show that Doppler-free spectra of Cs-D_2 line with no Doppler-broadened background can be observed using two GaAlAs lasers. Using these results, we emphasize the high potentiality of the semiconductor laser in the applications to the laser spectroscopy.

In chapter IV, we study on the frequency locking of the GaAlAs laser to one of the Doppler-free spectra of the Cs-D_2 line. We have stabilized the laser frequency, after stabilizing the diode temperature, by controlling the injection current, and obtained extremely high frequency-stability. We discuss on the system of the frequency stabilization and its experimental results. We discuss also on the limitation of the frequency stability, recalling the theory of the frequency stability and noise. We next estimate the frequency stability of the GaAlAs laser locked at the Cs-D_2 line and discuss on these results. For further improvement of the frequency stability, we have constructed a system with double-loop temperature-control. The preliminary result shows fairly high stability of the diode temperature. For various practical applications, a compact system of the stabilized GaAlAs laser must be useful. To this end, we constructed a compact optical system with some improvements. We mention about this system in the last section of this chapter.

In chapter V, we summarize the results of the present work

and discuss on the possible applications of the frequency-stabilized GaAlAs laser.

CHAPTER II

THEORY OF SATURATED ABSORPTION SPECTROSCOPY

II-1 Introduction

II-1-1 Outline of Theory

In this chapter, we present a theoretical consideration of the saturated absorption spectroscopy for some simplified cases of atomic system. We consider an absorption cell of atomic vapor and to which quasi-monochromatic laser beams are applied. The vapor pressure of atom is assumed to be very low, so that atomic collisions are almost negligible. In this case, absorption spectrum of each atom is very narrow, however, absorption spectrum of vapor is broadened due to thermal motion of atoms.

In this chapter, we firstly consider a simplified two-level atomic system and discuss on the rate equation treatment of atoms using a semiclassical theory of atom-field interaction.[90),91)] We derive an absorption characteristic in the case of Doppler-broadened atomic absorption line. We next discuss on the saturation of atomic absorption by using a steady state solution of rate equation of atoms. We also consider about the optical pumping using a three-level atomic system with two lower energy

levels. We show that the optical pumping can significantly decrease the light intensity to cause the saturation. Finally, we present a theoretical treatment of the saturated absorption spectroscopy and show appearance of narrow Doppler-free spectra "Lamb dip" and "crossover resonance" and also present formulas describing depth and width of these Doppler-free spectra.

As a preparation of the analysis of this chapter, we present a conception of a simplified model of atom and the density matrix ρ by which we treat atoms in the following sections.

II-1-2 Simplified Model of Atom in Vapor

Consider the case that a single atom is irradiated by a monochromatic light beam. An interaction between atom and light can be described by using an atomic Hamiltonian H, which can be written as a sum of free-atom Hamiltonian H_0 and interaction term V as

$$H = H_0 + V. \qquad \text{(II.1)}$$

According to Dirac's formula,[92] an atomic state is represented by a state vector $|\psi\rangle$, and its time evolution is determined by the Schrödinger equation as

$$i\hbar\frac{\partial}{\partial t}|\psi> = H\ |\psi>. \qquad \text{(II.2)}$$

Let $|\phi_i>$ be the eigenvector with the eigenvalue E_i, which presents the energy of the state, namely,

$$H_0|\phi_i> = E_i|\phi_i>. \qquad \text{(II.3)}$$

An atomic state is therefore written by a superposition of the eigenstates as

$$|\psi> = \sum_i C_i|\phi_i>, \qquad \text{(II.4)}$$

where C_i is complex number. The atom-light interaction is treated as a transition problem between eigenstates due to the perturbation V. In many problems of atom-light interaction, the light frequency ω is almost resonant to only one transition frequency ω_{ab} between eigenstates $|\phi_a>$ and $|\phi_b>$,

$$\omega \sim \frac{E_a - E_b}{\hbar} = \omega_{ab}. \qquad \text{(II.5)}$$

and no other transition frequencies come into resonance. In this case, we can consider on the behavior of atom using a state vector $|\psi'>$ in the sub-space spanned by $|\phi_a>$ and $|\phi_b>$ instead of a proper state vector $|\psi>$, where the vector $|\psi'>$ is produced from $|\psi>$ by a projection operator P as

$$|\psi'\rangle = P|\psi\rangle, \tag{II.6}$$

where P is

$$P = |\phi_a\rangle\langle\phi_a| + |\phi_b\rangle\langle\phi_b|. \tag{II.7}$$

Such simplified model of atom in the subspace is called as "two-level system", and similarly we can have a "three-level system" where three atomic eigenstates come into transition problem.

In this chapter, we are interested in the atom-light interaction in an atomic vapor, where we cannot observe the state of each atom, and a possible observation of some atomic observable A gives always its mean value $\langle A\rangle$ averaged over all atoms in the vapor. In this case, an atom should be treated not individually but as an ensemble. Let us represent the atomic state to be considered in the ensemble as $|\phi_i\rangle$ and the rest of the atomic state not to be observed as $|\theta_k\rangle$. An ensemble of atom can be expressed as a product of these state vectors as

$$|\psi\rangle = \sum_{ik} C_{ik}|\phi_i\rangle|\theta_k\rangle . \tag{II.8}$$

In this case, the mean value of atomic observable A, which is independent of the state $|\theta_k\rangle$, is calculated as

$$< A > = <\psi|A|\psi> = \sum_{ijkl} <\theta_l|<\phi_j|C^*_{jl}AC_{ik}|\phi_i>|\theta_k>$$

$$= \sum_{ijk} C^*_{jk}C_{ik}<\phi_j|\ A\ |\phi_i> . \qquad \text{(II.9)}$$

The ensemble atom is represented usually by using a Hermitian operator ρ called as density operator[93] with matrix elements

$$\rho_{ij} = \sum_k C^*_{jk}\ C_{ik}, \qquad \text{(II.10)}$$

and <A> is calculated by the formula as

$$< A > = \sum_i <\phi_i|\rho A|\phi_i> = Tr\{\rho A\}\ , \qquad \text{(II.11)}$$

where the trace "Tr" means a sum over all diagonal matrix elements of ρA. When atoms are in thermal equilibrium and free from external purturbation, ρ can be diagonalized by using the energy eigenstate $|\phi_i>$ and eigenvalue w_i as

$$\rho = \sum_i w_i\ |\phi_i><\phi_i| . \qquad \text{(II.12)}$$

The eigenvalue w_i can be interpreted as a probability of finding an atom in the state $|\phi_i>$ because a simple calculation shows $w_i \geq 0$ and $\sum_i w_i = 1$.

The time variation of the atomic eigenstates are expressed from Eqs. (II.2) and (II.3) as

$$|\phi_i(t)> = e^{-\frac{i}{\hbar}Ht} |\phi_i(0)>, \qquad \text{(II.13)}$$

and therefore the time variation of ρ can be written by unitary transform as

$$\rho(t) = e^{-\frac{i}{\hbar}Ht} \rho(0) e^{+\frac{i}{\hbar}Ht}. \qquad \text{(II.14)}$$

By taking the derivative of Eq. (II.14), the Schrödinger equation for the density operator is derived as

$$i\hbar\frac{\partial\rho}{\partial t} = [H , \rho], \qquad \text{(II.15)}$$

where $[H,\rho]$ is a comutator of H and ρ.

We can add relaxation term to Eq. (II.15), and such equation is usually called as the Liouville equation.[53] When atomic Hamiltonian is given, we can calculate the motion of atoms using the Liouville equation.

In atomic vapor, atom moves thermally, so one atom is also considered to be an ensemble of atoms moving with all possible thermal velocity.[94] In usual problem of light absorption, the energy separations between levels are much larger than thermal energy of atoms. In this case, we can specify atomic state independently of thermal velocity. So we can consider the atomic ensemble for a group of atoms with velocity between v and v+dv. Whole atoms in vapor are represented by using the Maxwellian

velocity distribution and the atomic ensemble for each velocity group as

$$\rho = \int_{-\infty}^{\infty} \frac{1}{\sqrt{\pi}u} e^{-(\frac{v}{u})^2} \rho_v \, dv, \qquad \text{(II.16)}$$

where

$$\rho_v = \sum_i w_i |iv><iv| . \qquad \text{(II.17)}$$

In Eq. (II.16), u is the most-probable velocity given by

$$u = \left(\frac{2k_B T}{M} \right) \frac{1}{2}, \qquad \text{(II.18)}$$

where k_B is the Boltzmann constant, T is the temperature and M is the mass of atom.

In the following sections, we discuss on the saturated absorption spectra using a simplified atomic system described by density matrix ρ_v defined in Eq. (II.17) for each velocity group of atoms. Such assumption has validity in the case that velocity changing collision can be negligible. In this case, mean value of atomic observable A can be calculated at first by taking the trace of $\rho_v A$ similarly to Eq. (II.11) for each velocity group of atoms and next by integrating over all possible velocity with Maxwellian velocity distribution as

$$< A > = \frac{1}{\sqrt{\pi}u} \int_{-\infty}^{\infty} e^{-(\frac{v}{u})^2} \mathrm{Tr}\{\rho_v A\} dv. \qquad \text{(II.19)}$$

In this representation, we may normalize the density operator for each velocity group of atoms as

$$\mathrm{Tr}\{ \rho_v \} = 1. \qquad \text{(II.20)}$$

II-2 Absorption Spectrum of Atomic Vapor

II-2-1 Semiclassical Theory of Atom-Light Interaction

For simplicity, we at first consider the case of two-level atom, with an upper level $|a\rangle$ and a ground level $|b\rangle$, irradiated by a monochromatic laser beam with frequency ω on the frame where the atom is at rest. The atom and the laser beam interact through the electric dipole moment $\vec{d}$ of atom and the electric field $\vec{E}$ of light, and the interaction term of the Hamiltonian can be written as

$$V = - \vec{d} \cdot \vec{E}. \qquad \text{(II.21)}$$

Since $\vec{d}$ is a vector operator having odd parity, $\vec{d}$ and V have no diagonal matrix elements. If we use the representation of the state vector as

$$|a\rangle = \begin{pmatrix} 1 \\ 0 \end{pmatrix} , \quad |b\rangle = \begin{pmatrix} 0 \\ 1 \end{pmatrix} , \tag{II.22}$$

V can be written down as

$$V = \begin{pmatrix} 0 & V_{ab} \\ V_{ab} & 0 \end{pmatrix} . \tag{II.23}$$

The Liouville equation is written down by its components as

$$\begin{aligned} \frac{d\rho_{aa}}{dt} &= -\frac{i}{\hbar}(V_{ab}\rho_{ba}-\rho_{ab}V_{ba})-\gamma_a(\rho_{aa}-\rho_{aa}^{(0)}) , \\ \frac{d\rho_{bb}}{dt} &= -\frac{i}{\hbar}(V_{ba}\rho_{ab}-\rho_{ba}V_{ab})-\gamma_b(\rho_{bb}-\rho_{bb}^{(0)}) , \\ \frac{d\rho_{ab}}{dt} &= -\frac{i}{\hbar}(E_a-E_b)\rho_{ab}-\frac{i}{\hbar}(V_{ab}\rho_{bb}-\rho_{aa}V_{ab})-\gamma_{ab}\rho_{ab} . \end{aligned} \tag{II.24}$$

where γ_a and γ_b are decay rates of ρ_{aa} and ρ_{bb}, γ_{ab} is decay rate of ρ_{ab}, and $\rho^{(0)}$ means the matrix element in the thermal equilibrium. In these equations, the diagonal elements ρ_{aa} and ρ_{bb} are usually called as "population" because they give the probability of finding atoms at the states $|a\rangle$ and $|b\rangle$, and the off-diagonal element ρ_{ab} is called as "coherence", which is concerned with the induced electric dipole moment of atom.[95] When atoms are in thermal equilibrium, the populations in $|a\rangle$ and $|b\rangle$ are distributed according to the Boltzmann distribution with random phase. Since $E_a-E_b \gg k_BT$ for light absorbing states, $\rho_{aa}^{(0)} \sim 0$ and $\rho_{bb}^{(0)} \sim 1$, and also $\rho_{ab}^{(0)} = \rho_{ba}^{(0)} = 0$.

Let us write the electric field of the monochromatic laser

beam as

$$\vec{E} = \frac{E_0}{2}\{\vec{e}\cdot e^{-i(\omega t-\vec{k}\cdot\vec{r})} + \vec{e}^{*}\cdot e^{i(\omega t-\vec{k}^{*}\cdot\vec{r})}\}, \qquad \text{(II.25)}$$

where $\vec{e}$ is the polarization vector of light. Here we represent $\vec{d}$ using its off-diagonal element $\vec{d}_{ab}$ as

$$\vec{d} = \begin{pmatrix} 0 & \vec{d}_{ab} \\ \vec{d}_{ab}^{*} & 0 \end{pmatrix}. \qquad \text{(II.26)}$$

Let us consider that the atom is rest at $\vec{r} = 0$. By substituting Eqs. (II.25) and (II.26) into Eq. (II.24), the equation for coherence is written expricitly as

$$\frac{d\rho_{ab}}{dt} = -(i\omega_{ab}+\gamma_{ab})\rho_{ab} - \frac{i}{\hbar}\frac{E_0}{2}\{\vec{d}_{ab}\cdot\vec{e}\, e^{-i\omega t}+\vec{d}_{ab}^{*}\cdot\vec{e}^{*}e^{i\omega t}\}(\rho_{aa}-\rho_{bb}), \qquad \text{(II.27)}$$

where the transition frequency ω_{ab} in Eq. (II.5) is used.

Next, we consider ρ_{ab} on a rotating frame as

$$\rho_{ab} = e^{-i\omega t}\rho_r, \qquad \text{(II.28)}$$

and obtain the equation

$$\frac{d\rho_r}{dt} = -\{i(\omega_{ab}-\omega)+\gamma_{ab}\}\rho_r - \frac{iE_0}{2\hbar}\{\vec{d}_{ab}\cdot\vec{e}(\rho_{aa}-\rho_{bb})+ \text{rapidly oscillating term}\}. \qquad \text{(II.29)}$$

We can consider that ρ_r is slowly varying with respect to time, and we can neglect the rapidly oscillating term and the derivative of ρ_r in Eq. (II.29). We obtain the solution of Eq. (II.27) as

$$\rho_{ab} = -\frac{iE_0}{2\hbar} \vec{d}_{ab}\cdot\vec{e}\, e^{-i\omega t} \frac{\rho_{aa}-\rho_{bb}}{(\omega_{ab}-\omega)^2+\gamma_{ab}^2}. \tag{II.30}$$

By using this, the interaction term in Eq. (II.24) is calculated as

$$\frac{i}{\hbar}(V_{ab}\rho_{ba}-\rho_{ab}V_{ba}) = \frac{E_0^2|\vec{d}_{ab}\cdot\vec{e}|^2}{2\hbar^2\gamma_{ab}} \frac{\gamma_{ab}^2}{(\omega_{ab}-\omega)^2+\gamma_{ab}^2}(\rho_{aa}-\rho_{bb}), \tag{II.31}$$

where rapidly oscillating terms are again neglected. Here we define the transition rate R_{ab} and Lorentzian $\mathcal{L}(\omega_{ab})$ by

$$R_{ab} = \frac{E_0^2 p_{ab}^2}{2\hbar^2\gamma_{ab}} \mathcal{L}(\omega_{ab}), \tag{II.32}$$

$$\mathcal{L}(\omega_{ab}) = \frac{\gamma_{ab}^2}{(\omega_{ab}-\omega)^2+\gamma_{ab}^2}, \tag{II.33}$$

where p_{ab} is defined as

$$p_{ab} = |\vec{d}_{ab}\cdot\vec{e}|. \tag{II.34}$$

Substituting Eq. (II.32) into Eq. (II.24), we can obtain the following equations of slowly varying terms.

$$\frac{d\rho_{aa}}{dt} = -R_{ab}(\rho_{aa}-\rho_{bb})-\gamma_a(\rho_{aa}-\rho_{aa}^{(0)}), \qquad \text{(II.35)}$$

$$\frac{d\rho_{bb}}{dt} = +R_{ab}(\rho_{aa}-\rho_{bb})-\gamma_b(\rho_{bb}-\rho_{bb}^{(0)}). \qquad \text{(II.36)}$$

These equations consist of only the populations ρ_{aa} and ρ_{bb}, which give the rate equation of atoms. The first term in each equation presents the induced transition, the stimulated absorption and emission. The second term presents the relaxation process including the spontaneous decay and other nonradiative decay. In Eqs. (II.35) and (II.36), total population of atoms is conserved, and we consider hereafter the total population is normalized to be unity;

$$Tr\{\ \rho\ \} = \rho_{aa} + \rho_{bb} = 1. \qquad \text{(II.37)}$$

Consequently, we can discuss on the behavior of atom by using the transition rate R_{ab} and the set of rate equations. The solution of the coherence ρ_{ab} presents a dielectric interaction between light and atomic vapor and determines the light propagation characteristics, on which we will discuss in the following sections.

II-2-2 Resonant Light Absorption in Atomic Vapor

The light propagation in a dielectric medium is described by the wave equation as follows.

$$\left(\nabla^2 - \frac{1}{c^2} \frac{\partial^2}{\partial t^2} \right) \vec{E} = \frac{4\pi}{c^2} \frac{\partial^2}{\partial t^2} \vec{P}. \qquad \text{(II.38)}$$

The macroscopic polarization $\vec{P}$ of the atomic vapor is related to the light field $\vec{E}$ by dielectric susceptibility $\langle \chi \rangle$ as

$$\vec{P} = \vec{E} \langle \chi \rangle. \qquad \text{(II.39)}$$

The imaginary part of the susceptibility gives the light absorption coefficient, and its real part gives the refractive index.[96] Namely, for the plane wave propagating along z axis, the wave number k is given from wave equation as

$$k \simeq \frac{\omega}{c} (1 + 2\pi \langle \chi \rangle), \qquad \text{(II.40)}$$

The imaginary part represents attenuation of the light field, and the real part presents the dispersion relation. Therefore, the absorption coefficient α of light intensity per unit length and the refractive index n are related to the susceptibility as

$$\alpha = \frac{4\pi\omega}{c} \mathrm{Im}\{ \langle \chi \rangle \}, \qquad \text{(II.41)}$$

$$n = 1 + 2\pi \, \mathrm{Re}\{ \langle \chi \rangle \}, \qquad \text{(II.42)}$$

where Im and Re means the imaginary and real part of $\langle \chi \rangle$

respectively.

The polarization of atomic vapor can be easily calculated from Eq. (II.11). Let us consider that N atoms are in the unit volume, and the macroscopic polarization is N times of the atomic polarization $\langle\vec{d}\rangle$ as

$$\vec{P} = N \langle \vec{d} \rangle . \tag{II.43}$$

The mean value of the electric dipole moment $\vec{d}$ is calculated from Eq. (II.11) as

$$\langle\vec{d}\rangle = Tr\{\rho\vec{d}\} = \rho_{ab}\vec{d}^{*}_{ab} + \rho^{*}_{ab}\vec{d}_{ab} . \tag{II.44}$$

By using the solution of ρ_{ab} in Eq. (II.30), we can obtain the representation of $\langle\chi\rangle$, α and n as

$$\langle\chi\rangle = - \frac{Np^2_{ab}}{\hbar\gamma^2_{ab}} \mathcal{L}(\omega_{ab})\{(\omega_{ab}-\omega)+i\gamma_{ab}\}(\rho_{aa}-\rho_{bb}), \tag{II.45}$$

$$\alpha = - \frac{4\pi p^2_{ab}}{\hbar\gamma_{ab}} \frac{\omega}{c} N\mathcal{L}(\omega_{ab})(\rho_{aa}-\rho_{bb}), \tag{II.46}$$

$$n = 1 - \frac{2\pi p^2_{ab}}{\hbar\gamma^2_{ab}} N(\omega_{ab}-\omega)\mathcal{L}(\omega_{ab})(\rho_{aa}-\rho_{bb}). \tag{II.47}$$

This results show that an atomic absorption spectrum shows a frequency dependence of Loretzian shape, and its natural linewidth is γ_{ab} (HWHM). The absorption coefficient is proportional to the population difference between levels where

the absorption transition is concerned. Therefore, by calculating the population difference from the rate equation in Eqs. (II.35) and (II.36), we can obtain the absorption spectrum of the atomic vapor.

II-2-3 Doppler-Broadened Absorption Spectrum

In above section, we have discussed the atom-light interaction on the atomic frame. In the vapor, atoms move with thermal velocity with Maxwellian velocity distribution, and the light frequency on each atomic frame is shifted due to the Doppler effect. As shown in Fig. II-1(a), consider an atom on the laboratory frame, in which atom moves along x_1 axis with velocity V, and the light with frequency ω is propagated along z axis, and the angle between x_1 and z axes is θ. This can be translated to the atomic frame as shown in Fig. II-1(b), in which the light source moves along x_1' axis with velocity -V, and the light with frequency ω' propagates along z' axis, and the angle between these axes is θ'. The light frequencies ω and ω', and the angles θ and θ' are related to each other by the Lorentz transformation of vector[97] as

$$k = (k' - \frac{V}{c} k_1') \{1 - (\frac{V}{c})^2\}^{\frac{1}{2}}, \qquad \text{(II.48)}$$

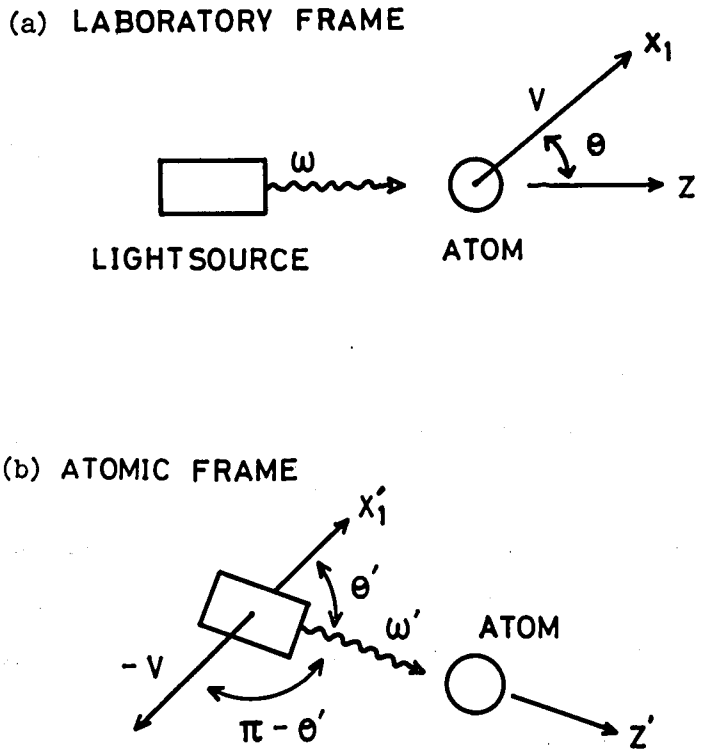

Fig.II-1 Relationship between the laboratory frame (a) and the atomic frame (b). The light frequency is shifted in the atomic frame due to Doppler effect.

$$\cos\theta = \frac{\cos\theta' + \frac{V}{c}}{1 + \frac{V}{c}\cos\theta'}, \qquad \text{(II.49)}$$

where c is the light velocity, and k is the wavenumber

$$k = \frac{\omega}{c}, \quad k_1' = k'\cos(\pi-\theta') = -\frac{\omega'}{c}\cos\theta. \qquad \text{(II.50)}$$

By using these transformations, the relation between the light frequencies in both frame is derived as

$$\omega' = \omega(1-\frac{V^2}{c^2})^{\frac{1}{2}}\{1+\frac{V}{c}(\cos\theta-\frac{V}{c})(1-\frac{V}{c}\cos\theta)^{-1}\}^{-1}. \qquad \text{(II.51)}$$

By reserving the second-order terms of V/c, this can be rewritten as

$$\omega' = \omega\ \{\ 1 - \frac{v}{c} - (\frac{v}{c})^2 - \frac{1}{2}(\frac{V}{c})^2\ \}, \qquad \text{(II.52)}$$

where $v = V\cos\theta$. The thermal velocity of atom at ordinary temperature is of the order of 10^4 cm/s which gives $V/c \sim 10^{-6}$. For visible or infrared light, the frequency is of the order of 10^{14} Hz, and the second order Doppler-shift is of the order of 100 Hz, which presents small ambiguity of the center of the absorption spectrum.

In the following calculations, we take account of the first order Doppler-shift, and the atomic transition frequency ω_{ab} in Eq. (II.46) is replaced by $\omega_{ab} + kv$. By integrating Eq. (II.46)

over all possible value of v, the absorption coefficient in the atomic vapor is obtained as

$$\alpha = -\frac{1}{\sqrt{\pi}u}\int_{-\infty}^{\infty} e^{-(\frac{v}{u})^2} \frac{4\pi p_{ab}^2}{\hbar\gamma_{ab}} \frac{\omega}{c} N_0 \mathcal{L}(\omega_{ab}+kv)(\rho_{aa}-\rho_{bb})_v dv, \quad \text{(II.53)}$$

where N_0 is the density of atom and $(\rho_{aa}-\rho_{bb})_v$ means the population difference calculated from the rate equations for each velocity group of atoms. This shows that the absorption spectrum of atomic vapor is the superposition of narrow Lorentzian absorption lines which are shifted due to Doppler effect.

II-2-4 Absorption Spectrum of Atomic Vapor

For a very weak light intensity, the population difference $(\rho_{aa}-\rho_{bb})_v$ is almost equal to $(\rho_{aa}^{(0)}-\rho_{bb}^{(0)})_v$, and some calculation gives the absorption coefficient α as

$$\alpha = -\frac{\alpha_0}{\pi ku} \mathrm{Im}\{ Z(\frac{\omega_{ab}-\omega+i\gamma_{ab}}{ku}) \}, \quad \text{(II.54)}$$

where $Z(\zeta)$ is the plasma dispersion function,[98] and Im indicates its imaginary part, u is the most probable velocity, k is the wavenumber of light, and α_0 is the linear absorption coefficient at $\omega = \omega_{ab}$ defined as

$$\alpha_0 = \frac{4\pi^2 p_{ab}^2 \omega_{ab}}{\hbar c} N_0 (\rho_{aa}^{(0)} - \rho_{bb}^{(0)})_{v=0} . \qquad \text{(II.55)}$$

The plasma dispersion function is defined as

$$Z(\zeta) = \begin{cases} \frac{1}{\sqrt{\pi}} \int_{-\infty}^{\infty} \frac{e^{-t^2}}{t - \zeta} \, dt & ; \ \mathrm{Im}\{\zeta\}>0, \quad \text{(II.56)} \\ \frac{1}{\sqrt{\pi}} \int_{-\infty}^{\infty} \frac{e^{-t^2}}{t - \zeta} \, dt + 2\sqrt{\pi}\, i\, e^{-\zeta^2} & ; \ \mathrm{Im}\{\zeta\}<0. \quad \text{(II.57)} \end{cases}$$

This function is connected to the complex error function erf(iζ) by[99]

$$Z(\zeta) = i\sqrt{\pi}\, e^{-\zeta^2} \{1+\mathrm{erf}(i\zeta)\}, \qquad \text{(II.58)}$$

$$\mathrm{erf}(i\zeta) = \frac{2}{\sqrt{\pi}} \int_0^{i\zeta} e^{-t^2} \, dt . \qquad \text{(II.59)}$$

The typical value of ku is more than 100 MHz at ordinary temperature, and the homogeneous width γ_{ab} is of the order of 1 MHz and is much smaller than ku. In this case, so called Doppler-limit, the function Z(ζ) can be approximated by

$$Z\left(\frac{\omega_{ab} - \omega + i\gamma_{ab}}{ku} \right) \simeq e^{-\left(\frac{\omega_{ab}-\omega}{ku}\right)^2} \left\{ i\sqrt{\pi} - 2\int_0^{\frac{\omega_{ab}-\omega}{ku}} e^{-x^2} dx \right\}, \qquad \text{(II.60)}$$

and we have obtained

$$\alpha \simeq \alpha_0 \frac{1}{\sqrt{\pi}ku} e^{-\left(\frac{\omega_{ab}-\omega}{ku} \right)^2} . \qquad \text{(II.61)}$$

This result shows that the absorption spectrum of atomic vapor is observed to be a Gaussian shape with width ω_D

$$\omega_D = 2\omega_{ab}\left(\frac{k_B T}{Mc^2} \cdot 2\ln 2 \right)^{1/2} \quad \text{(FWHM)}, \qquad \text{(II.62)}$$

which is usually referred as inhomogeneous or Doppler-broadened linewidth and is much larger than the homogeneous linewidth γ_{ab}.

II-3 Saturation Effect

II-3-1 Two-Level system

It has been shown that the absorption coefficient for light propagating in atomic vapor is proportional to the population difference between atomic energy levels where light absorption transition takes place. In this section, we show absorption coefficient in atomic vapor and consider saturation effect by using a steady-state solution of the rate equation for two typical cases of atomic systems. One is a two-level system, and another is a three-level system with two lower levels, one of which is absorbing level and the other is nonabsorbing level. In the case of the three-level system, the optical pumping is caused between two lower levels, so that the saturation effect is

strongly enhanced.

We at first consider the two-level system with a relaxation scheme as shown in Fig. II-2, in which lower level is in atomic ground state. The population in $|a\rangle$ decays to $|b\rangle$ with a rate γ, and populations in both levels also decay to its thermal equilibrium with rate γ_T. In the present work, γ_T is considered to be reciprocal to the time duration of atom-field interaction. In this case, the rate equation is given for each velocity group of atoms as

$$\frac{d\rho_{aa}}{dt} = -R_{ab}(\rho_{aa}-\rho_{bb})-(\gamma_T+\gamma)(\rho_{aa}-\rho_{aa}^{(0)}), \qquad (II.63)$$

$$\frac{d\rho_{bb}}{dt} = R_{ab}(\rho_{aa}-\rho_{bb})-\gamma_T(\rho_{bb}-\rho_{bb}^{(0)})+\gamma(\rho_{aa}-\rho_{aa}^{(0)}), \qquad (II.64)$$

in which we will normalize the population so that

$$Tr\{\rho\} = \rho_{aa} + \rho_{bb} = 1. \qquad (II.65)$$

The transition rate R_{ab} also depends on the atomic velocity v. The steady state solution of the rate equation gives the population difference between two levels for each velocity group of atoms as

$$(\rho_{aa}-\rho_{bb})_v = (\rho_{aa}^{(0)}-\rho_{bb}^{(0)})_v\left(1+\frac{2R_{ab}}{\gamma_T+\gamma}\right)^{-1}. \qquad (II.66)$$

Using R_{ab} in Eq. (II.32) and taking account of the Doppler shift, the population difference is calculated as

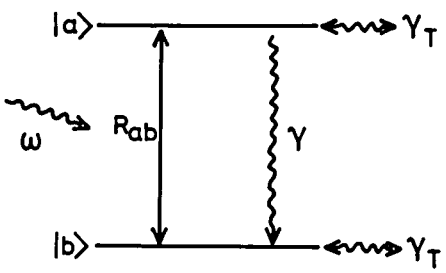

Fig. II-2 Energy diagram and relaxation scheme of the two-level atomic system. The decay rate of the coherence between two levels is γ_{ab}.

$$(\rho_{aa}-\rho_{bb})_v = (\rho_{aa}^{(0)}-\rho_{bb}^{(0)})_v\{1 - \frac{I_s}{1+I_s} L(\omega_{ab}+kv)\}. \quad \text{(II.67)}$$

I_s is the saturation parameter defined by

$$I_s = \frac{E_0^2 p_{ab}^2}{2\hbar^2 \gamma_{ab}} \frac{2}{\gamma_T+\gamma}, \quad \text{(II.68)}$$

and $L(\omega_{ab}+kv)$ is power-broadened Loretzian defined as

$$L(\omega_{ab}+kv) = \frac{(1+I_s)\gamma_{ab}^2}{(\omega_{ab}+kv-\omega)^2 + (1+I_s)\gamma_{ab}^2}. \quad \text{(II.69)}$$

where γ_{ab} is the natural width (HWHM) of the absorption line. In Eq. (II.68), usually $\rho_{aav}^{(0)} \sim 0$ since $h\omega_{ab} >> k_B T$, hence $\rho_{bbv}^{(0)} \sim 1$. Consider the Maxwellian velocity-distribution of atoms, the steady state distribution of the population in both levels are calculated as

$$\rho_{aav} = \frac{1}{\sqrt{\pi}u} e^{-(\frac{v}{u})^2} \frac{I_s}{2(1+I_s)} L(\omega_{ab}+kv), \quad \text{(II.70)}$$

$$\rho_{bbv} = \frac{1}{\sqrt{\pi}u} e^{-(\frac{v}{u})^2} \{1- \frac{I_s}{2(1+I_s)} L(\omega_{ab}+kv)\}. \quad \text{(II.71)}$$

This shows that, an intense light field of $I_s > 1$ burns a hole with a Lorentzian shape in the velocity distribution in the ground level $|b\rangle$ at $v = (\omega-\omega_{ab})/k$. The hole burning stationary decreases the population difference between two levels and saturates the light absorption. Substituting the result of

Eqs. (II.70) and (II.71) into Eq. (II.53) and evaluating the integral, we can obtain the absorption coefficient as

$$\alpha = -\frac{1}{\sqrt{\pi}u}\int_{-\infty}^{\infty} \frac{\alpha_0}{\pi\gamma_{ab}} e^{-(\frac{v}{u})^2} \mathcal{L}(\omega_{ab}+kv)\{1-\frac{I_s}{1+I_s}L(\omega_{ab}+kv)\}dv \quad \text{(II.72)}$$

$$= -\frac{1}{\pi ku}\frac{1}{\sqrt{1+I_s}} \mathrm{Im}\{ Z(\frac{\omega_{ab}-\omega+i\sqrt{1+I_s}\gamma_{ab}}{ku}) \}. \quad \text{(II.73)}$$

Comparing this with Eq. (II.54), we can see that the homogeneous linewidth is broadened by $\sqrt{1+I_s}$ times of the natural linewidth, and the light absorption is reduced due to saturation by $1/\sqrt{1+I_s}$ times. Usually the decay rate in the ground state γ_T is much smaller than that of the upper level $\gamma = 1/\tau$, so that I_s can be approximated by

$$I_s \simeq \frac{E_0^2 p_{ab}^2}{2\hbar^2\gamma_{ab}} 2\tau . \quad \text{(II.74)}$$

The square of the electric field is related to the energy flux of light or light power I by the Poynting theorem as

$$I = \frac{cE_0^2}{8\pi}. \quad \text{(II.75)}$$

It should be noted that, the saturation parameter for the two level system depends on the lifetime τ of the upper level. Namely, in order to achieve the saturation threshold $I_s \sim 1$, the light must pump the population to the upper level against the fast relaxation. Typically $\tau \sim 10^{-8}$ s, $p_{ab}^2 \sim 10^{-36}$ esu^{2}s^2, and

$\gamma_{ab} \sim 10^7$ Hz, so that the light power of about 100 mW/cm^2 is required to obtain the saturation threshold $I_s \sim 1$.

II-3-2 Three-Level System with Optical Pumping

We consider a three-level atomic system with relaxation scheme as shown in Fig. II-3. The lower levels $|b\rangle$ and $|c\rangle$ are respectively the light-absorbing level and the nonabsorbing level in the atomic ground state. The atom is selectively excited from $|b\rangle$ to $|a\rangle$ and quickly decay back to $|b\rangle$ and also to $|c\rangle$. In this pumping cycle, some amount of atoms in the lower levels are effectively transferred to $|c\rangle$. Since the relaxation time from $|c\rangle$ to $|b\rangle$ is generally very slow, and a large amount of atoms are pumped from $|b\rangle$ to $|c\rangle$ after many cycles of optical pumping. The rate equation describing this three-level system is written for each velocity group of atoms as

$$\frac{d\rho_{aa}}{dt} = -R_{ab}(\rho_{aa}-\rho_{bb})-(\gamma_T+\gamma_b+\gamma_c)(\rho_{aa}-\rho_{aa}^{(0)}), \tag{II.76}$$

$$\frac{d\rho_{bb}}{dt} = R_{ab}(\rho_{aa}-\rho_{bb})+\gamma_b(\rho_{aa}-\rho_{aa}^{(0)})-\gamma_T(\rho_{bb}-\rho_{bb}^{(0)})-\gamma_{bc}(\rho_{bb}-\rho_{cc}), \tag{II.77}$$

$$\frac{d\rho_{cc}}{dt} = \gamma_c(\rho_{aa}-\rho_{aa}^{(0)})-\gamma_T(\rho_{cc}-\rho_{cc}^{(0)})+\gamma_{bc}(\rho_{bb}-\rho_{cc}), \tag{II.78}$$

where γ_{bc} is the decay rate of the population difference between lower levels, and the population is normalized as

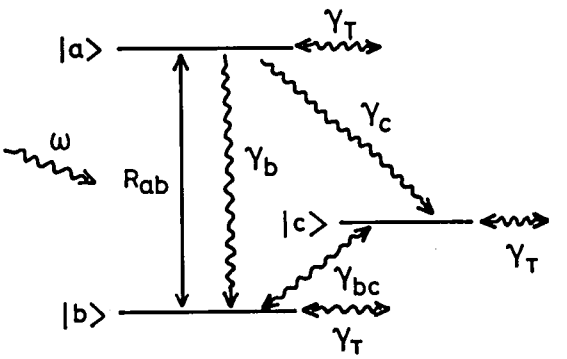

Fig. II-3 Energy diagram and relaxation scheme of the three-level atomic system. The decay rate of the coherence between levels |a> and |b> is γ_{ab}. The level |c> is nonabsorbing level close to the level |b>.

$$\mathrm{Tr}\{\rho\} = \rho_{aa} + \rho_{bb} + \rho_{cc} = 1. \qquad \text{(II.79)}$$

The steady-state solution gives the population difference similarly to Eq. (II.67) as

$$(\rho_{aa}-\rho_{bb})_v=(\rho_{aa}^{(0)}-\rho_{bb}^{(0)})_v\{1+\frac{\gamma_c+2\gamma_T+3\gamma_{ab}}{(2\gamma_{bc}+\gamma_T)(\gamma_T+\gamma_b+\gamma_c)}R_{ab}\}^{-1}. \qquad \text{(II.80)}$$

By using R_{ab} in Eq. (II.32), the population difference is written similarly to the case of the two-level system as

$$(\rho_{aa}-\rho_{bb})_v = (\rho_{aa}^{(0)}-\rho_{bb}^{(0)})_v\{1-\frac{I_s}{1+I_s} L(\omega_{ab}+kv)\}, \qquad \text{(II.81)}$$

where $L(\omega_{ab}+kv)$ is the power-broadened Lorentzian defined in Eq. (II.69). The saturation parameter is defined for the three-level system as

$$I_s = \frac{1}{2\gamma_{bc}+\gamma_T} \{ \frac{\gamma_c+2\gamma_T+3\gamma_{bc}}{\gamma_T+\gamma_b+\gamma_c} \} \frac{E_0^2 p_{ab}^2}{2\hbar^2\gamma_{ab}}. \qquad \text{(II.82)}$$

Usually the decay rate γ_b and γ_c are much larger than γ_T and γ_{bc}, and the saturation parameter is approximated as

$$I_s \simeq \frac{E_0^2 p_{ab}^2}{2\hbar^2\gamma_{ab}} \xi T, \qquad \text{(II.83)}$$

where we introduced the relaxation-branching ratio ξ and the relaxation time T between lower levels defined as

$$\xi = \frac{\gamma_c}{\gamma_b + \gamma_c}, \tag{II.84}$$

$$T = \frac{1}{2\gamma_{bc} + \gamma_T}. \tag{II.85}$$

I_s in the three-level system is proportional to the relaxation time T between lower levels in contrast with two-level system in which I_s is proportional to lifetime τ of the upper level. Comparing these results of I_s, the ratio of the saturation parameters becomes

$$\frac{I_s\ (\text{ three level })}{I_s\ (\text{ two level })} \sim \frac{\xi T}{2\tau} \simeq \frac{\gamma_c T}{2}. \tag{II.86}$$

Usually τ is much smaller than the ground state relaxation time T. We can conclude that the saturation parameter is sizably increased due to the optical pumping. In the three-level system, the population distributions of atoms are calculated for the light intensity giving $I_s \sim 1$ as

$$\rho_{aav} \simeq 0, \tag{II.87}$$

$$\rho_{bbv} \simeq \frac{\rho_{bb}^{(0)}}{\sqrt{\pi}u} e^{-(\frac{v}{u})^2} \{1 - \frac{I_s}{1+I_s} L(\omega_{ab}+kv)\}, \tag{II.88}$$

$$\rho_{ccv} \simeq \frac{\rho_{cc}^{(0)}}{\sqrt{\pi}u} e^{-(\frac{v}{u})^2} \{1 + \frac{\rho_{bb}^{(0)}}{\rho_{cc}^{(0)}} \frac{I_s}{1+I_s} L(\omega_{ab}+kv)\}. \tag{II.89}$$

This shows that, the hole burning with Lorentzian shape is

produced in the level |b>, and the population burned is repopulated to |c> conserving thermal velocity v and the Lorentzian shape. A relatively intense light can almost completely deplete the level |b> at $v = (\omega_{ab}-\omega)/k$. It should be noted that the absorption coefficients for both cases of two- and three-level systems are formally equal, except a difference in the magnitudes of the saturation parameters. This makes it possible to treat both atomic systems formally as a two-level system.

II-4 Doppler-Free Saturated Absorption Spectroscopy

In this section, we consider an experimental scheme of the saturated absorption spectroscopy as shown in Fig. II-4, in which an absorption cell of atomic vapor is subjected to two counter-propagating laser beams. One of the laser beams is relatively intense and used as a pump beam which burns a hole in the velocity distribution of atoms in the ground level. The other laser beam is weak and used as a probe beam which detects the hole burning. Both laser beams are assumed to be quasi-monochromatic and tuned to the same frequency. An absorption signal of the probe beam is observed as laser frequency is swept through the atomic absorption line. In this experiment, we can observe a narrow Doppler-free spectrum on the Doppler-broadened absorption signal.

We present in this section the theoretical treatment of the

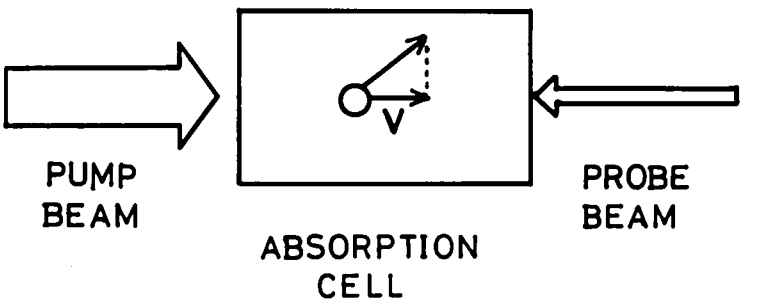

Fig. II-4 Experimental scheme of the saturated absorption spectroscopy. The relatively intense pump beam and the weak probe beam are applied into the cell from the opposite direction to each other.

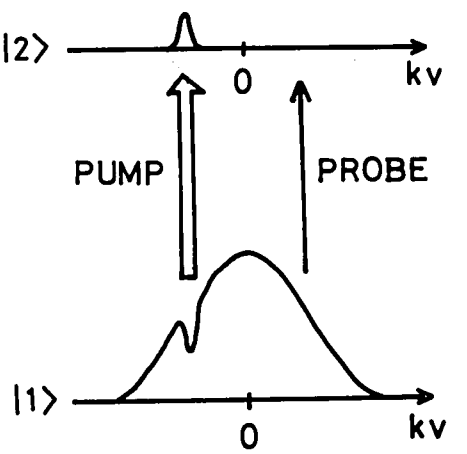

Fig. II-5 Velocity distribution of two-level atomic system. The relatively intense pump beam burns a hole in the velocity distribution of atoms in the lower level |1>.

saturated absorption spectroscopy for two typical cases of simplified atomic systems. One to be considered is a two-level system in which a narrow Doppler-free spectrum "Lamb dip"[46] appears. The other is a three-level system with two closely spaced excited levels, in which a narrow Doppler-free spectrum "crossover resonance"[47] appears in addition to two Lamb dips. As is mentioned in Sec. II-3-4, the population difference between the ground and excited levels can be calculated by using Eqs. (II.67) and (II.81). The difference between these two cases is only in the magnitude of the saturation parameter I_s. Therefore, we consider the atomic systems with one ground level in this section, which may include the case that another nonabsorbing level exists in the ground state.

In following calculations, we assume that the probe beam is weak and does not affect largely to the population distribution between levels. Therefore, the population distribution in each level is determined due to interaction of atoms with the pump beam. The absorption of the probe beam is calculated by using the population distribution produced by the pump beam.

II-4-1 Lamb Dip

Consider the case of two-level system with resonance frequency ω_{21} as shown in Fig. II-5. According to the result of Eq. (II.67), the population difference produced by the pump beam is calculated for each velocity group of atoms as

$$(\rho_{22}-\rho_{11})_v = (\rho_{22}^{(0)}-\rho_{11}^{(0)})_v\{1-\frac{I_s}{1+I_s}L(\omega_{21}+kv)\}. \quad (II.90)$$

The pump beam produces the hole burning at $\omega_{21}+kv = \omega$. The absorption of the probe beam is proportional to the population difference in Eq. (II.90). The absorption coefficient α_p for the probe beam is calculated by using Eq. (II.53) as

$$\alpha_p = -\frac{1}{\sqrt{\pi}u}\int_{-\infty}^{\infty}\frac{\alpha_0}{\pi\gamma_{21}}e^{-(\frac{v}{u})^2}\mathcal{L}(\omega_{21}-kv)\{1-\frac{I_s}{1+I_s}L(\omega_{21}+kv)\}dv, \quad (II.91)$$

where

$$\alpha_0 = \frac{4\pi^2 p_{21}^2\omega_{21}}{\hbar c}N_0(\rho_{22}^{(0)}-\rho_{11}^{(0)})_{V=0}, \quad (II.92)$$

$$\mathcal{L}(\omega_{21}-kv) = \frac{\gamma_{21}^2}{(\omega_{21}-kv-\omega)^2+\gamma_{21}^2}, \quad (II.93)$$

$$L(\omega_{21}+kv) = \frac{(1+I_s)^2\gamma_{21}^2}{(\omega_{21}+kv-\omega)^2+(1+I_s)\gamma_{21}^2}. \quad (II.94)$$

Because of the counter propagation of the laser beams, the Doppler-shifts kv have positive sign for the pump beam and negative sign for the probe beam. Equation (II.91) consists of two terms, the first term α_{p1} presents an ordinary Doppler-broadened absorption as Eq. (II.54), and the second term α_{p2} presents a saturated absorption spectrum as

$$\alpha_{p2} = \frac{1}{\sqrt{\pi}u}\int_{-\infty}^{\infty}\frac{\alpha_0}{\pi\gamma_{21}}e^{-(\frac{v}{u})^2}\frac{I_s}{1+I_s}\mathcal{L}(\omega_{21}-kv)L(\omega_{21}+kv)dv, \quad (II.95)$$

It is easy to see that this integral has nonzero value only in the case that the arguments in both Lorentzian are simultaneously in the narrow vicinity of resonance as

$$\omega \simeq \omega_{21} - kv \simeq \omega_{21} + kv. \qquad \text{(II.96)}$$

This gives $v = 0$ and $\omega = \omega_{21}$. Simple calculation gives α_{p2} in the form of the plasma dispersion function as

$$\alpha_{p2} = -\frac{\alpha_0}{\pi ku}\frac{I_s}{\sqrt{1+I_s}}\,\mathrm{Im}\Big\{ Z\Big(\frac{\Delta+i\gamma_{21}}{ku}\Big)\frac{\gamma^2}{(\gamma_{21}-2i\Delta)^2-\gamma^2} + Z\Big(\frac{\Delta+i\gamma}{ku}\Big)\frac{\gamma_{21}^2}{(\gamma-2i\Delta)^2-\gamma_{21}^2}\Big\}, \qquad \text{(II.97)}$$

where the detuning $\Delta = \omega_{21} - \omega$ and the power-broadened linewidth $\gamma = \sqrt{1+I_s}\,\gamma_{21}$ are used. In the Doppler-limit $\gamma \ll ku$, the whole absorption coefficient $\alpha = \alpha_{p1} + \alpha_{p2}$ is approximately given as

$$\alpha = -\frac{\alpha_0}{\sqrt{\pi}ku}\, e^{-\left(\frac{\omega_{21}-\omega}{ku}\right)^2} \times\Big\{ 1 - \frac{I_s}{\sqrt{1+I_s}(1+\sqrt{1+I_s})}\,\frac{\{(1+\sqrt{1+I_s})\gamma_{21}/2\}^2}{(\omega_{21}-\omega)^2+\{(1+\sqrt{1+I_s})\gamma_{21}/2\}^2}\Big\}. \qquad \text{(II.98)}$$

The second term in the bracket shows a narrow decrease of the absorption at the center of the Doppler-broadened spectrum. This spectrum is the Doppler-free spectrum, so-called Lamb dip. The

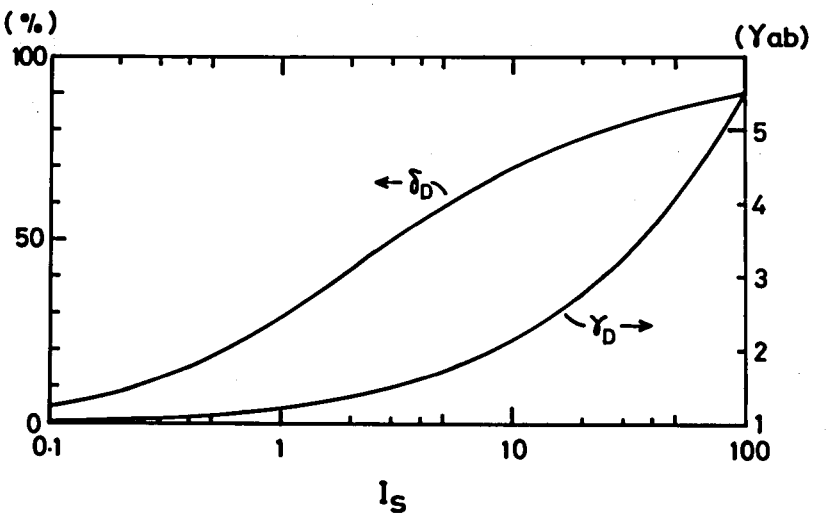

Fig. II-6 The power-broadened width γ_D and the depth δ_D of the saturated absorption spectrum as a function of the saturation parameter I_s.

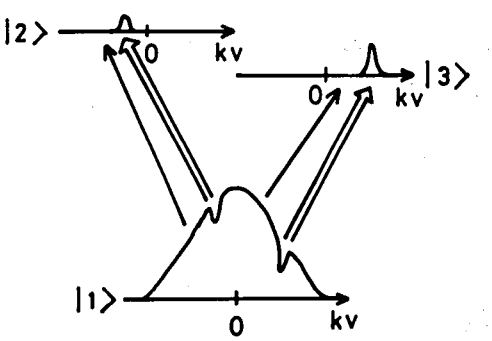

Fig. II-7 Velocity distribution of three-level atomic system. The pump beam burns two holes in the velocity distribution of atoms in the lower level |1>.

Lamb dip is the Lorentzian spectrum with the spectral width γ_D (HWHM) given as

$$\gamma_D = (1+ \sqrt{1+I_s}) \gamma_{21} /2. \qquad \text{(II.99)}$$

The depth δ_D of Lamb dip is given as

$$\delta_D = \frac{I_s}{\sqrt{1+I_s} (1+ \sqrt{1+I_s})}, \qquad \text{(II.100)}$$

which is the relative value to the Doppler-broadened background. The theoretical values of γ_D and δ_D are shown in Fig. II-6 according to a change of the saturation parameter.

In the case that, the absorption cell is optically thin, Eqs. (II.97) and (II.98) give directly the shape of observed signal of the Lamb dip. In the case that, the cell is optically thick, the observed shape of the Lamb dip is calculated from a nonlinear absorption equation as

$$\frac{dI(z)}{dz} = - \alpha(z) I(z), \qquad \text{(II.101)}$$

where I(z) is the light intensity at the point z along the laser beam.

II-4-2 Crossover Resonance

Consider a three-level system as shown in Fig. II-7, in which the excited state consists of two closely spaced sublevels $|2\rangle$ and $|3\rangle$ such as hyperfine levels. Let us write the transition frequencies as ω_{21} and ω_{31}. We assume that two absorption lines overlap to each other due to Doppler-broadening. In the case of the hyperfine levels, the frequency separation $(\omega_{31}-\omega_{21})$ is usually much larger than the natural linewidth. Therefore, we can neglect the case that atoms in the same velocity group are excited simultaneously to the upper levels $|2\rangle$ and $|3\rangle$. In this case, we can neglect the coherence between two upper levels as $\rho_{32} \sim 0$, which reduces a complication of the problem.[100] The results of Sec. II-2 can be utilized for this case.

In the case of the three-level system, hole burnings are produced by the pump beam at two different velocities v in the velocity distribution of atoms in the ground level. The population difference between the upper and the lower levels are calculated by using Eq. (II.67) as

$$(\rho_{22}-\rho_{11})_v \simeq (\rho_{22}^{(0)}-\rho_{11}^{(0)})_v\{1- \frac{I_2}{1+I_2} L_2(\omega_{21}+kv) - \beta_3 \frac{I_3}{1+I_3} L_3(\omega_{31}+kv)\}, \quad \text{(II.102)}$$

$$(\rho_{33}-\rho_{11})_v \simeq (\rho_{33}^{(0)}-\rho_{11}^{(0)})_v\{1-\frac{I_3}{1+I_3}L_3(\omega_{31}+kv) - \beta_2\frac{I_2}{1+I_2}L_2(\omega_{21}+kv)\}, \quad \text{(II.103)}$$

where I_2 and I_3 are respectively the saturation parameters for $|1\rangle$ to $|2\rangle$ and $|1\rangle$ to $|3\rangle$ excitations, and L_2 and L_3 are the power-broadened Lorentzians which include I_2 and $_{21}$, and I_3 and γ_{31}, respectively. In the case that $(\rho_{22}-\rho_{11}) \sim (\rho_{33}-\rho_{11})$, the coefficient β_i is given by $\beta_i \sim 1$ when the optical pumping occurs in the ground state and by $\beta_i \sim 1/2$ when no optical pumping occurs. For instance, let us consider Eq. (II.102). The second term in the large bracket represents the hole burning due to $|1\rangle$ to $|2\rangle$ excitation by the pump beam similarly to the case of the two-level system. The third term represents a contribution of the $|1\rangle$ to $|3\rangle$ excitation by the pump beam to the population difference $(\rho_{22}-\rho_{11})$. In the case that no optical pumping occurs, the change of ρ_{11} due to $|1\rangle$ to $|3\rangle$ excitation is the half of the change of $(\rho_{33}-\rho_{11})$, so that the coefficient β_i is about 1/2. In the case that optical pumping occurs, the change of ρ_{11} is approximately equal to the change of $(\rho_{33}-\rho_{11})$ because the population change in the upper level is negligibly small, so that the coefficient β_i is unity.

The absorption coefficient of the probe beam is calculated from Eq. (II.53) as

$$\alpha_p = -\frac{1}{\sqrt{\pi}u}\int_{-\infty}^{\infty} e^{-(\frac{v}{u})^2}\frac{\alpha_{21}}{\pi\gamma_{21}}\mathcal{L}(\omega_{21}-kv)(\rho_{22}-\rho_{11})_v/(\rho_{21}-\rho_{11})_{v=0}dv$$

$$-\{\text{interchange 2 and 3 in above expression}\}, \qquad \text{(II.104)}$$

where α_{21} and α_{31} are the linear absorption coefficients defined as

$$\alpha_{ij} = \frac{4\pi p_{ij}^2 \omega_{ij}}{\hbar c} N_0(\rho_{ii}^{(0)}-\rho_{jj}^{(0)})_{v=0}. \qquad \text{(II.105)}$$

Substituting the Eqs. (II.102) and (II.103) into Eq. (II.104) and integrating over all possible velocity, the absorption coefficient of the probe beam is obtained as a sum of following two terms.

$$\alpha_{p1} = \frac{-1}{\sqrt{\pi}u}\int_{-\infty}^{\infty}\frac{\alpha_{21}}{\pi\gamma_{21}} e^{-(\frac{v}{u})^2}\mathcal{L}(\omega_{21}-kv)\{1-\frac{I_2}{1+I_2}L_2(\omega_{21}+kv)\}dv$$

$$-\{\text{interchange 2 and 3 in above expression}\}, \qquad \text{(II.106)}$$

$$\alpha_{p2} = \frac{-1}{\sqrt{\pi}u}\int_{-\infty}^{\infty}\beta_3\frac{\alpha_{21}}{\pi\gamma_{21}} e^{-(\frac{v}{u})^2}\mathcal{L}(\omega_{21}-kv)\frac{I_3}{1+I_3}L_3(\omega_{31}+kv)dv$$

$$-\{\text{interchange 2 and 3 in above expression}\}. \qquad \text{(II.107)}$$

The former term α_{p1} represents the ordinary Doppler-broadened absorption and two Lamb dips appeared at both centers of the teansitions. The later term α_{p2} represents another type of the

saturated absorption spectrum, so called crossover resonance, in which the integral has nonzero value only in the case that the arguments of two Lorentzians satisfy the resonance conditions as

$$\omega \simeq \omega_{21} - kv \simeq \omega_{31} + kv, \tag{II.108}$$

$$\omega \simeq \omega_{31} - kv \simeq \omega_{21} + kv. \tag{II.109}$$

These results show that the crossover resonance appears at the arithmetic mean frequency of two transitions as

$$\omega \simeq \omega_c = \frac{\omega_{21} + \omega_{31}}{2}. \tag{II.110}$$

Simple calculation gives α_{p2} in the form of the plasma dispersion function as

$$\alpha_{p2} = -\frac{\alpha_{21}\beta_3}{\pi ku}\frac{I_3}{\sqrt{1+I_3}}\,\mathrm{Im}\Big\{ Z\Big(\frac{\Delta_{21}+i\gamma_{21}}{ku}\Big)\frac{\gamma_3^2}{(\gamma_{21}-2i\Delta_c)^2-\gamma_3^2} + Z\Big(\frac{\Delta_{31}+i\gamma_3}{ku}\Big)\frac{\gamma_{21}^2}{(\gamma_3-2i\Delta_c)^2-\gamma_{21}^2}\Big\}$$

$$- \{\text{interchange 2 and 3 in above expression}\}, \tag{II.111}$$

where we used the detunings $\Delta_{21} = \omega_{21}-\omega$, $\Delta_{31} = \omega_{31}-\omega$ and $\Delta_c = \omega_c-\omega = (\omega_{21}+\omega_{31})/2-\omega$, and the power-broadened linewidths $\gamma_2 = \sqrt{1+I_2}\,\gamma_{21}$ and $\gamma_3 = \sqrt{1+I_3}\,\gamma_{31}$. In the Doppler-limit, α_{p2} can be approximated as

$$\alpha_{p2} \simeq \frac{\alpha_{21}\beta_3}{\sqrt{\pi}ku} e^{-\left(\frac{\Delta_{32}}{2ku}\right)^2} \frac{I_3}{\sqrt{1+I_3}(1+\sqrt{1+I_3})} \frac{\{(\gamma_{21}+\sqrt{1+I_3}\gamma_{31})/2\}^2}{(\omega_c-\omega)^2+\{(\gamma_{21}+\sqrt{1+I_3}\gamma_{31})/2\}^2}$$

$$+ \{\text{interchange 2 and 3 in above expression}\}, \quad \text{(II.112)}$$

where we used $\Delta_{21} \sim \Delta_{31} \sim \Delta_{32} = \omega_{31} - \omega_{21}$. The crossover resonance is the superposition of two Lorentzian spectra with different width and depth, which correspond to the hole burning due to $|1\rangle$ to $|2\rangle$ pumping and its detection by $|1\rangle$ to $|3\rangle$ absorption, and vice versa.

When many energy levels are closely spaced in the excited state of atom, and Doppler-broadened absorption lines are overlapping, Lamb dips appear at the centers of the transitions, and crossover resonances appear at arithmetic means of possible pairs of transitions. If the energy separation between levels are larger than the homogeneous width of absorption lines, the discussion of this section can be applied to discussion on these Doppler-free spectra.

II-5 Conclusion and Discussions

In this chapter, we have discussed on the theoretical treatment of the saturated absorption spectroscopy by using a semiclassical theory of atom-light interaction. We have shown that the Doppler-free spectra, Lamb dip and crossover resonance, are appeared in the case of two- and three-level atomic systems. We have derived the representations of the width and depth of

these Doppler-free spectra as the function of the saturation parameter. The expression of the saturation parameter was derived for both cases of two-level system and three-level system with the optical pumping. Comparing these two cases, we show that the optical pumping can strongly increase the saturation parameter. In the case of alkali-metal atom, the optical pumping occurs between hyperfine levels in the ground state, and we can use a weak laser beam for the saturated absorption spectroscopy. By using these results, one can calculate an expected depth and linewidth of a saturated absorption spectrum. Such estimations are useful to optimize the laser powers and beam diameters in the saturated absorption setup of the frequency-stabilization system which is discussed in the followings of this thesis.

In the present theory, we have considered the steady state of atoms. The transit-time effect across the laser beam has been treated as if it is relaxation between hyperfine levels in the ground state. However, this assumption may be sometimes invalid, and the transient effect may manifest itself as a deformation of the absorption spectrum.[110),111)] A consideration on such transient effects will show interesting phenomena, although it is very complicated.

CHAPTER III

SATURATED ABSORPTION SPECTRA OF THE Cs-D_2 LINE

III-1 Introduction

The Cs-D_2 line at 852.1 nm lies within the tunable range of 820 nm band GaAlAs laser operating on a single mode at room temperature. In this chapter, we report the details of the experiments on the Doppler-free saturated absorption spectroscopy of the Cs-D_2 line using a GaAlAs laser.

Some experiments to observe the Cs-D_2 line have been performed by using GaAs laser operating at the liquid N_2 temperature. In 1969, Hochuri et al.[58] observed the hyperfine components of the Cs-D_2 line in Cs atomic beam. Sigh et al.,[101] in 1971, Bykowskii et al.,[102] in 1973, and Picqué,[103] in 1974, observed the Doppler-broadened absorption or emission spectra of the Cs-D_2 line using Cs cell with buffer gas. They reported on an appearance of the effects of optical pumping in the ground state of Cs. Picqué et al.[60),61] utilized the optical pumping of the Cs atomic beam to improve the precision of the atomic-beam clock. For the case of the Cs-D_2 line, the optical pumping between two hyperfine levels with F = 4 and 3 in the ground state is easily achieved. The optical pumping between hyperfine levels

is called the hyperfine pumping. As mentioned in Sec. I-3-3, the hyperfine pumping enhances considerably the saturation of absorption, and we can observe the saturated absorption spectra of the Cs-D_2 line by using a semiconductor laser with output power less than 1 mW.

Because of high frequency-tunability of a semiconductor laser, it is possible to observe the Doppler-free spectrum in details. However, as a reflection of high frequency-tunability, the frequency stability is rather poor in free-running condition. The frequency is greatly influenced by small changes of the injection current and the diode temperature. Because typical linewidth of a saturated absorption spectrum is of the order of 10 MHz in the case of the Cs-D_2 line, it is very important to suppress the fluctuation of the laser frequency at least within 10 MHz. In the case of GaAlAs laser which operates at several 10 mA and at room temperature, the 10 MHz change of the laser frequency is caused by about 1 μA fluctuation of the injection current or by about 10^{-3} °C fluctuation of the diode temperature. Although it is easy to prepare a regulated current source with stability of 10^{-4}, special devices are required to stabilize the diode temperature within 10^{-3} °C. We have achieved such stability of the diode temperature only by using a carefully constructed electronic system.

In this chapter, we study firstly on the saturated absorption spectra of the Cs-D_2 line theoretically utilizing the results of the Chap. II. Secondly, we report on the temperature

stabilization of GaAlAs laser as the first stage of the frequency stabilization. Thirdly, we present the experimental results on the observation of the Doppler-free saturated absorption spectra of the Cs-D_2 line. We also show an experimental evidence of the hyperfine pumping in which we monitor the velocity distribution of atoms in both of two hyperfine levels in the ground state, using two GaAlAs lasers. Furthermore, we can observe the Doppler-free resonances completely free from Doppler-broadened background. These experiments show high potentiality of the semiconductor lasers in applications to the laser spectroscopy.

III-2 Saturated Absorption Spectra of the Cs-D_2 Line

III-2-1 D_2 Absorption Line of Cs

The electronic ground state of the ^{133}Cs atom is $6^2S_{1/2}$, and $6^2P_{1/2}$ and $6^2P_{3/2}$ are the first excited states, which have electron angular momentum J = 1/2 and 3/2 respectively. The absorption lines corresponding to the $6^2S_{1/2} \rightarrow 6^2P_{1/2}$ and $6^2S_{1/2} \rightarrow 6^2P_{3/2}$ transitions are the D_1 line (894.35 nm) and D_2 line (852.112 nm) respectively.[104] The Cs-D_2 line lies within the tunable range of GaAlAs laser. The Cs atom has nuclear spin I = 7/2, so the energy levels split into hyperfine levels, which are identified by the quantum number F of the total angular momentum, i. e. $\vec{F} = \vec{I} + \vec{J}$.

The energy diagram of the Cs-D_2 line is shown in Fig. III-

1. The ground state consists of two hyperfine levels with F = 3 and 4. The hyperfine separation in the ground state is 9192631770 Hz, which is used in the definition of time.[105] The $6^2P_{3/2}$ state consists of four hyperfine levels with F = 2, 3, 4 and 5. The theoretical values of the hyperfine separations in the $6^2P_{3/2}$ state[58] are Δ_{54} = 212.8 MHz, Δ_{43} = 169.3 MHz and Δ_{32} = 128.3 MHz, which are indicated also in Fig. III-1. These values are calculated from the hyperfine energy W_F due to the magnetic dipole and electric quadrupole interactions.[106] W_F is given as

$$W_F = \frac{1}{2} hAK + \frac{3}{2} hB \frac{K(K+1) - 2I(I+1)J(J+1)}{2I(2I-1)2J(2J-1)}, \quad \text{(III.1)}$$

where

$$K = F(F+1) - I(I+1) - J(J+1). \quad \text{(III.2)}$$

The experimental determination of A and B was performed by Violino,[107] who used the level-crossing technique. The experimental results show that, A = 50.45 MHz and B = -0.66 MHz, and these values give Δ_{54} = 251.8 MHz, Δ_{43} = 202.0 MHz and Δ_{32} = 151.8 MHz, which are about 1.2 times larger than those in shown in Fig. III-1.

The selection rules of the electric dipole transitions are $\Delta F = 0, \pm 1$, which allow three transitions from each hyperfine level in the ground state as shown in Fig. III-1. The lifetime

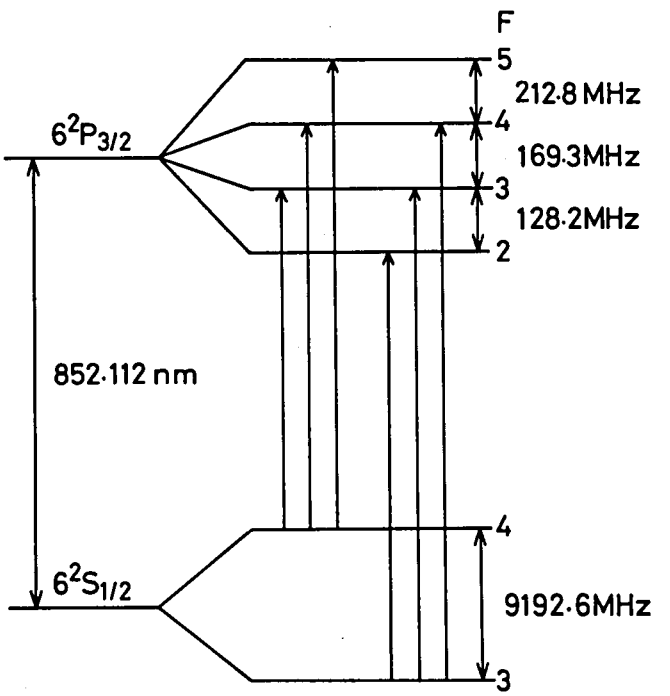

Fig. III-1 Energy diagram of Cs corresponding to the D_2 line and allowed transitions from the $6^2S_{1/2}$ state. The theoretical values of the frequency separation between the hyperfine levels in the $6^2P_{3/2}$ state are indicated. (The spacing between energy levels is not to scale.)

of the $6^2P_{3/2}$ state was measured by Link[108] to be 30.5 ns, which gives the natural homogeneous linewidth 2.6 MHz (HWHM) and the oscillator strength $f_{D2} = 0.732$. The oscillator strength is related to the dipole matrix element p_{ij} as[91),92)]

$$p_{ij}^2 = \frac{\hbar e^2 f_{D2} S_{ij}}{4\pi m_e \nu_{ij}} = 8.95\times10^{-35}\ S_{ij} \qquad (cm^2 esu^2), \quad \text{(III.3)}$$

where e is the electron charge, m_e is the electron mass, ω_{ij} and S_{ij} are the frequency and the relative weight of the transition[91] from the hyperfine level with F = j in the ground state to the hyperfine level with F = i in the $6^2P_{3/2}$ state. We normalize the values of S_{ij} so that the sum of S_{ij} over all tansitions from the ground state becomes unity. The theoretical values of S_{ij} are listed in Table III-1, and the relative magnitudes of the absorption lines from the hyperfine levels with F = 3 and 4 in the ground state are 7 and 9. The lifetime τ_i of each hyperfine level in the $6^2P_{3/2}$ state is related to the lifetime τ of the $6^2P_{3/2}$ state by

$$\frac{1}{\tau_i} = \frac{g}{\tau} \sum_j S_{ij}, \qquad \text{(III.4)}$$

where g = 4 is the number of the hyperfine levels in the excited state. We show in Tables III-2 and III-3 the values of the dipole matrix element p_{ij}, and the lifetime τ_i and the natural linewidth γ_{ij} of each absorption line calculated from the values of f_{D2} and S_{ij}, respectively.

S_{ij}

i \ j	4	3
5	0.344	0
4	0.164	0.117
3	0.055	0.164
2	0	0.156
sum	0.563	0.437

Table III-1 The relative weight S_{ij} of the transition from the hyperfine level $6^2S_{1/2}$ F = j to the hyperfine level $6^2P_{3/2}$ F = i of Cs.

p_{ij}^2

i \ j	4	3
5	3.08	0
4	1.46	1.04
3	0.50	1.46
2	0	1.40

$\times 10^{-35}$ (cm^2esu^2)

Table III-2 The dipole matrix element p_{ij} of Cs corresponding to the transition from $6^2S_{1/2}$ F = j to $6^2P_{3/2}$ F = i.

i	τ_i (ns)	γ_{ij} (MHz)
5	22.2	7.2
4	27.1	5.9
3	34.8	5.5
2	48.9	3.3

Table III-3 The lifetime τ_i of the hyperfine level with F = i in the $6^2P_{3/2}$ state of Cs, and the natural linewidth γ_{ij} (HWHM) of the absorption line corresponding to the transition from $6^2S_{1/2}$ F = j to $6^2P_{3/2}$ F = i.

ξ_{ij}

i \ j	4	3
5	0	0
4	0.416	0.584
3	0.749	0.251
2	0	0

Table III-4 The relaxation branching ratio ξ_{ij} of Cs excited from $6^2S_{1/2}$ F = j to $6^2P_{3/2}$ F = i.

Let us consider the absorption spectroscopy of the Cs-D_2 line by using a Cs cell with low vapor pressure, and by using a single-mode laser with a narrow spectrum. In such a case, atomic collisions are almost negligible, and the atomic absorption line is broadened by the thermal motion of atoms, whereas each Cs atom has a narrow natural linewidth. The Doppler-broadened linewidth is about 185 MHz (HWHM) at room temperature, which is much smaller than the hyperfine separation 9 GHz in the ground state, so that the absorption lines from F = 3 and 4 levels in the ground state can be observed separately. The hyperfine separations in the $6^2P_{3/2}$ state are smaller than the Doppler-broadened linewidth, so the three absorption lines from each of the hyperfine levels with F = 3 and 4 in the ground state are almost completely overlapping.

As is mentioned in Sec. III-1, the hyperfine pumping is caused between the levels with F = 3 and 4 in the ground state by a laser beam tuned to either of the absorption lines. Namely, atoms in one of the hyperfine levels in the ground state are selectively excited to the $6^2P_{3/2}$ state, and a part of the excited atoms quickly decay to the other hyperfine level in the ground state, if such decay branch agrees with the selection rule. Repeating above pumping cycles, the atoms are depopulated from one of the hyperfine levels in the ground state and repopulated to the other. The hyperfine pumping can strongly enhance the saturation of absorption and significantly increase the saturation parameter. According to the theoretical

calculations in Chap. II, the saturation parameter I_{sij} is given by

$$I_{sij} = \frac{E_0^2 p_{ij}^2}{2\hbar^2 \gamma_{ij}} 2\tau_i \left(1 + \frac{\xi_{ij} T}{2\tau_i} \right)$$

$$= 7.54 \times 10^{51} \, p_{ij}^2 \tau_i^2 \left(1 + \frac{\xi_{ij} T}{2\tau_i} \right) W, \qquad \text{(III.5)}$$

where T is the relaxation time between the hyperfine levels in the ground state, τ_i is the lifetime of the hyperfine level in the $6^2P_{3/2}$ state, W is the laser power density in W/cm^2, and ξ_{ij} is the ratio of relaxation branching from one to the other hyperfine levels in the ground state for the F = j to i excitation. In the case that, $\xi_{ij} \neq 0$, the second term in the bracket of Eq. (III.5) is dominant. We show, in Table III-4, the values of the relaxation-branching ratio ξ_{ij}, where we have assumed that no collisional transfer takes place between the hyperfine levels in the $6^2P_{3/2}$ state.

Here we give data on Cs for later use. The melting point of Cs metal is 28.8 °C. The vapor pressure p and the vapor density n of Cs atoms were measured by Rozwadowski et al.,[109] and the results give the experimental formula as

$$p, \, n = 10^{\left(A - B \log_{10} T - C/T \right)} \qquad (\text{torr}, \, \text{cm}^{-3}), \qquad \text{(III.6)}$$

where, at a temperature T °K below the melting point, (A,B,C) =

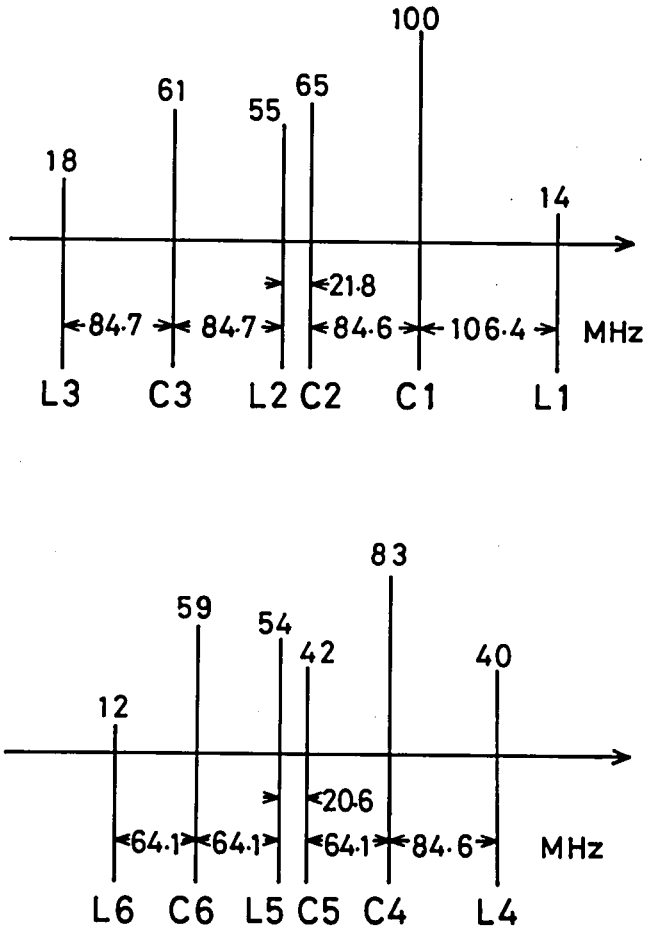

Fig. III-2 The positions of the Doppler-free saturated absorption spectra of the Cs-D_2 line calculated from the theoretical values of the hyperfine separations in the $6^2P_{3/2}$ state. The symbols L and C represent the Lamb dip and crossover resonance respectively. The relative magnitudes of the spectra are theoretically calculated under the condition shown in Table III-5.

(10.5460, 1.00, 4150) in the case of p, and (A,B,C) = (29.531, 2.00, 4150) in the case of n, and at the temperature above the melting point, (A,B,C) = (11.0531, 1.35, 4041) in the case of p, and (A,B,C) = (30.0379, 2.35, 4041) in the case of n. Typical values of p and n are about 3×10^{-7} torr and 1×10^{10} cm^{-3} at 10 °C, which is enough to observe the saturated absorption spectra by using a Cs cell with length of 1 cm.

III-2-2 Saturated Absorption Spectra of the Cs-D_2 Line

The three transitions are allowed from hyperfine level in the ground state of Cs, and the corresponding spectral components are overlapped to each other by the Doppler-broadening. Therefore, we can expect to observe six Doppler-free spectra on the Doppler-broadened absorption signal; three Lamb dips at the centers of the transition frequencies, and three crossover resonances at the arithmetic mean frequencies of pairs of the transitions.

The positions of the Doppler-free spectra are shown in Fig. III-2, which are calculated from the theoretical values of the hyperfine separations. The symbols L1, L2 and L3 represent the Lamb dips due to the transitions from the hyperfine level with F = 4 in the ground state to the hyperfine levels with F = 5, 4 and 3 in the $6^2P_{3/2}$ state, and C1, C2 and C3 represent the crossover resonances due to the pairs of the transitions to the hyperfine levels with F = 5 and 4, F = 5 and 3, and

	PUMP BEAM	I_s	PROBE BEAM	γ_D (MHz)	δ_D (%)	RELATIVE MAGNITUDE
L1	4→5	0.2	4→5	3.9	10	14
L2	4→4	31	4→4	17	83	55
L3	4→3	25	4→3	14	81	18
L4	3→4	31	3→4	17	83	40
L5	3→3	24	3→3	14	81	54
L6	3→2	0.5	3→2	1.2	19	12
C1	4→4 4→5	31 0.2	4→5 4→4	17 3.9	83 10	100
C2	4→3 4→5	25 0.2	4→5 4→3	14 3.9	81 10	65
C3	4→4 4→3	31 25	4→3 4→4	17 14	83 81	61
C4	3→4 3→3	31 24	3→3 3→4	17 14	83 81	83
C5	3→4 3→2	31 0.5	3→2 3→4	17 1.2	83 19	42
C6	3→3 3→2	24 0.5	3→2 3→3	14 1.2	81 19	59

Table III-5 The width γ_D and the relative magnitude of each saturated absorption spectrum of the Cs-D_2 line calculated in the case that the power density and diameter of the pump beam are 2 mW/cm^2 and 5 mm, and the Cs cell temperature is 10 °C. The symbols such as L1 and C1 represent the Lamb dip and the crossover resonance, respectively, which are shown in Fig. III-2.

F = 4 and 3 in the $6^2P_{3/2}$ state, respectively. The symbols L4, L5 and L6 represent the Lamb dips from the hyperfine level with F = 3 in the ground state to the hyperfine levels with F = 4, 3 and 2 in the $6^2P_{3/2}$ state, and C4, C5 and C6 represent the crossover resonances due to the pairs of transitions to the hyperfine levels with F = 4 and 3, F = 4 and 2, and F = 3 and 2 in the $6^2P_{3/2}$ state, respectively.

In Fig. III-2, we also show the relative magnitudes of the Doppler-free spectra expected from the theoretical calculation, in the case that the power density and diameter of the pump beam are 2 mW/cm^2 and 5 mm, and the Cs cell temperature is 10 °C. Because no hyperfine pumping takes place in the case of L1 and L6, these Doppler-free spectra are small. All of other Doppler-free spectra are associated with the transitions which cause the hyperfine pumping.

By using the saturation parameter I_{sij} defined in Eq. (III.5), the width of the saturated absorption spectrum γ_{Dijkl} (HWHM) are given from the results of Chap. II as

$$\gamma_{Dijkl} = (\gamma_{kl} + \sqrt{1+I_{sij}}\ \gamma_{ij})/2, \qquad \text{(III.7)}$$

where the pump beam excites atoms from F = j to i, and the probe beam is absorbed by F = l to k transition. The normalized depth of the Doppler-free spectrum δ_{Dij} is given as

$$\delta_{Dij} = \frac{I_{sij}}{\sqrt{1+I_{sij}}\,(1+\sqrt{1+I_{sij}})} \times 100 \quad (\%). \quad \text{(III.8)}$$

When the hyperfine relaxation by atomic collisions in the ground state is negligible, the relaxation time T between hyperfine levels in the ground state is mainly determined by transit time of atoms across the laser beam. In rough estimation, the transit time is given by

$$T \simeq \frac{d}{u}, \quad \text{(III.9)}$$

where d is the beam diameter, and u is the most probable velocity of atoms across the laser beam. At room temperature, u is about 200 m/s, and T is $\sim 10^{-5}$ s for the beam diameter of several 1 mm. The values of τ_i and ξ_{ij} in Eq. (III.5) are of the order of 10^{-8} s and 0.1, so that the saturation parameter is increased due to the hyperfine pumping by a factor

$$\frac{\xi T}{2\tau} \sim 100. \quad \text{(III.10)}$$

For instance, as shown in Fig. III-2, consider the case of laser beam with 5 mm diameter and 2 mW/cm^2 power density and of a Cs cell at 10 °C. In this case u is about 200 m/s and T is roughly 2.5×10^{-5} s, and the saturation parameter becomes about 31 for the F = 4 to 4 transition which give the normalized depth of Lamb dip about 83 %. We show in Table III-5 the calculated values of I_s

and δ_D. In this way, the Doppler-free spectra of Cs-D_2 line can be observed with good signal-to-noise ratio by using a weak laser beam with power less than 1 mW, and we can use a semiconductor laser in the saturated absorption spectroscopy of the Cs-D_2 line. It should be noted that the transit of atoms across the laser beam may not give the exponential decay as seen in ordinary relaxation. To calculate the line shape more precisely, one must consider carefully the transient phenomenon.[110),111)]

III-3 Temperature Stabilization of GaAlAs Laser

III-3-1 Property of GaAlAs Laser

The GaAlAs laser used was a double-heterostructure type operating on a single longitudinal mode at a room temperature with the maximum output power of 5 mW. Generally the oscillation frequency of a semiconductor laser shifts toward the high-frequency side repeating a continuous change and a mode hopping according to decrease of the injection current or to decrease of the diode temperature. Typical oscillation characteristic of a GaAlAs laser is shown in Fig. III-3. The oscillation wavelength was measured by using a monochromator, as changing the diode temperature. Similar characteristic can be observed by changing the injection current. The intervals between the mode hopping are not regular and vary for each laser diode individually. A more careful measurement shows that the oscillation wavelength

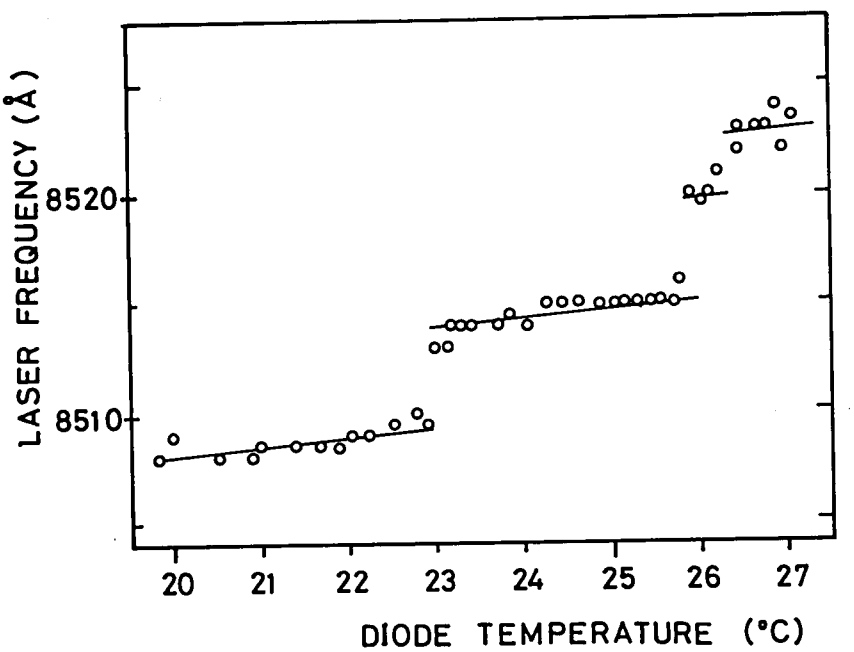

Fig. III-3 Typical oscillation characteristic of a GaAlAs laser measured by changing the diode temperature. Similar characteristic can be obtained by changing the injection current.

depends on the diode temperature and on the injection current with a good linearity in the continuously changing region. In the case of the GaAlAs laser used in this work, the rates of change in wavelength were measured to be 0.04 nm/°C and 0.02 nm/mA respectively in the continuously changing region. These values in frequency are about 20 GHz/°C and 8 GHz/mA at 852.1 nm respectively. The laser diode with the oscillation frequency close to Cs-D_2 line was selected among commercially available semiconductor lasers. The laser frequency could be tuned to the Cs-D_2 line when the injection current was around 43 mA at the diode temperature 30 °C. Since the continuously tunable region of the GaAlAs laser was more than 10 GHz, we can observe continuously, i. e. without mode hopping, the two absorption components of the Cs-D_2 line from the hyperfine levels with F = 3 and 4 in the ground state.

In order to observe an absorption spectrum in details, it is required to control the laser frequency with a stability better than the spectral separation or width of the absorption line. For the Cs-D_2 line, typical width of the Doppler-free spectrum is about 10 MHz. Especially in the frequency locking of GaAlAs laser to one of the Doppler-free spectra, it is very important to stabilize the diode temperature at least within 1×10^{-3} °C which gives about 20 MHz change of the laser frequency. We have tried to control and stabilize the diode temperature with stability better than 1×10^{-3} °C for a high resolution spectroscopy of the Cs-D_2 line and also as the first stage of the frequency

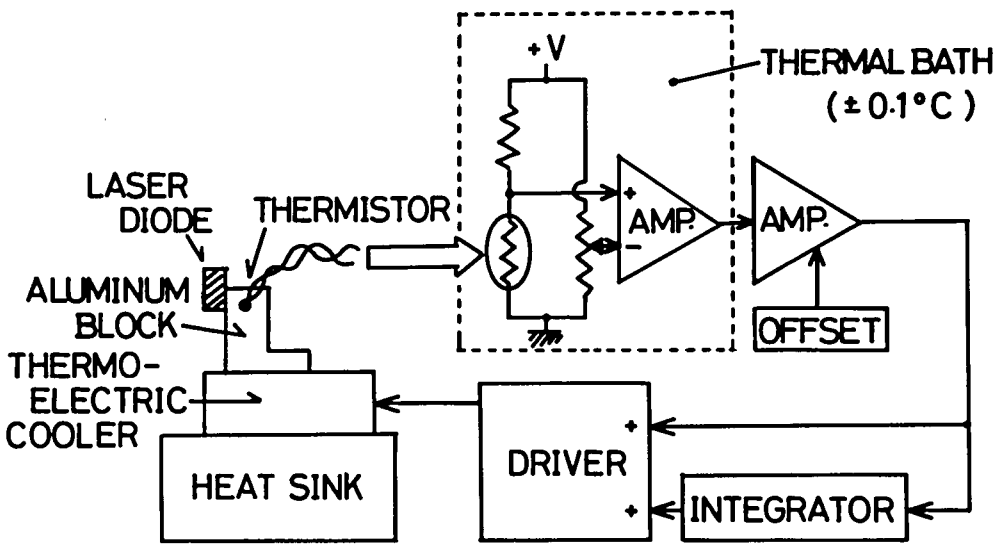

Fig. III-4 Schematic diagram of the system for the temperature stabilization of the semiconductor laser.

stabilization of the GaAlAs laser.

III-3-2 System of Temperature Stabilization

The temperature of the GaAlAs laser is stabilized by using the system shown in Fig. III-4. The laser diode is mounted tightly on a small aluminum block, whose temperature is controlled by a thermoelectric cooler (Peltier element) by which both heating and cooling are possible. The thermoelectric cooler used was a 3 cm square with the maximum thermal absorption of 20 W, which makes it possible to control the temprtature of laser diode within ± 20 °C from room temperature. The diode temperature is measured as a resistance change of a thermistor which is mounted on the aluminum block at the position close to the laser diode. The thermistor used was 0.8 mm in diameter and 5 mm in length with resistance 4 KΩ at 30 °C, and the B coefficient was about 3500 °K which relates the change of resistance R to that of temperature T as

$$\frac{\Delta R}{\Delta T} = - \frac{RB}{T^2}. \qquad \text{(III.11)}$$

In the case of the thermistor used, the resistance change was 4 % for 1 °C change at 30 °C, which is about 10 times larger than other metal sensor such as Pt and Ni. Because of its small size and high B coefficient, the thermistor is very sensitive of minute temperature fluctuation. To measure a small change of the

diode temperature, the thermistor is inserted into a bridge circuit where the resistance of the thermistor is compared with a reference resistance as shown in Fig. III-4. The bias voltage of the bridge circuit is supplied by a thermally compensated zener diode with zener voltage of 7 V. A relatively large series resistance of 30 KΩ is connected to the thermistor in order to limit self heating of the thermistor. The other side of the bridge circuit consists of a voltage divider with impedance 10 KΩ, which can be adjusted by 0.01 % step. Thus, the change of the diode temperature is converted to the output voltage of the bridge circuit. In order to stabilize the diode temperature, the output of the bridge circuit is amplified and fed back, through a lowpass filter with 3 Hz cutoff, to the current source of the thermoelectric cooler. To improve the long-term stability of the diode temperature, integrated output of the bridge circuit is fed back simultaneously with the proportional feedback. Small misadjustment of the bridge circuit can be compensated by an offset circuit, and we can easily stabilize the diode temperature at a desired value with stability better than 10^{-3} °C. Since the bridge circuit and the first stage amplifier of its output may easily be affected by a drift of room temperature, the components with low temperature-dependence are used in these circuits. The temperature coefficients of the series resistor and the voltage divider used are 25 ppm/°C and 10 ppm/°C, and the nominal value of the input-offset drift of the first-stage amplifier is 0.2 μV/°C. However, these values are not sufficiently small

because the bridge circuit must measure about 0.1 Ω change of the thermistor to measure the temperature fluctuation less than 10^{-3} °C, which corresponds to 20 μV output of the bridge circuit. In this system, 1 °C fluctuation of room temperature causes 150 and 70 μV uncertainity of the bridge output due to fluctuations of the series resistor and the voltage divider. To improve the problem, the bridge circuit and its first-stage amplifier are put into a 0.1 °C temperature-controlled thermal bath.

It should be noted that the change of the bridge output is regarded to be approximately proportional to that of the laser frequency, if the change of the diode temperature is small and slow enough. This makes it possible to observe the absorption spectra of the Cs-D_2 line by utilizing the output of the bridge circuit as a measure of frequency or wavelength. The frequency scale can be calibrated by utilizing the hyperfine separation in the ground state of Cs as the standard. Of course, it is better to use an external Fabry-Perot cavity as frequency marker. As to be shown in later, a frequency scanning of the GaAlAs laser with resolution better than 10 MHz is achieved by sweeping the diode temperature using above temperature-control system.

The semiconductor laser and the thermoelectric cooler are packed into an aluminum case in order to avoid external electrostatic noise, and an aluminum heat radiator is attached to its outside surface as a heat sink of the thermoelectric cooler. The current line of the laser diode comes into the aluminum case

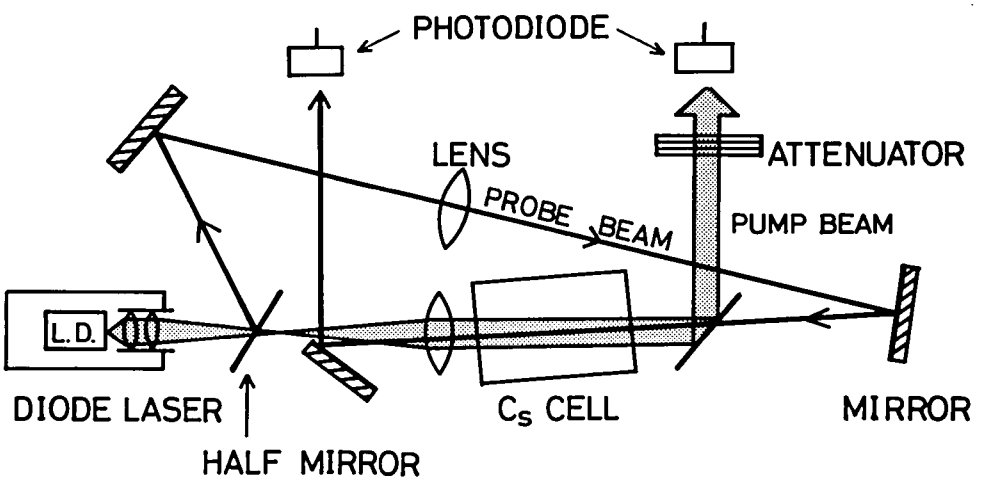

Fig. III-5 Experimental alignment of the optical system for the saturated absorption spectroscopy of Cs. The laser beam emitted is focused by a lens with focal length 18 mm, and split into the pump and probe beams by a half mirror. The Cs cell is used at a room temperature.

through a passive noise-filter at the entrance. The injection current is supplied by a voltage-regulated power source with residual noise of the order of 1 μA in the injection current. To avoid the destruction of the laser diode by a spike noise arised when the current source is turned on or off, a protection circuit is equipped, in which the injection current of under threshold is turned on and off when the power source operates stationary. A small alternative current can also be applied to the laser diode together with the direct current, by which the laser frequency is modulated directly. It is possible to observe the atomic absorption line on a CRT by scanning the injection current.

III-4 Observation of Doppler-Free Spectra of the Cs-D_2 Line

III-4-1 Experimental Setup for Saturated Absorption

An experimental setup for the saturated absorption spectroscopy is shown in Fig. III-5. The laser beam is focused by a lens with focal length 18 mm and split into two beams by a half mirror, one of which is used as a relatively intense pump beam and the other is used as a weak probe beam. The pump beam is collimated and applied into a Cs cell with a relatively large beam diameter in order to saturate the atomic absorption in a large region of the cell. The probe beam with a relatively small diameter is applied into the cell from the opposite direction to the pump beam. The pump beam and the probe beam form a small

misalignment angle in order to avoid the laser beam returning back to the laser diode. The two laser beams overlap to each other within the cell, i. e. the probe beam is completely contained by the pump beam within the cell. Since laser beam is invisible, the beam path is found out by using an IR-phospher which emits visible light as infrared light is irradiated. After transmitted through the cell, both beams are reflected by mirrors and detected by silicon photodiodes.

When the laser frequency is swept through the Cs-D_2 line by sweeping the injection current or the diode temperature, narrow Doppler-free spectra are expected to be observed on the Doppler-broadened background in the absorption signal of the probe beam. On the other hand, an intensity change of the relatively strong pump beam shows mainly the Doppler-broadened background, which can be used to reduce the Doppler-broadened background in the signal of the probe beam. It should be noted that one must be careful to avoid the laser beam returning back to the laser diode, which causes an instability of the laser oscillation and sometimes spoils the laser diode.[112),113)]

The Cs cell used in this experiment is cylindrical, which is made of Pyrex glass with 3 cm inner diameter and length 5 cm. The cell was evacuated and enclosed distilled Cs metal after sufficient cleaning of the cell by baking. The cell contains no buffer gas. The vapor pressure and density of the Cs atoms are 3.0×10^{-7} torr and 1.0×10^{-3} cm^{-3} at 11 °C, at which the following experiments were carried out. The length of the Cs cell is 5 cm,

which is more than enough when the cell is used at room temperature. This cell is optically so thick at temperature above 25 °C that the absorption line is distorted as the light is propagated through the cell. The length of 1 cm is thought to be sufficient to observe the saturated absorption spectra.

In order to avoid a mechanical vibration and acoustic noise, all optical components are fastened by using magnetic basements on an iron surface plate of 30×40 cm^2 in size, which is isolated from the laboratory floor by using air cushons.

III-4-2 Doppler-Broadened Absorption Spectrum of the Cs-D_2 Line

In order to tune the laser frequency to the Cs-D_2 line, we have to at first measure the oscillation characteristic of the GaAlAs laser, which is largely dependent on the changes of the injection current and the diode temperature, as mentioned already. Rather wide frequency range can be put into a continuously changing region by choosing an adequate combination of the injection current and the diode temperature, however some frequency range still remain within a gap of mode hopping. Rough tuning of the laser frequency to the Cs-D_2 line is obtained by monitoring it with a monochromator, to which the light from a Cs lamp is also applied as a frequency reference. Since the spectral width of the Cs-D_2 line is of the order of 0.001 nm, a precise tuning is carried out by observing directly the light absorption of the Cs cell. The laser frequency is modulated with

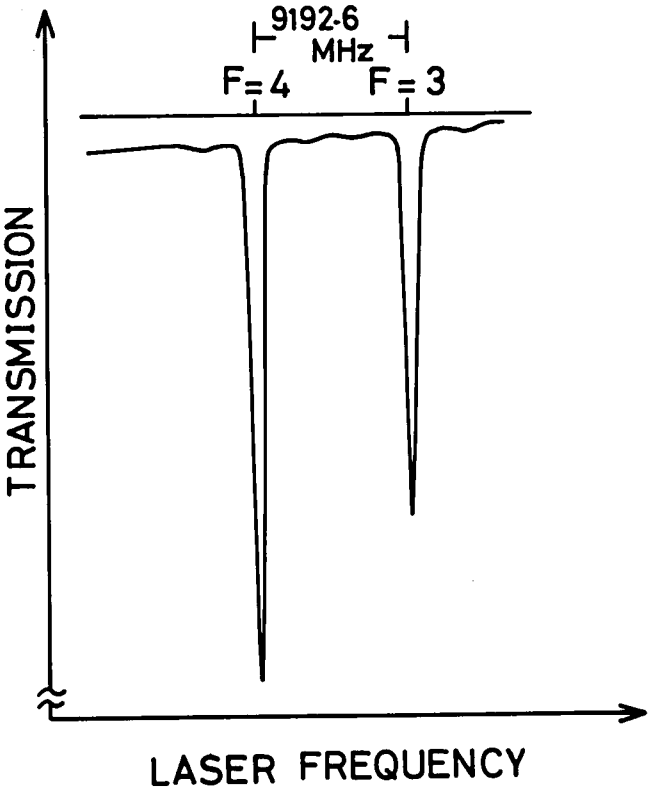

Fig. III-6 Typical Doppler-broadened absorption spectra of the Cs-D_2 line at 852.1 nm obtained when the laser frequency was swept by varying the diode temperature. The three absorption lines from each one of hyperfine levels with F = 4 and 3 in the ground state are overlapping to each other due to Doppler-broadening.

a few GHz by modulating the injection current, and an absorption signal of the laser beam is observed on a CRT. A Doppler-broadened absorption spectrum of the Cs-D_2 line can be observed on the CRT by sweeping either the injection current or the diode temperature.

One of the observed Doppler-broadened absorption spectrum of the Cs-D_2 line is shown in Fig. III-6, as an intensity change of the transmitted laser beam as a function of the change of the diode temperature measured by the system described in Sec. III-3. We can see in Fig. III-6 two Doppler-broadened absorption lines from the hyperfine levels with F = 3 and 4 in the ground state, whose frequency separation is known to be 9192.6 MHz. The power of the laser beam was about 400 μW, and the Cs cell was cooled by ice at 0 °C (Corresponding vapor pressure is 8×10^{-8} torr.). A slight increase of the laser output can be seen when the diode temperature is decreased.

In Fig. III-6, small absorption signals can be seen beside the main absorption signals, which are considered to be due to the spectral characteristics of the GaAlAs laser. Similar absorption signal could also be observed when the laser frequency was swept by varying the injection current. In this case the laser output was increased slightly with the increase of the injection current.

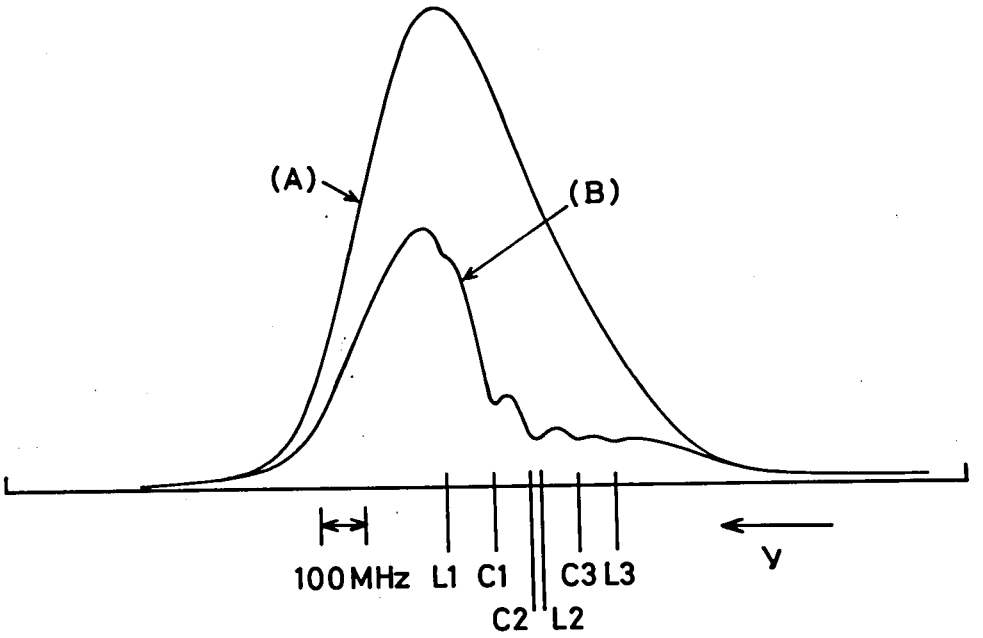

Fig. III-7 Typical absorption signal of the probe beam obtained when the laser frequency ν was swept through the absorption line from the hyperfine level with F = 4 in the ground state of Cs, in two cases that (A) the pump beam was not applied and (B) the pump beam was applied. The positions of the Doppler-free spectra indicated are estimated from the theoretical calculation (see Fig. III-2).

III-4-3 Observed Doppler-Free Spectra of the Cs-D_2 Line

The Doppler-free spectra of the Cs-D_2 line were observed. Figure III-7 shows a typical absorption signal of the probe beam which was obtained when the laser frequency ν was swept, by varying the diode temperature, through the absorption line from the hyperfine level with F = 4 in the ground state. In Fig. III-7, the horizontal axis actually shows the output voltage of the bridge circuit, which is approximately proportional to the change of the diode temperature. The change of the diode temperature can be regarded to be proportional to that of the laser frequency because the change was slow and small, less than 0.1 °C.

In Fig. III-7, the curve A shows the absorption signal of the probe beam observed when the pump beam was not applied, the curve B shows the signal observed when the pump beam was applied. In the curve A, we see a Doppler-broadened absorption spectrum, which is asymmetrical because of the overlap of three hyperfine components with different intensities. Small but sharp Doppler-free spectra can be seen on the Doppler-broadened background in the curve B. In Fig. III-7, five Doppler-free dips are clearly observed. The spectral widths of the observed Doppler-free spectra are about 20 $\sim$ 30 MHz (HWHM). These are much larger than the natural linewidth 2.6 MHz (HWHM) of the D_2 line, because of the spectral broadenings due to the power broadening, misalignment of laser beams and spectral width of the laser light. These absorption signals were obtained by recording on a chart the amplified and inverted output of the photodiode

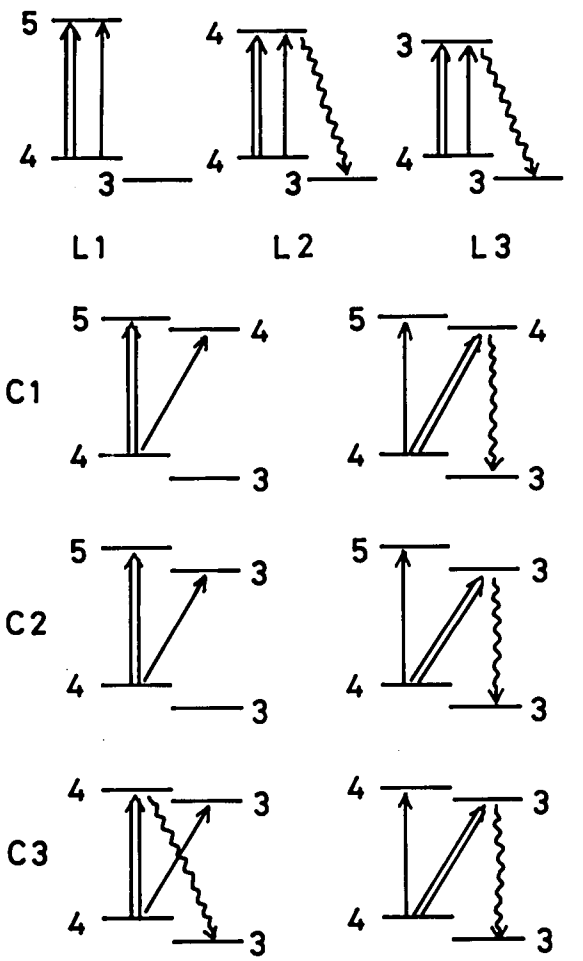

Fig. III-8 The transitions corresponding to the Doppler-free spectra shown in Fig. III-7. Each hyperfine level is identified by the quantum number F.

detecting the probe beam after transmitted through the Cs cell. The Doppler-free spectra with very high signal-to-noise ratio could be obtained in only one scan, without any data processing. The spectra indicated by symbols L1, L2 and L3 are Lamb dips due to the transitions to the hyperfine levels with F = 5, 4 and 3 in the $6^2P_{3/2}$ state, and those indicated by symbols C1, C2 and C3 are the crossover resonances between these Lamb dips, which have been discussed in details in Sec. III-2. In Fig. III-7, the frequency scale was determined by fitting the separation between dips of C1 and L3 to the theoretical value (275.8 MHz). The indicated positions of the Doppler-free spectra L1, L2, C2 and C3 indicated in Fig. III-7 were determined by the theoretical values of the hyperfine separations in $6^2P_{3/2}$ state. One can see in Fig. III-7, the relative positions of the Doppler-free spectra are in good agreement with these expected theoretically.

The transitions corresponding to each Doppler-free spectrum are shown in Fig. III-8, in which the excitation by the pump beam is indicated by ⇗ , that of the probe beam is indicated by ↗ , and the relaxation which causes hyperfine pumping is indicated by ∿ . As mentioned in Sec. III-2, the hyperfine pumping enhances strongly the saturation of absorption. Comparing Figs. III-7 and III-8, one may see that the Doppler-free spectra associated with the hyperfine pumping are strong.

In this experiment, the powers of the pump and probe beams were 910 μW and 20 μW, and the beam diameters at the cell were about 7 mm and 1 mm, respectively, and hence the power densities

	PUMP BEAM		PROBE BEAM
$^2P_{3/2}$	I_s	LINE BROADENING (MHz)	I_s
F=5	0.2	7.2 + 0.3	0.03
4	50	5.9 + 20	7
3	40	5.5 + 10	5

	PUMP BEAM	PROBE BEAM	γ_D (MHz)	δ_D (%)	RELATIVE MAGNITUDE
L1	4→5	4→5	7.2 + 0.3	9	10
L2	4→4	4→4	5.9 + 20	90	60
L3	4→3	4→3	5.5 + 10	80	20
C1	4→4 4→5	4→5 4→4	5.9 + 20 7.2 + 0.3	90 9	100
C2	4→3 4→5	4→5 4→3	5.5 + 10 7.2 + 0.3	80 9	60
C3	4→4 4→3	4→3 4→4	5.9 + 20 5.5 + 10	90 80	60

Table III-6 The values of the saturation parameter I_s for the pump and probe beams, and the width and relative magnitude of each saturated absorption spectrum of the Cs-D_2 line theoretically calculated in the case that the signal shown in Fig. III-7 was obtained.

of both beams were about 2 mW/cm^2. The misalignment angle between the pump and probe beams was at least 2×10^{-2} rad. The Cs cell was used at room temperature 11 °C, at which the vapor pressure and density of Cs atom are 3.0×10^{-7} torr and 1.0×10^{10} cm^{-3}, respectively. The Doppler-broadened width of the D_2 absorption line is about 185 MHz (HWHM) at 11 °C. In Fig. III-7, we can see in the curve B that the Doppler-broadened background was also reduced by the pump beam. This was due to the fact that the fluorescence induced by the pump beam was also detected by the photodiode to detect the intensity of the transmitted probe beam.

In the present experiment, the most probable velocity of atom is about 200 m/s, and the transit time across the pump beam is roughly estimated to be about 4×10^{-5} s, so that the saturation parameters can be calculated from Eq. (III.6) to be $I_s\sim 50$ for the F = 4 to 4 transition, and $I_s\sim 40$ for the F = 4 to 3 transition, which give the power-broadened linewidths about 20 and 15 MHz (HWHM) respectively. On the other hand, the transit time across the probe beam is about 5×10^{-6} s, and $I_s\sim 7$ for the F = 4 to 4 transition and, $I_s\sim 4$ for the F = 4 to 3 transition, which are relatively small in comparison with I_s in the case of the pump beam. Using these values of I_s, one may find that the power-broadened linewidths of the Doppler-free spectra L2, L3, C1, C2, and C3 are within the range between 10 and 30 MHz (HWHM). These values are larger than the natural linewidth 2.6 MHz (HWHM) of the D_2 line by a factor about 10. The

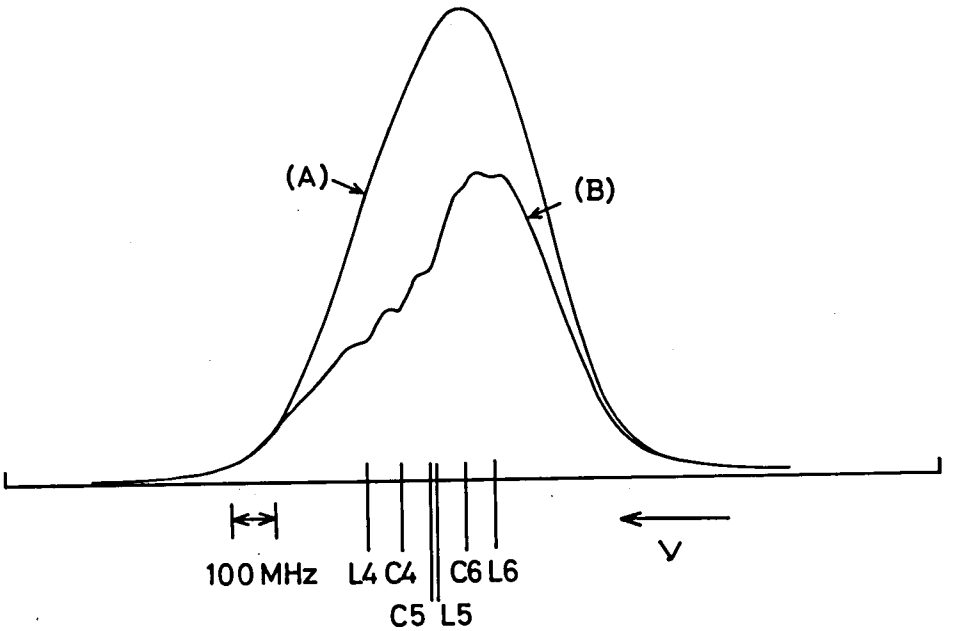

Fig. III-9 Typical absorption signal of the probe beam obtained when the laser frequency ν was swept through the absorption line from the hyperfine level with F = 3 in the ground state of Cs, in two cases that (A) the pump beam was not applied and (B) the pump beam was applied. The positions of the Doppler-free spectra indicated are estimated from the theoretical calculation (see Fig. III-2).

normalized depths of these Doppler-free signals are in the range between 80 and 90 %. We have assumed in above calculations that the saturation broadening due to the probe beam is negligibly small. In the case of L1, no hyperfine pumping occurs because F = 5 to 3 relaxation branch is forbidden, and the saturation parameter I_s is about 0.2 for the pump beam, which gives the linewidth and depth of L1 about 8 MHz (HWHM) and 10 % respectively. These results of the theoretical calculation are listed in Table III-6. Additional line broadenings to be considered are those due to the misalignment between the pump and probe beams, which give a line broadening with Gaussian shape, and due to the spectral width of the GaAlAs laser, which are estimated to be about 5 MHz and 10 MHz (HWHM) respectively. Owing to these line broadenings, the Doppler-free spectra L2 and C2, whose frequency separation is 21 MHz, could not be well resolved as seen in Fig. III-7.

Similar Doppler-free spectra could be observed for the absorption line from the hyperfine level with F = 3 in the ground state. A typical absorption signal of the probe beam is shown in Fig. III-9, in the case that the power of the pump beam was about 220 μW. In Fig. III-9, L4, L5 and L6 represent Lamb dips due to the transitions to the hyperfine levels with F = 4, 3 and 2 in the $6^2P_{3/2}$ state. The spectra indicated by symbols C4, C5 and C6 are the crossover resonances. The frequency scale shown in Fig. III-9 was determined by fitting the separation between dips of C4 and L6 to the theoretical value (212.9 MHz). The

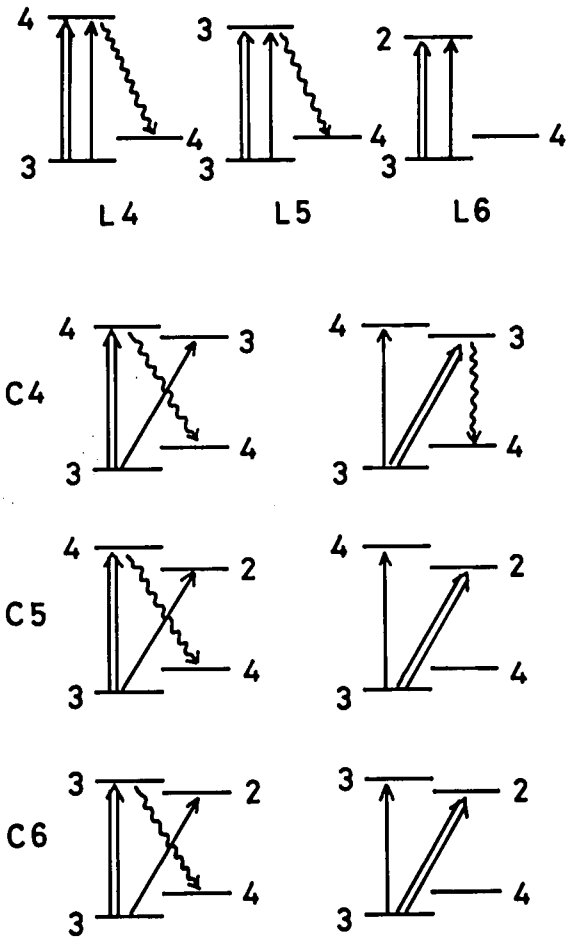

Fig. III-10 The transitions corresponding to the Doppler-free spectra shown in Fig. III-9. Each hyperfine level is identified by the quantum number F.

	PUMP BEAM		PROBE BEAM
$^2P_{3/2}$	I_s	LINE BROADENING (MHz)	I_s
F=4	20	5.9 + 10	3
3	10	5.5 + 6	2
2	0.2	3.3 + 0.2	0.04

	PUMP BEAM	PROBE BEAM	γ_D (MHz)	δ_D (%)	RELATIVE MAGNITUDE
L4	3→4	3→4	5.9 + 10	80	50
L5	3→3	3→3	5.5 + 6	70	60
L6	3→2	3→2	3.3 + 0.2	9	7
C4	3→4 3→3	3→3 3→4	5.9 + 10 5.5 + 6	80 70	100
C5	3→4 3→2	3→2 3→4	5.9 + 10 3.3 + 0.2	80 9	50
C6	3→3 3→2	3→2 3→3	5.5 + 6 3.3 + 0.2	70 9	60

Table III-7 The values of the saturation parameter I_s for the pump and probe beams, and the width and relative magnitude of each saturated absorption spectrum of the Cs-D_2 line theoretically calculated in the case that the signal shown in Fig. III-9 was obtained.

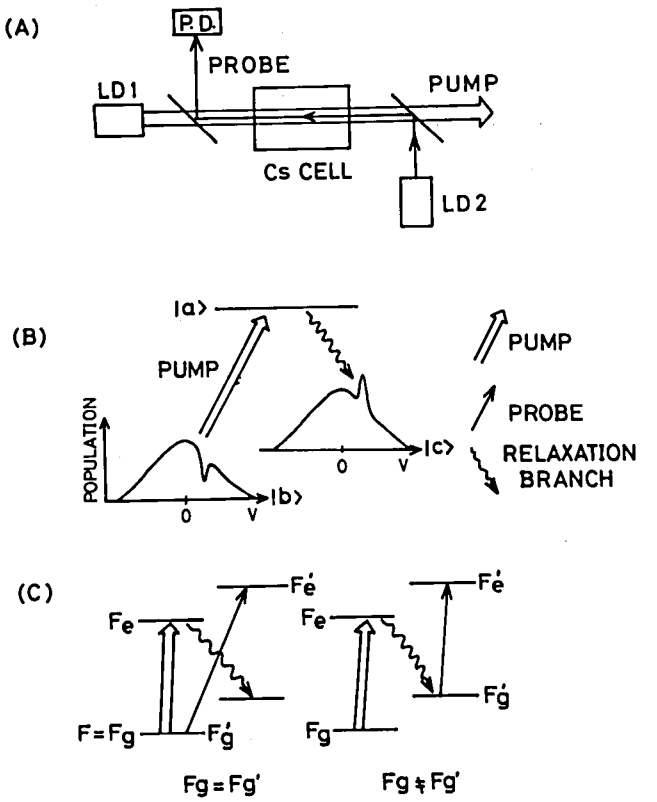

Fig. III-11 Experimental scheme of the velocity-selective hyperfine pumping (A). The pump and probe frequencies are tuned to ω_1 and ω_2 respectively. The pump beam burns a hole and produces a swell in the velocity distribution of atoms in the ground state, and the probe beam monitors the velocity distribution (B). Combinations of the pump excitation and the probe detection (C).

positions of the Doppler-free spectra L4, L5, C5 and C6 indicated in Fig. III-9 were determined by the theoretical values of the hyperfine separations. One can see in Fig. III-9, the relative positions of the Doppler-free spectra are in good agreement with these expected theoretically. The transitions corresponding to the Doppler-free spectra are shown in Fig. III-10. The estimated values of the saturation parameters and the line broadenings are listed in Table III-7. Owing to the line broadenings mentioned already, the Doppler-free spectra L5 and C5, whose frequency separation is 20.6 MHz, could not be well resolved.

III-5 Experimental Evidence of Hyperfine Pumping

III-5-1 Experimental Setup of Velocity-Selective Hyperfine Pumping

An experimental test has been performed to show the velocity-selective hyperfine pumping[55] in the ground state of Cs, in which we have monitored the velocity distribution of atoms in both of the hyperfine levels in the ground state, using two GaAlAs lasers. A scheme of the experiment is shown in Fig. III-11, where a relatively intense laser beam tuned to the frequency ω_1 is applied into the Cs cell as a pump beam, and a weak laser beam tuned to ω_2 is applied as a probe beam from opposite direction to the pump beam.

For a simple discussion, consider a three-level system with

an excited level $|a\rangle$ and two ground level $|b\rangle$ and $|c\rangle$, and suppose the pump frequency ω_1 is tuned to $|b\rangle \rightarrow |a\rangle$ absorption line. The pump beam causes the velocity-selective hyperfine pumping and burns a hole in the velocity distribution of atoms in the ground level $|b\rangle$ as shown in Fig. III-11. When the vapor pressure of atoms is low enough, the velocity-changing collision of atoms is negligible. As the result, the atoms are pumped conserving their velocity, so that a narrow swell is produced in the velocity distribution of atoms in ground level $|c\rangle$. When the probe frequency ω_2 is swept through the $|b\rangle \rightarrow |a\rangle$ absorption line, a narrow decrease of absorption due to the hole burning appears on the Doppler-broadened signal of the probe beam. On the other hand, when the probe frequency is swept through the $|c\rangle \rightarrow |a\rangle$ absorption line, where the swell in the velocity distribution is produced, a narrow peak appears in the Doppler-broadened signal of the probe beam.

Let us assume that no population difference exists between ground levels $|b\rangle$ and $|c\rangle$ in the thermal equilibrium. Let us write the transition frequencies as ω_{ab} and ω_{ac}. When the probe frequency is swept through the $|c\rangle \rightarrow |a\rangle$ absorption line, where the swell is produced in the velocity distribution, the absorption signal of the probe beam is described in terms of the absorption coefficient α_{pc} as

$$\alpha_{pc} = \frac{-1}{\sqrt{\pi}u} \int_{-\infty}^{\infty} \frac{\alpha_{0ac}}{\pi\gamma_{ac}} e^{-(\frac{v}{u})^2} \frac{\gamma_{ac}^2}{(\omega_{ac}-kv-\omega_2)^2+\gamma_{ac}^2}$$
$$\times\{ 1+ \frac{I_s}{B^2} \frac{B^2\gamma_{ab}^2}{(\omega_{ab}+kv-\omega_1)^2+B^2\gamma_{ab}^2} \}dv, \quad \text{(III.12)}$$

where $B = \sqrt{1+I_s}$, and α_{0ac} represents the linear absorption coefficient for the $|c\rangle \rightarrow |a\rangle$ transition. By the similar method used for the crossover resonances in Sec. II-4-2, the second term of α_{pc} can be calculated as

$$\alpha_{pc2} = \frac{\alpha_{0ac}}{\pi ku} \frac{I_s}{B} \mathrm{Im}\{ Z(\frac{\Delta_{2c}+i\gamma_{ac}}{ku}) \frac{B^2\gamma_{ab}^2}{(\gamma_{ac}-2i\Delta_{mc})^2-B^2\gamma_{ab}^2}$$
$$+ Z(\frac{\Delta_{1b}+iB\gamma_{ab}}{ku}) \frac{\gamma_{ac}^2}{(B\gamma_{ab}-2i\Delta_{mc})^2-\gamma_{ac}^2} \}, \quad \text{(III.13)}$$

where

$$\Delta_{1b} = \omega_{ab} - \omega_1, \qquad \Delta_{2c} = \omega_{ac} - \omega_2, \qquad \omega_m = (\omega_1 - \omega_2)/2, \qquad \Delta_{mc} = \omega_c - \omega_m, \qquad \omega_c = (\omega_{ab} - \omega_{ac})/2. \quad \text{(III.14)}$$

In the Doppler-limit, this can be approximated by

$$\alpha_{pc2} = - \frac{\alpha_{0ac}}{\sqrt{\pi}ku} e^{-(\frac{\omega_{bc}-\omega_{12}}{2ku})^2} \frac{I_s}{B(\gamma_{ac}+B\gamma_{bc})}$$
$$\times [\frac{\{(\gamma_{bc}+B\gamma_{ab})/2\}^2}{(\omega_c-\omega_m)^2+\{(\gamma_{bc}+B\gamma_{ab})/2\}^2}], \quad \text{(III.15)}$$

where

$$\omega_{12} = \omega_1 - \omega_2 ,$$

$$\omega_{bc} = \omega_{ab} - \omega_{ac} . \qquad \text{(III.16)}$$

On the other hand, when the probe frequency ω_2 is swept through the absorption line where the hole burning is produced, the absorption coefficient α_{pb2} is presented as a similar form as Eq. (III.15) by replacing subscripts c with b, and by changing the sign of the right-hand side. From above analysis, we see that the narrow dips and peaks can be observed in the absorption signal of the probe beam respectively when one of the following conditions is satisfied.

$$\omega_{ab} = \omega_m \quad ; \quad \omega_{ab} - \omega_1 = \omega_2 - \omega_{ab} , \qquad \text{(III.17)}$$

$$\omega_c = \omega_m \quad ; \quad \omega_{ab} - \omega_1 = \omega_2 - \omega_{bc} . \qquad \text{(III.18)}$$

These show that the probe and pump beams simultaneously interact with atoms in the same velocity group.

In the case of the Cs-D_2 line, three transitions are allowed from each of the hyperfine levels with F = 3 and 4 in the ground state. Two of the transitions to F = 3 and 4 levels in the $6^2P_{3/2}$ state cause the hyperfine pumping. So, two holes are burned by the hyperfine pumping in the velocity distribution of atoms in either ground level, from which the pump beam excites atoms. The atoms are pumped to nonabsorbing ground level conserving their velocity, and two swells are produced in the velocity distribution of atoms in the nonabsorbing level. The

pump beam detects one of the holes and swells by three transitions. When the probe frequency ω_2 is swept through either absorption line from F = 3 or 4 level in the ground state, two holes or swells manifest themselves as six narrow dips or peaks of absorption in the signal of the probe beam. Two of dips or peaks overlap to each other.

To show the resonance conditions, let us indicate the signal of the hyperfine pumping as $(F_g F_e F'_g F'_e)$, which represents the signal appeared when the pump beam burns a hole by $F = F_g \rightarrow F_e$ transition, and the probe beam detects the hole or swell by $F = F'_g \rightarrow F'_e$ transition. A narrow dip or peak of absorption in the signal of the probe beam appears respectively when $F_g = F'_g$ or $F_g \neq F'_g$. When the pump frequency ω_1 is tuned to the absorption line from F = 4 level in the ground state, a narrow dips are observed at

$$(\omega_1-\omega_{34}) = \begin{pmatrix} 0 & (4343) \\ 169.3 & (4344)+(4443) \\ 338.6 & (4444) \\ 382.1 & (4345) \\ 551.4 & (4445) \end{pmatrix} - (\omega_2-\omega_{34}) \quad \text{in MHz}, \qquad \text{(III.19)}$$

and narrow peaks are observed at

$$(\omega_1-\omega_{34}) = \begin{pmatrix} -128.2 & (4332) \\ 0 & (4333) \\ 41.1 & (4432) \\ 169.3 & (4334)+(4433) \\ 338.6 & (4434) \end{pmatrix} - (\omega_2-\omega_{34}) + 9192.6 \quad \text{in MHz}. \qquad \text{(III.20)}$$

When the pump frequency ω_1 is tuned to the absorption line from F = 3 level in the ground state, narrow dips are observed at

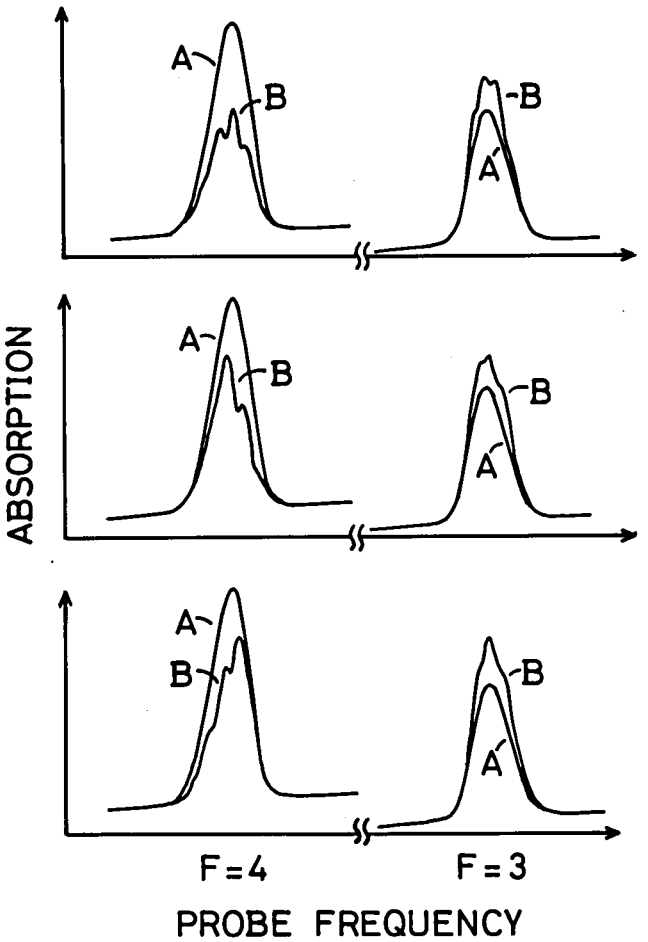

Fig. III-12 Typical absorption signal of the probe beam obtained when the pump frequency was tuned to three typical frequencies within the absorption line from the hyperfine level with F = 4 in the ground state, and the probe frequency was swept through both absorption lines from the ground state, in two cases that A the pump beam was not applied and B the pump beam was applied.

$$(\omega_1-\omega_{33}) = \begin{pmatrix} -128.2 & (3332) \\ 0 & (3333) \\ 41.1 & (3432) \\ 169.3 & (3334)+(3433) \\ 338.6 & (3434) \end{pmatrix} - (\omega_2-\omega_{33}) \quad \text{in MHz}, \qquad \text{(III.21)}$$

and narrow peaks are observed at

$$(\omega_1-\omega_{33}) = \begin{pmatrix} 0 & (3343) \\ 169.3 & (3344)+(3443) \\ 338.6 & (3444) \\ 382.1 & (3345) \\ 551.4 & (3445) \end{pmatrix} - (\omega_2-\omega_{33}) + 9192.6 \quad \text{in MHz}. \qquad \text{(III.22)}$$

These conditions are also satisfied when the pump frequency ω_1 is swept and the probe frequency ω_2 is fixed. These narrow peaks and dips in the probe absorption are free from Doppler-broadening.

III-5-2 Experiment of Velocity-Selective Hyperfine Pumping

We have observed absorption signals of the probe beam showing the velocity-selective hyperfine pumping. Three typical absorption signals of the probe beam are shown in Fig. III-12, which were obtained when the pump frequency was fixed by using the temperature control at three typical frequencies within the absorption line from the hyperfine level with F = 4 in the ground state, and the probe frequency was swept, by varying the injection current, through both absorption lines from F = 3 and 4 in the ground state. The curve A shows the signal of the probe beam obtained when the pump beam was not applied, in which we see

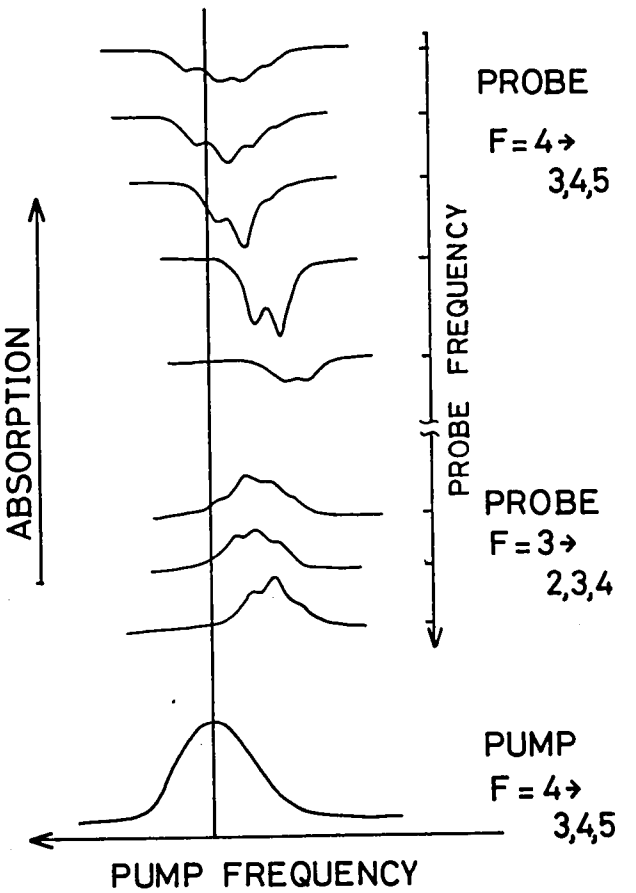

Fig. III-13 Typical absorption signal of the probe beam obtained when the pump frequency was swept through the absorption line from the hyperfine level with F = 4 in the ground state, and the probe frequency was tuned to typical frequencies within both absorption lines from the ground state.

Doppler-broadened absorption spectrum, and the curve B shows the signal obtained when the pump beam was applied. We can see, in the curve B, some narrow dips and peaks on the Doppler-broadened absorption signals from F = 4 and F = 3 levels in the ground state respectively. These results show the evidence that the pump beam burns holes in the velocity distribution of F = 4 hyperfine level in the ground state, and produces swells in the velocity distribution of the F = 3 level, conserving the total population.

In this experiment, the powers and the diameters of the pump and probe beams were about 400 μW and 10 mm and 20 μW and 1 mm respectively. The Cs cell was cooled down to 0 °C, at which the Cs vapor pressure is $\sim 8\times10^{-8}$ torr. The saturation parameters in this case are $I_s \sim$ 20 and 10 for the F = 4 to 4 and 4 to 3 transitions respectively. Because the misalignment angle of the pump and probe beams was relatively large, the observed spectra were broadened and not resolved well.

III-5-3 Doppler-Free Spectra on the Flat Background

In contrast with the previous experiment, it is very interesting to observe the absorption signal of the probe beam when the probe frequency is fixed and the pump frquency is swept. In this case, narrow Doppler-free spectra due to the velocity-selective optical pumping can be observed with no Doppler-broadened background.

Figure III-13 shows the observed absorption signal of the probe beam versus the frequency of the pump beam, which was swept through the absorption line from F = 4 in the ground state by varying the injection current. The probe frequency, which was stabilized by the temperature control, was changed discretely through both absorption lines from F = 3 and 4 levels in the ground state. In this experiment, the absorption signal of the pump beam was simultaneously observed, by which the positions of the probe signals were determined. In Fig. III-13, some narrow dips and peaks can be seen on the flat background in the signal of the probe beam. These dips are due to the hole burning of the pump beam, each of which the probe beam detects by three transitions. The peaks are due to the swells produced by the hyperfine pumping in the velocity distribution of atoms in F = 3 level in the ground state. Because these peaks are as sharp as the dips, we can say with no doubt that the atoms are pumped from F = 4 to F = 3 levels in the ground state, conserving their velocity. These peaks and dips shift toward the lower frequency side when the probe frequency is increased. This agrees with the resonance conditions for ω_1 and ω_2 in Eqs. (III.19) and (III.20). The conditions of the Cs cell and laser beams were the same as those in Sec. III-5-2.

It should be noted that we could obtain completely Doppler-free resonances in this experiment, although these signals were broadened due to power broadening and a relatively large misalignment between pump and probe beams. A more careful

experiment may show more clear spectra of the velocity-selective hyperfine pumping, which can be applied, for instance, to determine the hyperfine separation. By other method, it is not easy to reduce the Doppler-broadened background of the Cs-D_2 line completely, because the Doppler width is not much larger than the homogeneous width owing to relatively heavy mass of Cs. Such completely Doppler-free signals can be obtained by using two single-mode and frequency-tunable lasers, however, an experiment becomes rather complicated if two dye lasers or other tunable lasers are used. This experiment shows a high potentiality of the semiconductor lasers in the applications to the laser spectroscopy. These narrow signals of the velocity-selective hyperfine pumping can also be used as a frequency reference in a frequency-offset locking of a GaAlAs laser to another stabilized GaAlAs laser.

III-6 Conclusion and Discussions

We could observe narrow Doppler-free spectra of the Cs-D_2 line by means of the saturated absorption spectroscopy. For each absorption line from one of the hyperfine levels with F = 3 and 4 in the ground state, two Lamb dips and two crossover resonances were observed clearly separated and the other Lamb dip and crossover resonance overlap to above signals. The spectral widths of the observed Doppler-free spectra were about 20 $\sim$ 30 MHz (HWHM) which were much broader than the natural

linewidth 2.6 MHz (HWHM) of the D_2 line. This was due to the power broadening, misalignment of laser beams and the spectral width of the laser. The power of the pump beam was 910 μW. Even for such relatively weak laser power, strong saturation of absorption was observed because of the presence of the hyperfine pumping.

We have constructed the system of the temperature stabilization of the laser diode, and shown that the laser frequency is precisely tunable to one of the narrow Doppler-free spectra by varying the injection current or the diode temperature. We could observe the saturated absorption spectra of the Cs-D_2 line by sweeping the diode temperature. The output valtage of the temperature-measurement circuit could be used as the frequency scale. The relative positions of the observed Doppler-free spectra were in good agreement with the theoretical spacing between Doppler-free spectra. This may indicate that the temperature-stabilized semiconductor laser can be a powerful tool for the high resolution laser spectroscopy, because the diode temperature can be locked to desired value, and the temperature stabilization never sacrifice the high frequency-tunability of the semiconductor laser.

We have also shown an experimental evidence of the velocity-selective hyperfine pumping in the ground state of Cs, in which we have monitored the velocity distribution of atoms in both hyperfine levels in the ground state, by using two GaAlAs lasers. In this experiment, we could observe the Doppler-free

spectra completely free from Doppler-broadened background. For its easy operation on a single-mode and high frequency-tunability, new types of the high-resolution laser spectroscopy may be possible if one use a combination of two or more semiconductor lasers.

CHAPTER IV

FREQUENCY STABILIZATION OF GaAlAs LASER

IV-1 Introduction

The Doppler-free atomic or molecular absorption spectrum is the most convenient frequency reference in the frequency stabilization of lasers. In Chapter III, we have obtained the Doppler-free saturated absorption spectra of the Cs-D_2 line by using the GaAlAs laser. The observed spectral width of the Doppler-free spectra was about 20 $\sim$ 30 MHz. To lock the laser frequency to such a narrow spectrum, the temperature of the GaAlAs laser was stabilized beforehand by using the temperature control system studied in Sec. III-2. By the temperature stabilization, the frequency fluctuation of the GaAlAs laser was suppressed to be less than 5 MHz. After the diode temperature was stabilized, the laser frequency was locked to one of the Doppler-free spectra, and the short-term frequency-stability was improved to be about 10 kHz. In this chapter, we report on the details of the system of the frequency stabilization and the experimental results.

The frequency stability of laser is usually estimated in terms of the Allan variance. We present a short review on the

theory of the frequency-stability analysis, and we discuss on the limitation of the frequency stability of the GaAlAs laser locked to the Cs-D_2 line. The experimental results show that the frequency stability of the GaAlAs laser was better than 10^{-11}, which is comparable to that of ordinary iodine-locked He-Ne laser.

By using the present method, it is possible to make frequency-stabilized laser system which is compact and portable. In this chapter, we study also on the improved and compact system of the stabilized GaAlAs laser, suitable for its practical use. Such compact system can be used such as a convenient standard of wavelength or optical frequency, and might be applicated to the optical telecommunications and the precision measurements of position and velocity.

IV-2 Frequency Stabilization of GaAlAs Laser

IV-2-1 Experimental System of Frequency Locking

The oscillation frequency of the GaAlAs laser is locked to one of the Doppler-free spectra of the Cs-D_2 line. A system used for the frequency locking is shown in Fig. IV-1, in which the diode temperature is stabilized in the way described in Chap. III. In Fig. IV-1, the dotted area shows the same optical system as that used in the saturated absorption spectroscopy, which is shown in Fig. III-5. The photodiodes detecting the

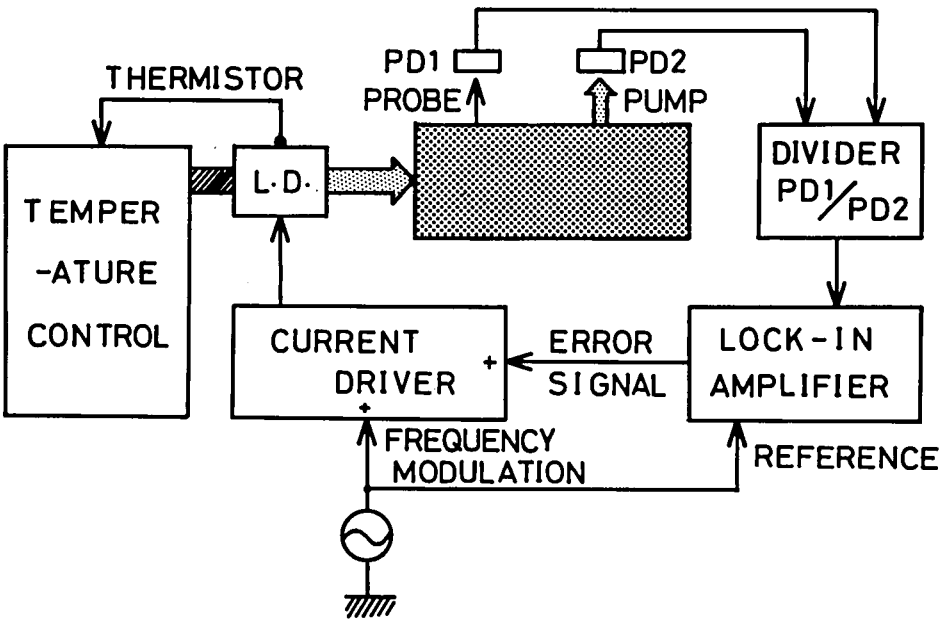

Fig. IV-1 Block diagram of the experimental setup for the frequency stabilization of the GaAlAs laser. Dotted area shows the same optical system of the saturated absorption spectroscopy of Cs as shown in Fig. III-5. The first derivative of Doppler-free spectrum is used as an error signal to lock the laser frequency.

probe beam and the pump beam are indicated as PD1 and PD2, respectively. In order to reduce the Doppler-broadened background appearing in the absorption signal of the probe beam, the output of PD1 is divided by that of PD2. The output of PD2 shows only Doppler-broadened background because the pump beam is much stronger than the probe beam. A flat background in the output of the photodiodes are reduced, and the output of PD1 and PD2 are applied to the divider circuit.

In this experiment, the first derivative of the signal of the Doppler-free spectrum is used as an error signal to lock the laser frequency. The center frequency of the Doppler-free spectrum is just the zero-crossing frequency of the first derivative. In the central region of the Doppler-free spectrum, the frequency deviation from the resonance is approximately proportional to the first derivative. The difference of frequencies giving two extrema of the first derivative is smaller than FWHM of the Doppler-free spectrum by a factor $1/\sqrt{3}$.

To get the first derivative of Doppler-free spectra the laser frequency is modulated by adding a small alternative current to the injection current. The output of the divider circuit is applied to a lock-in amplifier tuned at the modulation frequency of the injection current. Let us write $f(\omega)$ as the output of the divider circuit, and suppose that the laser frequency ω is modulated at the frequency ω_m with frequency deviation ω_1 as

$$\omega = \omega_0 + \omega_1 \cos \omega_m t, \qquad \text{(IV.1)}$$

where ω_0 is the center frequency. Since ω_1 is small in comparison with the width of the Doppler-free spectrum, $f(\omega)$ can be expanded as

$$f(\omega) = f(\omega_0) + \frac{\partial f(\omega)}{\partial \omega}\Big|_{\omega=\omega_0} \omega_1 \cos\omega_m t + o(\omega_1^2). \qquad \text{(IV.2)}$$

Thus, one can obtain the first derivative of $f(\omega)$ by taking out the component synchronizing with $\cos\omega_m t$, by means of the lock-in detection. When the Doppler-free signal is written as $S(\omega)$, and the Doppler-broadened background as $D_1(\omega)$ for PD1 and $D_2(\omega)$ for PD2, $f(\omega)$ can be written as

$$f(\omega) = \frac{D_1(\omega) - S(\omega)}{D_2(\omega)}, \qquad \text{(IV.3)}$$

and its first derivative is

$$f'(\omega) = -\frac{S'(\omega)}{D_2(\omega)} - S(\omega)\frac{D'(\omega)}{D_2^2(\omega)}, \qquad \text{(IV.4)}$$

where the prime indicates the derivative with respect to ω. Since $S(\omega) \ll D_2(\omega)$ and the Doppler-broadened background is slowly varying with respect to ω, the second term in Eq. (IV.4) can be negligible, so that the frequency at zero-crossing of the first derivative of the divided signal gives approximately the

center frequency of the Doppler-free spectrum.

The modulation of the injection current causes also an intensity modulation of the laser output, which results in a small offset of the first derivative. The laser frequency can be locked to one of the Doppler-free spectra of the Cs-D_2 line by feeding back the output of the lock-in amplifier as an error signal to the current-driver of the GaAlAs laser. In this experiment, only the proportional servocontrol is employed in the feedback loop of the injection current.

In order to avoid an influence of external mechanical vibration and acoustic noise, all optical components are fastened by using magnetic basements on an iron surface plate with size of 30×40 cm^2 which is isolated from the laboratory floor by using air cushions.

IV-2-2 Experiment of Frequency Stabilization

Figure IV-2 shows the first derivative of the Doppler-free spectra of the Cs-D_2 line, which was obtained when the laser frequency ν was swept through the absorption line from the hyperfine level with $F = 4$ in the ground state. The laser frequency was swept by varying the diode temperature, whose change is approximately proportional to that of the laser frequency. The injection current was modulated at 1 kHz with the amplitude about 1 μA, and corresponding frequency-deviation of laser was about 8 MHz. Throughout the present experiment, the

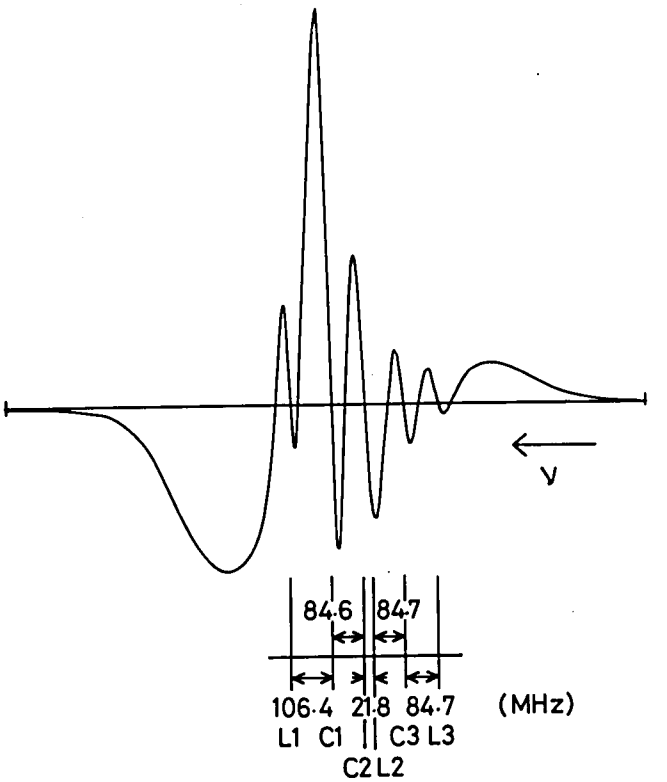

Fig. IV-2 First derivative of the Doppler-free spectra and their positions expected from the theoretical calculation. The laser frequency ν was swept through the absorption line from the hyperfine levl with F = 4 in the ground state of Cs.

time constant of the lock-in detection was fixed at 100 ms. The signal-to-noise ratio of the first derivative became worse for smaller frequency deviation, because the spectral width of the GaAlAs laser was about 10 MHz (HWHM), and the residual noise of the current source was of the order of 0.1 μA,

In Fig. IV-2, we show also the positions of the Doppler-free spectra expected from the theoretical calculation of the hyperfine separation. The frequency scale of the horizontal axis was estimated by fitting the separation between the Doppler-free spectra C1 and L3 to the theoretical value (275.8 MHz). The positions of the other Doppler-free spectra were determined by the theoretical values of the hyperfine separations in $6^2P_{3/2}$ state. The symbols L1, L2, L3 and C1, C2, C3 are the same as those in Fig. III-7. In this experiment, the powers of the pump and probe beams were 910 μW and 20 μW, and the beam diameters in the cell were about 7 mm and 1 mm, respectively. The Cs cell temperature was 11 °C, at which the vapor pressure of Cs atom is 3×10^{-7} torr, i. e. the Cs density is 1.0×10^{10} cm^{-3}. These conditions are the same as those in the experiment to observe the Doppler-free spectra shown in Fig. III-7.

In Fig. IV-2, the differences of frequencies at extrema of the first derivative were about 25 MHz for L1, 43 MHz for C1, 49 MHz for the overlapped signal of L2 and C2, 36 MHz for C3, and 39 MHz for L3. The output voltage of the lock-in amplifier is approximately proportional to the deviation of the laser frequency from the resonance in the central region of the

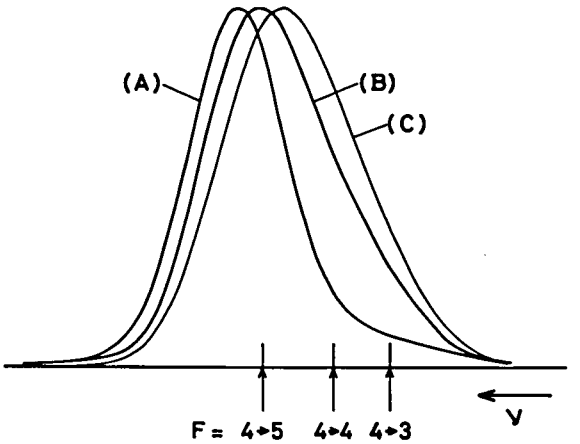

Fig. IV-3 The normalized Doppler-broadened absorption line from the hyperfine level with F = 4 in the ground state of Cs, observed by the pump beam (A) and the probe beam (B), and theoretically caluculated (C).

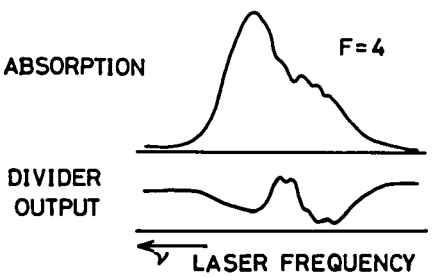

Fig. IV-4 Typical absorption signal of the probe beam and the output of the divider circuit obtained when the laser frequency ν was swept through the absorption line from the hyperfine level with F = 4 in the ground state of Cs.

Doppler-free spectrum. The voltage-frequency ratios were estimated to be 27 μV/kHz at L1, 71 μV/kHz at C1, 24 μV/kHz at the overlapped slope of L2 and C2, 12 μV/kHz at C3, and 6 μV/kHz at L3. The crossover resonance C1 is the strongest and sharpest one. If we use the values of the hyperfine separation measured by Violino instead of the theoretical ones, the frequency separations between Doppler-free spectra are estimated to be 1.2 times larger than the present values. Then the slopes of the first derivative in μV/kHz become less than these estimated above by a factor of 0.83. The ratios between the hyperfine separation are exactly the same for both cases, so that the relative positions of the Doppler-free spectra shown in Fig. IV-2 should not be changed.

In Fig. IV-2, there still exists a broad component, which comes from the incomplete elimination of Doppler-broadened background. This is mainly due to the difference of the magnitudes of saturation for the pump and probe beams, which results in a small difference of shapes of Doppler-broadened background for these beams. In Fig. IV-3, we show the normalized Doppler-broadened absorption signals from F = 4 level in the ground state, observed by the pump beam (curve A) and the probe beam (curve B). As seen in Fig. IV-3, the absorption of the pump beam was strongly saturated at about the frequencies of transitions from the F = 4 level in the ground state to the hyperfine levels with F = 3 and 4 in the $6^2P_{3/2}$ state owing to the hyperfine pumping and beam propagation in the optically thin

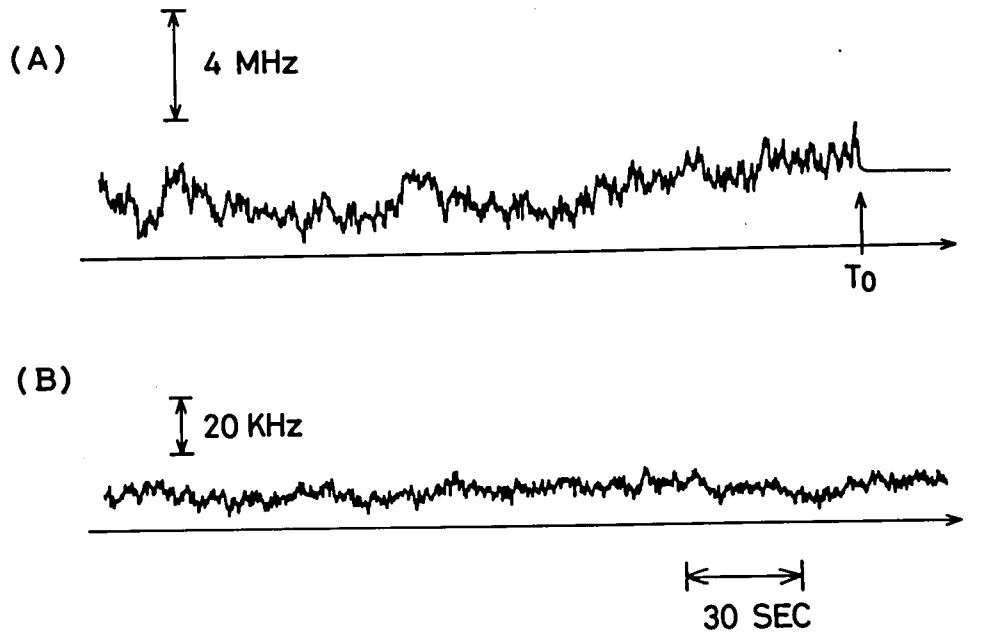

Fig. IV-5 Recorder traces showing the error signal from the lock-in amplifier in the two cases that (A) only the diode temperature was stabilized and (B) both of the diode temperature and the injection current were stabilized. The laser frequency was initially tuned at the crossover resonance C1 shown in Fig. IV-2. The frequency scale is estimated from the slope of the first derivative of the crossover resonance C1. In the case (A), the feedback loop of the injection current was turned on at the time T_0.

medium. In Fig. IV-3, the curve C shows the theoretically calculated shape of the Doppler-broadened absorption line in the case that the cell is optically thin. Comparing the curves B with C, we see that the absorption spectrum of the probe beam is also deformed because of the saturation and beam propagation. We show in Fig. IV-4, a typical output signal of the divider circuit, where a frequency-dependent offset appears.

Before locking the laser frequency to one of the Doppler-free spectra, the diode temperature was stabilized by using the temperature-control system described in Sec. III-3. In this experiment, the output of the bridge circuit integrated over the time interval of 12 s was fed back to the driver of the thermoelectric cooler, together with the proportional output, through a lowpass filter with $\sim$8 Hz cutoff. Figure IV-5A shows the recorder trace showing the error signal from the lock-in amplifier in the case that only the laser temperature was stabilized. In this case, the laser frequency was initially tuned at about the center of the crossover resonance C1. (The crossover resonance C1 is due to the simultaneous transitions of atoms with the same axial velocity from the hyperfine level with F = 4 in the ground state to the hyperfine levels with F = 5 and 4 in the $6^2P_{3/2}$ state.) The fluctuation of the error signal can be regarded as that of the laser frequency. The frequency-scale shown in Fig. IV-5 was estimated from the slope of the first derivative of the crossover resonance C1, i. e. about 71 μV/kHz. We found that the fluctuation of the laser frequency was

suppressed to be less than 5 MHz only by the temperature stabilization, which was kept so long as the fluctuation of the room temperature was within few degrees. The frequency fluctuation 5 MHz corresponds to the fluctuation of the diode temperature of 3×10^{-4} °C.

Under the control of the diode temperature, the laser frequency was locked to the crossover resonance C1 by feeding back the error signal to the current driver of the GaAlAs laser. In Fig. IV-5A, T_0 shows the time when the feedback loop of the injection current was turned on. Figure IV-5B shows a part of the recorder trace showing the fluctuation of the error signal after the time T_0. These traces were taken by the recorder with freuency response slower than 1 Hz. As seen in Fig. IV-5B, the short-term fluctuation of the laser frequency is less than 10 kHz, which corresponds to 5×10^{-4} parts of the width (FWHM) of the crossover resonance C1. The long-term fluctuation observed was less than 37 kHz for the time interval of 3000 s. The short-term frequency-stability 10 kHz is the best value reported so far on the frequency-stabilization of the semiconductor lasers. We will discuss on the limitation of the frequency stability in the following sections.

IV-3 Frequency Stability of GaAlAs Laser Locked at the Cs-D_2 Line

IV-3-1 Analysis of Frequency Stability

In this section, we present a brief review on the theoretical analysis of frequency stability of the laser,[105),114)-118)] which is used to estimate the limitation of the frequency stability of the GaAlAs laser locked at the Cs-D_2 line.

Suppose that the electromagnetic field u(t) of a stabilized laser oscillating at center frequency ω_0 with fluctuating phase $\phi(t)$ as

$$u(t) = u_0 \sin \{2\pi\nu_0 t + \phi(t)\}. \qquad \text{(IV.5)}$$

The instantaneous frequency $\nu(t)$ is defined as

$$\nu(t) = \nu_0 + \frac{1}{2\pi}\frac{d\phi(t)}{dt}, \qquad \text{(IV.6)}$$

and the normalized frequency-fluctuation y(t) as

$$y(t) = \frac{1}{2\pi\nu_0}\frac{d\phi(t)}{dt} = \frac{dx(t)}{dt}, \qquad \text{(IV.7)}$$

where

$$x(t) = \frac{\phi(t)}{2\pi\nu_0}. \qquad \text{(IV.8)}$$

We can analyze the stability or instability of the laser frequency in two ways. One is the analysis based on the frequency domain and the other is that based on the time domain. In the frequency-domain analysis, the spectral density $S_y(f)$ is generally used, which is defined usually as a Fourier transform of the autocovariance function $R_y(\tau)$ of y(t) by using Wiener-Khintchine theorem[119] as

$$R_y(\tau) = \lim_{T\to\infty} \frac{1}{T} \int_0^T y(t+\tau)\, y(t)\, dt, \qquad \text{(IV.9)}$$

$$S_y(f) = 4 \int_0^\infty R_y(\tau) \cos(2\pi f\tau)\, d\tau. \qquad \text{(IV.10)}$$

In the time domain, the frequency fluctuation is analyzed statistically in terms of the probability density. Since the frequency cannot be measured instantaneously, a possible measurement is done by averaging the instantaneous frequency y(t) over finite time-duration τ as

$$\bar{y}(t,\tau) = \frac{1}{\tau} \int_t^{t+\tau} y(t)\, dt. \qquad \text{(IV.11)}$$

This is equal to time variation of x(t) averaged over duration τ.

$$\bar{y}(t,\tau) = \frac{1}{\tau} \{x(t+\tau) - x(t)\}. \qquad \text{(IV.12)}$$

The statistical behavior of $\bar{y}(t)$ can be analyzed in terms of the variance, i. e. the second moment[115] calculated as

$$\sigma_y^2(\tau) = \langle \bar{y}^2(t,\tau) \rangle - \langle \bar{y}(t,\tau) \rangle^2, \qquad \text{(IV.13)}$$

where the broken bracket represents the time average:

$$\langle g(t) \rangle = \lim_{T \to 0} \frac{1}{T} \int_0^T g(t)\, dt. \qquad \text{(IV.14)}$$

Without any loss of generality, we can assume that $\langle \bar{y}(t,\tau) \rangle = 0$. With the relations in Eqs. (IV.12) and (IV.14), the variance of Eq. (IV.13) is calculated as

$$\sigma_y^2(\tau) = \frac{1}{\tau^2} \{\langle x^2(t+\tau) \rangle - 2\langle x(t+\tau)x(t) \rangle + \langle x^2(t) \rangle\} \qquad \text{(IV.15)}$$

$$= \frac{2}{\tau^2} \{ R_x(0) - R_x(\tau) \}. \qquad \text{(IV.16)}$$

The second term of Eq. (IV.15) corresponds to the autocovariance function $R_x(\tau)$, which is related to the spectral density of x(t) with the inverse Fourier transform of Eq. (IV.10) as

$$R_x(\tau) = \int_0^\infty S_x(f) \cos(2\pi f \tau)\, df. \qquad \text{(IV.17)}$$

Because $S_x(f)$ is related to $S_y(f)$ as

$$S_y(f) = S_{\frac{dx(f)}{dt}} = (2\pi f)^2 S_x(f), \qquad \text{(IV.18)}$$

$R_x(\tau)$ can be written in terms of the spectral density $S_y(f)$ as

$$R_x(\tau) = \int_0^\infty \frac{S_y(f)}{(2\pi f)^2} \cos(2\pi f\tau)\, df. \qquad \text{(IV.19)}$$

Substituting Eq. (IV.19) into Eq. (IV.16), we can obtain the relation between the variance and the spectral density as

$$\sigma_y^2(\tau) = \frac{1}{\pi\tau} \int_0^\infty S_y\left(\frac{u}{\pi\tau}\right) \frac{\sin^2 u}{u^2}\, du, \qquad \text{(IV.20)}$$

where the frequency f has been replaced by u as $\pi f \tau = u$.

In the practical measurements, it is impossible to obtain sample $\bar{y}(t)$ over infinite time-duration of observation as in above calculations. More realistic case is that N samples of $\bar{y}(t)$ are measured with sampling duration τ, sampling interval T and dead time $T - \tau$:

$$\bar{y}_k(kT,\tau) = \frac{1}{\tau} \int_{kT}^{kT+\tau} y(t)\, dt. \qquad \text{(IV.21)}$$

An average of $\bar{y}_k$ is written as

$$< \bar{y}_k >_N = \frac{1}{N} \sum_{K=1}^{N} \bar{y}_k, \qquad \text{(IV.22)}$$

and the variance is calculated as

$$\sigma_y^2(N,T,\tau) = \frac{1}{N-1} \sum_{k=1}^{N} \{\bar{y}_k - \langle \bar{y}_k \rangle_N\}^2. \qquad \text{(IV.23)}$$

This is not convenient because $\sigma_y(N,T,\tau)$ depends on all of the variables N, T, and τ. It was proposed by Allan[114] to analyze the frequency fluctuation y(t) by using an expectation value of the variance given as

$$\langle \sigma_y^2(N,T,\tau) \rangle = \lim_{M\to\infty} \frac{1}{M} \sum_{i=1}^{M} \sigma_{yi}^2(N,T,\tau). \qquad \text{(IV.24)}$$

The expectation value of Eq. (IV.24) is usually called as "Allan variance", and often its square root is called in the same term. Similarly to Eq. (IV.20), the Allan variance is related to the spectral density as follows.[117]

$$\langle \sigma_y^2(N,T,\tau) \rangle = \frac{N}{N-1} \int_0^\infty S_y(f) |H(f)|^2 \, df, \qquad \text{(IV.25)}$$

where H(f) is defined as

$$|H(f)| = \frac{\sin^2(\pi f\tau)}{(\pi f\tau)^2} \{1 - \frac{\sin^2(\pi fTN)}{N^2 \sin^2(\pi fT)}\}. \qquad \text{(IV.26)}$$

Especially in the case of N = 2 and T = τ, the Allan variance is given by a very simple formula as

$$\langle \sigma_y^2(2,\tau,\tau) \rangle = \frac{1}{2} \langle (\bar{y}_{k+1} - \bar{y}_k)^2 \rangle. \qquad \text{(IV.27)}$$

When we can measure a set of finite but large number of data y_k, the Allan variance can be calculated approximately by

$$\langle\sigma_y^2(2,\tau,\tau)\rangle \simeq \sigma^2(2,\tau) = \frac{1}{M-1}\sum_{k=1}^{M-1}\frac{1}{2}(\bar{y}_{k+1}-\bar{y}_k)^2. \qquad \text{(IV.28)}$$

An investigation was made by Tausworthe[120] on the convergence of $\sigma(2,\tau)$ to the Allan variance for infinite value of the sample number M. The formula of Allan variance given by Eq. (IV.28) is very convenient for practical use. Namely, $\sigma^2(2,\tau)$ can be calculated easily and directly from a set of data, i. e. from a trace of error signal of the laser frequency in our case. From Eq. (IV.25), we can obtain the relation between $\sigma(2,\tau)$ and the spectral density as

$$\sigma^2(2,\tau) \simeq \frac{2}{\pi\tau}\int_0^\infty S_y\left(\frac{u}{\pi\tau}\right)\frac{\sin^2 u\,\sin^2\left(\frac{T}{\tau}u\right)}{u^2}\,du. \qquad \text{(IV.29)}$$

It is known by experience that, in an analysis of the frequency stability or instability of an oscillator in the frequency domain, the important part of the spectral density can be expressed by a power-law[121),122)] as

$$S_y(f) = h_{-2}f^{-2}+h_{-1}f^{-1}+h_0f^0+h_1f^1+h_2f^2 = \sum_{i=-2}^{2}h_if^i. \qquad \text{(IV.30)}$$

The noise components with i = -2 is usually called as "random walk noise" frequency-modulation, i = -1 as "flicker noise" frequency-modulation, i = 0 as "white noise" frequency-

modulation, i = 1 as "flicker noise" phase-modulation, and i = 2 as "white noise" phase-modulation.[105] For the noise components with i = -2, -1 and 0, the Allan variance $\sigma(2,\tau)$ is calculated from Eq. (IV.29) as follows.[115]

$$\text{RANDOM WALK}, \quad h_{-2}f^{-2} \; ; \; \sigma^2(2,\tau)=\frac{4\pi^2}{6} h_{-2}\tau , \qquad \text{(IV.31)}$$

$$\text{FLICKER} \quad , \quad h_{-1}f^{-1} \; ; \; \sigma^2(2,\tau)=2\ln 2 \cdot h_{-1} , \qquad \text{(IV.32)}$$

$$\text{WHITE} \quad , \quad h_0 f^0 \; ; \; \sigma^2(2,\tau)=\frac{h_0}{2} \frac{1}{\tau} . \qquad \text{(IV.33)}$$

By using above results, it is possible to know the type of the noise component limitting the frequency stability, from the dependence of the Allan variance on the averaging time τ. In the case that the laser frequency fluctuates or it is modulated sinusoidally like $y = a \sin \omega t$, the Allan variance is calculated from Eq. (IV.29) as

$$\sigma(2,\tau) = a \frac{\sin^2(\omega\tau/2)}{\omega\tau/2} , \qquad \text{(IV.34)}$$

which is shown in Fig.IV-6 in the case that a = 1 and f = $\omega/2\pi$ = 1 Hz. The Allan variance in Eq. (IV.34) increases as $\sigma(2,\tau) \propto \tau$ and takes its maximum at $\tau = 0.37f^{-1}$ and decreases as $\sigma(2,\tau) \propto \tau^{-1}$.

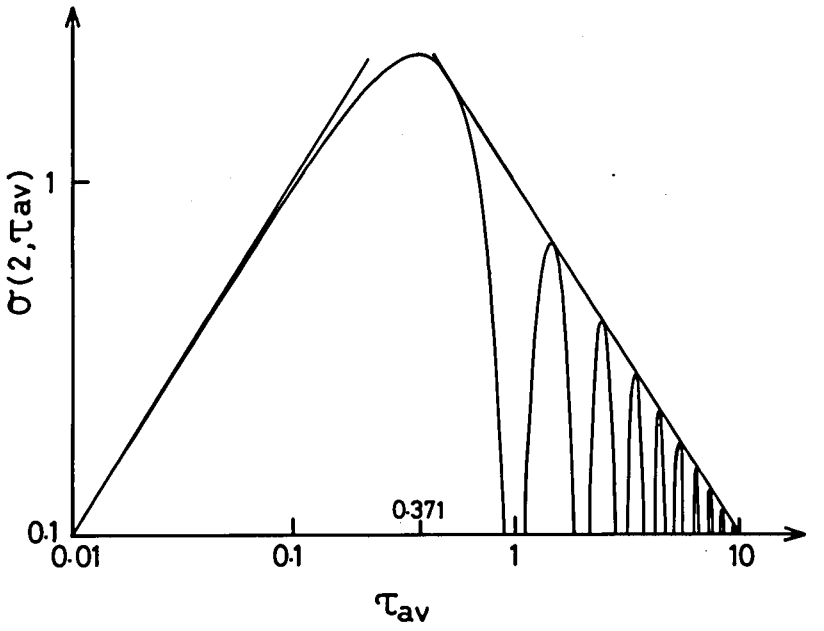

Fig. IV-6 Allan variance $\sigma(2,\tau_{av})$ for sinusoidal frequency-modulation y = sin $2\pi t$.

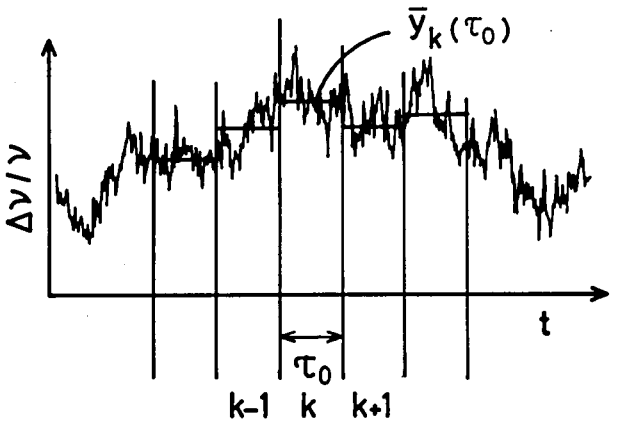

Fig. IV-7 Sampling of frequency fluctuation $\bar{y}_k(\tau_0)$ for calculation of Allan variance.

IV-3-2 Frequency Stability of GaAlAs Laser Locked at the Cs-D_2 Line

The frequency stability of the stabilized laser can be estimated from the recorder trace of the error signal in terms of the Allan varince as mentioned in Sec. IV-3-1. At first the error signal recorded on a chart is normalized by the mean frequency 3.518×10^{14} Hz of the Cs-D_2 line. The horizontal axis (time axis) of the trace of the error signal is divided into many sections with adequately short time-duration τ_0, and the error signal is averaged over τ_0 as shown in Fig. IV-7. The averaged values of the error signal are considered to be a basic set of normalized frequency-fluctuation $\bar{y}_k(\tau_0)$. The normalized frequency-fluctuations for larger averaging time, i. e. $\tau_{av}= i\tau_0$ (i: positive integer) are calculated from the basic set of $\bar{y}_k$ as

$$\bar{y}_n(ni\tau_0,i\tau_0) = \frac{1}{i}\sum_{k=ni}^{(n+1)i}\bar{y}_k(\tau_0). \qquad \text{(IV.35)}$$

Using the values of $\bar{y}_n$, the Allan variance $\sigma_M^2(2,\tau_{av})$ can be calculated as

$$\sigma_M^2(2,\tau_{av}) = \frac{1}{M-1}\sum_{n=1}^{N-1}\frac{1}{2}(\bar{y}_{n+1} - \bar{y}_n)^2, \qquad \text{(IV.36)}$$

where $\tau_{av}= i\tau_0$.

In an actual experiment, the sample number M is limitted. Lesage et al.[123] discussed on the uncertainity of the Allan

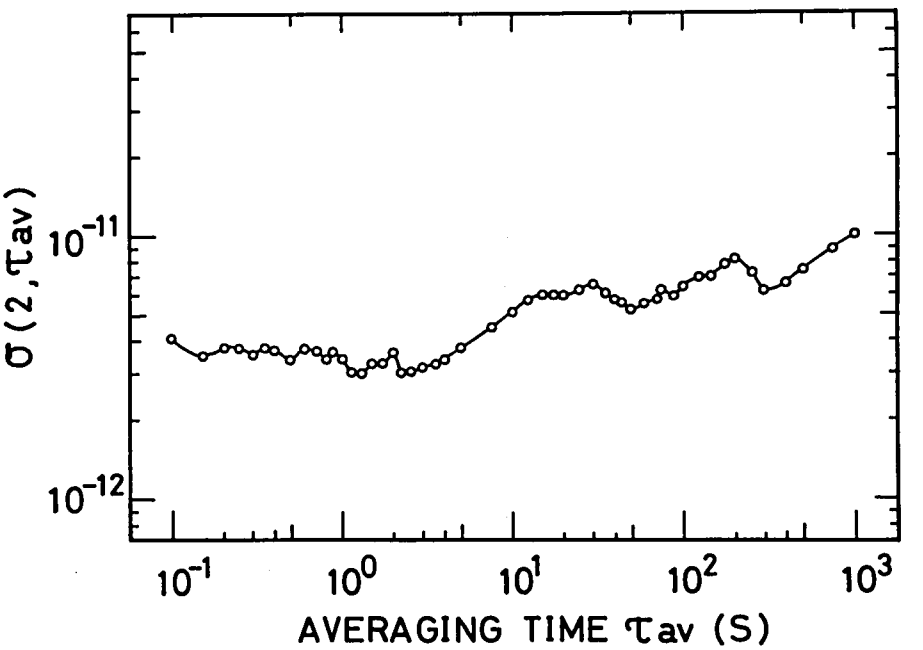

Fig. IV-8 Allan variance $\sigma(2,\tau_{av})$ calculated from the recorder trace of the output of the lock-in amplifier, a part of which is shown in Fig. IV-5. The recorder trace was taken for 3000 s.

variance for such a finite set of data using a "true" variance $\sigma^2(2,\tau_{av})$ and a relative uncertainity δ defined as

$$\delta = \frac{\sigma_M(2,\tau_{av}) - \sigma(2,\tau_{av})}{\sigma(2,\tau_{av})} . \qquad \text{(IV.37)}$$

They showed that a standard deviation of δ can be written as

$$\sigma(\delta) \simeq K_i \, M^{-\frac{1}{2}} , \qquad \text{(IV.38)}$$

with accuracy better than 10 percent for the sample number M larger than 10. In Eq. (IV.38), K_i is a constant close to unity but it is dependent on the type of the noise component. For the noise component $h_i f^i$, the values of K_i are given as $K_2 = K_1 = 0.99$, $K_0 = 0.89$, $K_{-1} = 1.19$ and $K_{-2} = 0.75$.

We have considered on the limit of the frequency stability of the GaAlAs laser locked at the Cs-D_2 line by using above results. Figure IV-8 shows the Allan variance $\sigma(2,\tau_{av})$ calculated from the recorder trace of error signal taken for 3000 s, a part of which is shown in Fig. IV-5B. The Allan variance for averaging time between 0.1 s and 5 s were calculated from the trace of error signal taken by a photo-recorder with fast response, and the basic set of data were taken for averaging duration of $\tau_0 = 0.025$ s. Since the time constant of the lock-in detection was 0.1 s, the Allan variance was calculated for the averaging time longer than 0.1 s. While, for the averaging time between 5 s and 1000 s, the Allan variance was calculated from

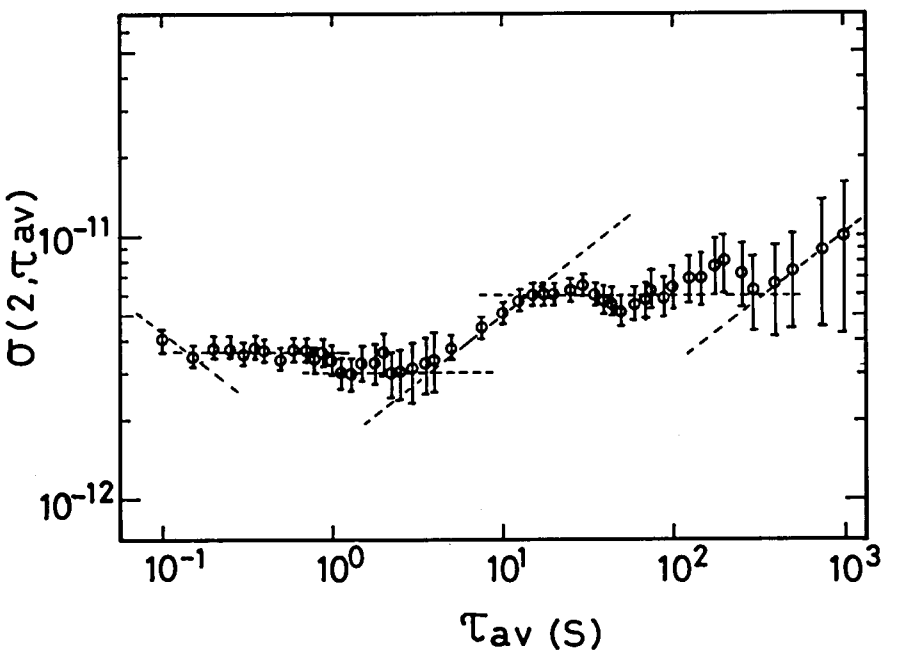

Fig. IV-9 The same Allan variance as shown in Fig. IV-8 together with the slopes of the Allan variance corresponding to white noise, flicker noise and random walk noise. The error bars show the standard deviation of the uncertainity of the Allan variance defined in Eq. (IV.37).

the trace of error signal taken by a pen recorder with frequency response below 1 Hz, and the time duration τ_0 for the basic set of data was 2.5 s. The maximum sampling number is 100 for each averaging time in the present case. In this case, the standard deviation of the normalized uncertainity $\sigma(\delta)$ was about 10 percent. The Allan variance between 3.0×10^{-12} and 1.0×10^{-11} was obtained at the averaging time between 0.1 s and 1000 s as seen in Fig. IV-8, and the minimum value was obtained at τ_{av}= 1.3 s. In our analysis, we used the theoretical values of the hyperfine separations in the $6^2P_{3/2}$ state. But when we use the hyperfine separations measured by Violino, the Allan variance becomes 1.2 times larger than that shown in Fig. IV-8, so that the minimum value becomes 3.6×10^{-12}. The frequency stability of a GaAlAs laser is usually of the order of 10^{-8} under free-running condition, so we see that it is significantly improved by the frequency-locking. It must be pointed out that the obtained frequency stability for the averaging time between 0.1 and 10 s is the best one reported so far in the case of semiconductor laser. This is as good as the stability of the ordinary iodine-stabilized He-Ne laser.

It should be noted that the frequency fluctuation used to estimate the stability was indirectly measured by using the first derivative of the Doppler-free spectrum. If there are fluctuation and drift in the first derivative of the spectrum itself, they must give error in estimation of the frequency stability. However, we believe that the obtained value of the

frequency stability is very close to the real one. In order to estimate the absolute frequency-stability, the oscillation frequencies of two stabilized GaAlAs laser must be compared by observing the beat frequency. In the present work, such absolute appreciation of the frequency stability has not been carried out yet.

Since the time constant of the lock-in detection was 0.1 s, the frequency stability at $\tau_{av} \sim$ 0.1 s was improved considerably. The Allan variance was almost constant between $\tau_{av} =$ 0.15 s and 4 s. This result indicates that the stability of the laser frequency in this region was mainly determined by the flicker noise frequency-modulation with the spectral density $\propto f^{-1}$. In these region of the averaging time, the frequency stability was also affected by the frequency modulation of the laser. According to the result in Eq. (IV.34), the frequency-modulation of at the frequency 1 kHz with the frequency deviation 8 MHz gives the Allan variance $\sigma \sim 4\times10^{-12}$ under the free-running condition.

When only the proportional feedback was utilized in the servocontrol of the injection current of the GaAlAs laser, the Allan variance increased slightly with longer averaging time. This was mainly due to a drift of the room temperature which caused a small drift of the diode temperature. The Allan variance increased between $\tau_{av} =$ 4 s and 12 s with a slope of 1/2, which indicates that the frequency instability was mainly due to a random wolk noise frequency-modulation with constant spectral

density. When the integral servocontrol with integration time of 12 s was done together with proportional control, the Allan variance was improved further and became constant in the region $\tau_{av} \sim$ 12 s. Figure IV-9 shows the same Allan variance as that shown in Fig. IV-8, together with the slopes of the Allan variance discussed above. The error bars in Fig. IV-9 show the standard deviation of the uncertainity of the Allan variance defined in Eq. (IV.37), in which we use $K_i = 1$. The error bars in the region $\tau_{av} > 30$ s are out of 10 % accuracy in this estimation. Two broad peakes and dips of the Allan variance can be seen in Fig. IV-8 in the region between $\tau_{av} = 20$ s and 400 s, which are considered to be due to the characteristic oscillation in the servocontrol system of the diode temperature. The time duration of the oscillation in the diode temperature was estimated to be about 50 s and 300 s from the positions of dips in the Allan variance. Actually, the oscillations at such frequencies could be seen in the trace of error signal. The Allan variance increased again in the region $\tau_{av} = 300$ s with the slope 1/2 of random walk noise frequency-modulation. This was due to a slow drift of room temperature, which caused an drift of output voltage of the bridge circuit and the drift of the diode temperature. The frequency stability of the GaAlAs laser must be improvrd, if we optimize the time constants and gains of the servocontrol loop taking account of these results.

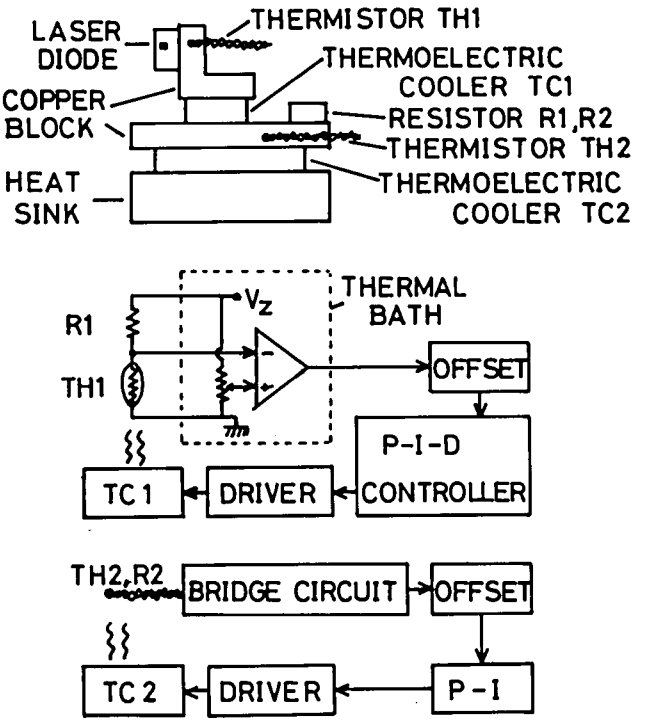

Fig. IV-10 Schematic diagram of the double-loop temperature-control of the semiconductor laser.

IV-4 Compact and Improved System of Frequency Stabilization

IV-4-1 Double-Loop Temperature Stabilization

In this section, we study on a small and portable system of the frequency-stabilization suitable for its practical use.

The long-term frequency-stability of the GaAlAs laser mainly depends on the stability of the diode temperature. In the previous system of the temperature control, the thermoelectric cooler was connected directly to the heat radiator exposed in open air. In this case, a drift of room temperature directly affects to the diode temperature. For instance, a few degree change of room temperature causes about 10 MHz change of the laser frequency even under the temperature stabilization. In above system, the aluminum block mounting the laser diode was not small enough, which resulted in the time lag about 12 s and caused instability when the loop-gain of feedback was raised. In practical use, a fluctuation of room temperature more than several degree should be taken into account.

Figure IV-10 shows an improved system of the temperature control. A copper block is temperature stabilized roughly by using a thermoelectric cooler with capacity of 20 W, which is used as a thermal buffer. The laser diode is mounted on a small copper block whose temperature is controlled by a small thermoelectric cooler, which is mounted on the larger temperature-stabilized copper block. The capacity and size of the small thermoelectric cooler are 2.4 W and 1 cm square. The

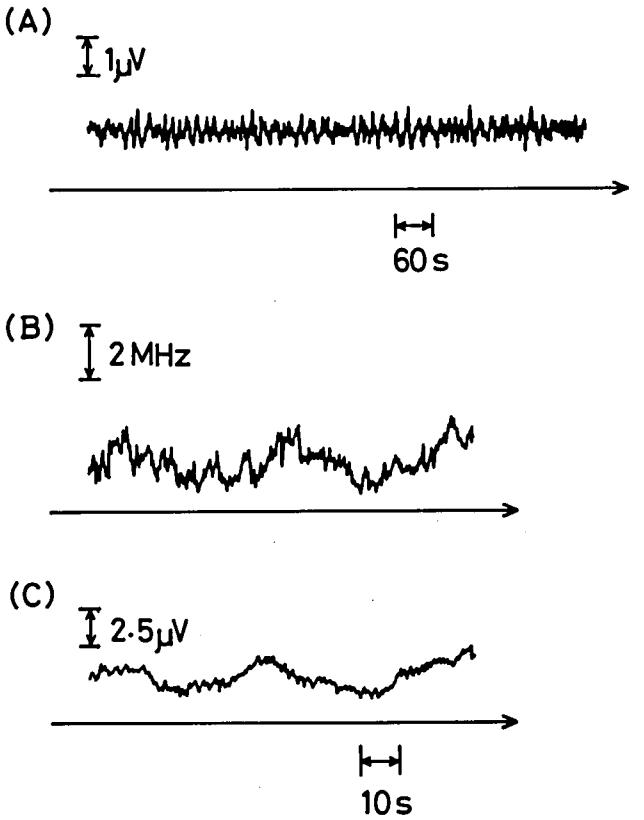

Fig. IV-11 Recorder trace of the output of the bridge circuit measuring the diode temperature obtained when the double-loop temperature-stabilization was carried out (A). And recorder traces showing the variation of the laser frequency (B) and corresponding output of the bridge circuit (C) obtained in the experiment of the temperature stabilization (Sec. IV-2-2).

temperature change of each copper block is measured by using thermistor and bridge circuit similar to that shown in Fig. III-4. By using this system, we can reduce the influence of room-temperature fluctuation. We can also reduce the time lag of the feedback loop, which enables us to improve the stability by increasing the gain. The series resistors in both of the bridge circuits are also mounted on the larger copper block in order to avoid thermal fluctuations of their resistance. As for the bridge circuit measuring the diode temperature, the voltage divider and the first-stage amplifier are placed in a small aluminum box whose temperature is controlled within ±0.1 °C. The stabilization of the diode temperature is done by using P-I-D servocontrol. The laser diode and two thermoelectric coolers are packed into a copper case which serves as a heat radiator of larger thermoelectric cooler.

A preliminary examination of this system was carried out, in which a fluctuation of the diode temperature was measured by recording the output of the bridge circuit. A part of the recorder trace in the case that the double-loop temperature control was carried out is shown in Fig. IV-11A. The fluctuation of the output voltage of the bridge circuit measuring the diode temperature could be reduced within 1 μV, which maintained at least for an hour. From the B coefficient 3500 °K of the thermistor and the temperature dependence of the laser frequency 20 GHz/°C, the changes of the diode temperature and the laser frequency as functions of the bridge output voltage were

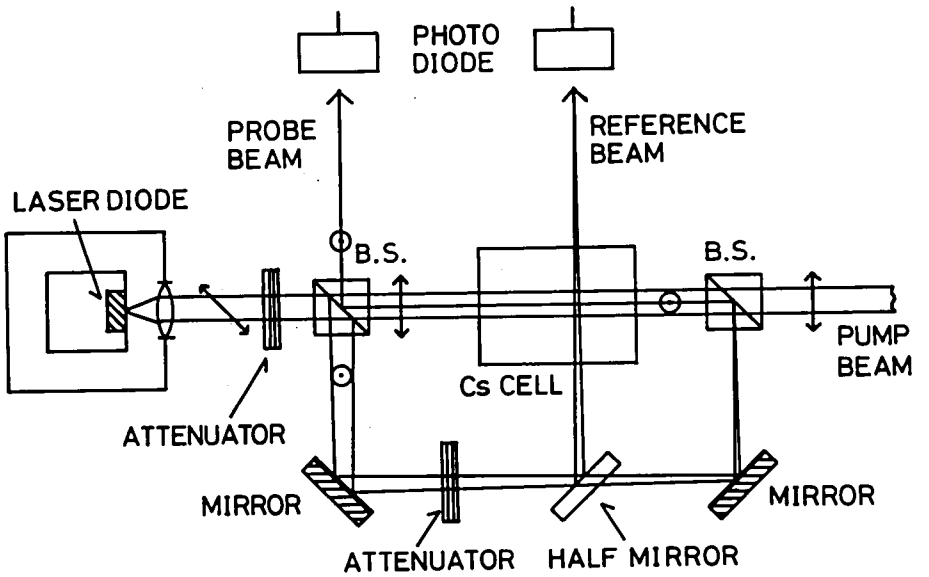

Fig. IV-12 Improved and compact optical system for the saturated absorption spectroscopy of Cs. The laser beam focused by a lens with focal length 1 cm is split into the pump and probe beams by a polarizing beam splitter. The polarization axes of the pump and probe beams are perpendicular to each other. A part of the probe beam is reflected by a half mirror and applied into the cell as a reference beam from the direction perpendicular to the probe beam.

estimated roughly to be 3×10^{-5} °C/μV and 0.6 MHz/μV respectively. Considering these values, we expect that the laser frequency can be stabilized within 1 MHz if the double-loop temperature-stabilization is adopted. For comparison, we show in Fig. IV-11 the recorder traces showing the variations of the laser frequency (B) and corresponding bridge output voltage (C) which were obtained in the experiment of the temperature stabilization (Sec. IV-2-2). In above experiments, the same types of the thermistor and the bridge circuit as in the present system were used. Looking at Fig. IV-11, one can see that the estimated value 0.6 MHz/μV agrees well with the experimental results.

IV-4-2 Compact and Improved Optical System

We have constructed a compact optical system as shown in Fig. IV-12. The laser beam is collimated by using a lens with focal length 10 mm and diameter 10 mm. A pinhole at the face of the lens provides a laser beam with a circular cross section with diameter of several 1 mm. The laser beam attenuated is split into two beams by using a polarizing beam splitter of 1 cm cube with the extinction rate 99 %. The polarizing beam splitter reflects almost completely the laser beam with the polarization perpendicular to the splitter axis and transmits almost completely the laser beam with polarization parallel to the splitter axis. The laser beam is linear polarized light, and we

can change the ratio of reflected and transmitted laser intensities by changing the polarization axis of the incident laser beam. The transmitted laser beam is applied to a small Cs cell as a relatively intense pump beam. The pump beam, after transmitted through the cell, goes out of the optical system through the second beam splitter whose polarization axis is oriented to the same direction as the first one. The laser beam reflected by the first beam splitter is used as weak probe beam, which is applied to the Cs cell from the opposite direction to the pump beam by using two mirrors and the second beam splitter, after attenuated by a neutral density filter. After transmitted through the cell, the probe beam is reflected by the first beam splitter and detected by a silicon photodiode. By focusing the probe beam slightly, the probe beam can be put completely into the pump beam, which has relatively large diameter, within the cell. All of the optical components have anti-reflection coat in order to avoid the reflection of the laser beam back to the laser diode. We could construct this optical system in the size $20 \times 10 \times 5$ cm^3 with sufficient spacing among the optical components.

Many improvements have been made in this compact optical system compared with that used in the previous experiment. Firstly, the misalignment between the pump and probe beams can be zero in principle, by using the polarizing beam splitter, which can identify the pump and probe beams by their polarizations. In the optical system used in the previous experiment, to avoid the

light returning back to the laser diode, small misalignment was necessary, which resulted in at least 5 MHz (HWHM) broadening of the Doppler-free spectra. Secondly, because of the short optical path and its low height from the basement, this optical system becomes stable against mechanical vibration and acoustic noise. So, no special apparatus such as air-floating table might be necessary.

As seen in Fig. IV-12, a part of the probe beam is reflected by a half mirror and is applied to the Cs cell from the direction perpendicular to the probe beam. Hereafter, let us call this beam "reference beam". After transmitted through the cell, the reference beam is detected by a silicon photodiode whose output is used to reduce the Doppler-broadened background in the signal of the probe beam. The outputs of both photodiodes are amplified so that the magnitude of the Doppler-broadened background in the signal of the probe beam is equal to that of the reference beam. Then, these amplified outputs are subtracted to reduce almost completely the Doppler-broadened background from the signal of the probe beam. In the previous system, we used a Cs cell with 5 cm length. For this length the cesium vapor becomes optically thick even at room temperature. This requires relatively strong laser intensity ($\sim$2 mW/cm^2) to observe the saturated absorption spectra. Such strong laser beam caused the large power-broadening (20$\sim$30 MHz) of the Doppler-free spectra. In addition, the shapes of both Doppler-broadened and Doppler-free spectra are deformed during beam propagation in the cell, which

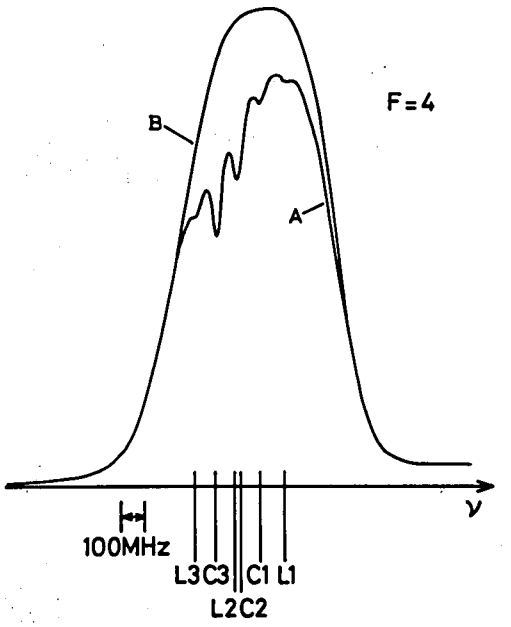

Fig. IV-13 Absorption signal of the probe beam A and the reference beam B obtained when the laser frequency ν was swept through the absorption line from the hyperfine level with F = 4 in the ground state of Cs.

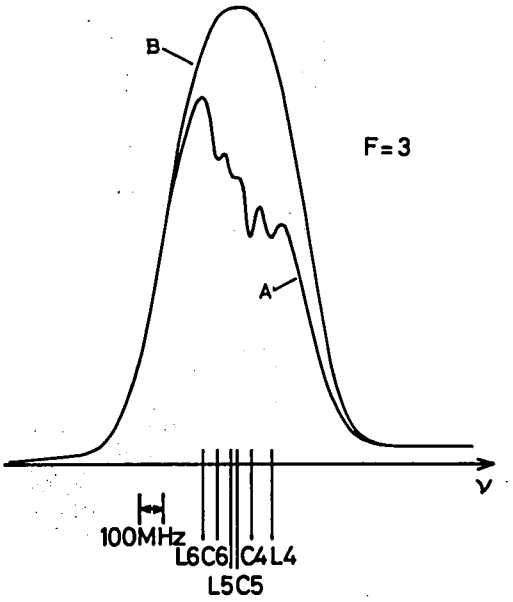

Fig. IV-14 Absorption signal of the probe beam A and the reference beam B obtained when the laser frequency ν was swept through the absorption line from the hyperfine level with F = 3 in the ground state of Cs.

makes it difficult to compensate the Doppler-broadened background in the signal of the probe beam. Since the signal-to-noise ratio of the observed Doppler-free spectra was sufficiently high, it is better to use a Cs cell with length ~1 cm, for which we can reduce considerably the laser power and hence power broadening of the Doppler-free spectra.

The saturated absorption spectra of the Cs-D_2 line were observed by using the improved optical system described above. The GaAlAs laser and the Cs cell used in this experiment were the same as those in the previous experiment (see Chap. III). The small cell did not obtained at that time. Figures IV-13 and IV-14 show typical absorption signals of the probe beam, which were obtained when the laser frequency was swept through the absorption lines from the hyperfine levels with F= 4 and 3 in the ground state, respectively. The frequency scanning was made by sweeping the injection current. In this experiment, the cell temperature was 25 °C, corresponding vapor pressure and density of Cs were 1.4×10^{-6} torr and 4.5×10^{10} cm^{-3} respectively, and the power and diameters of the pump and probe beams were about 1 mW and 20 μW, and 4 mm and 2 mm, respectively. In Figs. IV-13 and IV-14, we show also the Doppler-broadened absorption signal of the reference beam. The frequency scales of these figures were estimated by fitting the separations between the dips of C1 and L3, and L4 and C6 to the theoretical values (275.4 MHz and 233.4 MHz), respectively. The positions of the Doppler-free spectra shown were determined from the theoretical calculation.

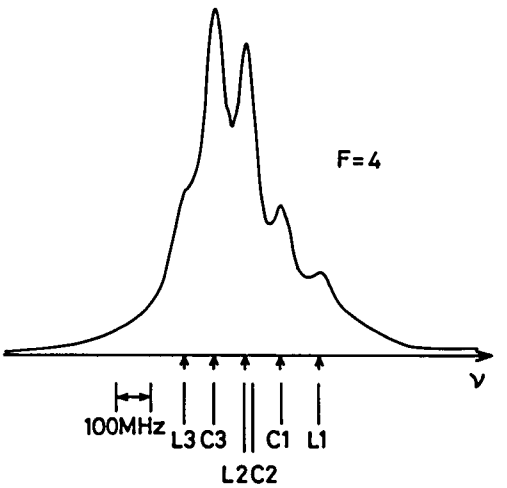

Fig. IV-15 Doppler-free spectra obtained by subtracting the signal of the reference beam from that of the probe beam, which are shown in Fig. IV-13.

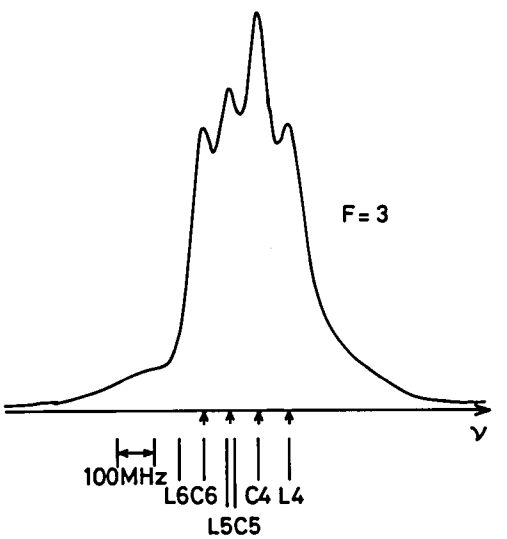

Fig. IV-16 Doppler-free spectra obtained by subtracting the signal of the reference beam from that of the probe beam, which are shown in Fig. IV-14.

The indications such as L1 and C1 are the same as those in Figs. III-7 and III-9. Comparing Figs. IV-13 and IV-14 with Figs. III-7 and III-9, one can see that the spectral sharpness of the Doppler-free spectra were improved in the present case, so that the centers of the Doppler-free spectra became pointed, and their depths were several times increased. This was mainly due to the fact that the misalignment between the pump and probe beams could be reduced to about zero. We can see slight deformation of the Doppler-broadened background in both signals at around their peaks. This was mainly due to the effect of beam propagation in optical thin medium.

Figures IV-15 and IV-16 show the Doppler-free spectra obtained by subtracting the Doppler-broadened absorption signal of the reference beam from that of the probe beam. In these figures, we see the Doppler-broadened background is almost disappeared. The expected positions of the Doppler-free resonances, which are calculated in the same way as Figs. IV-13 and IV-14, are also shown in Figs. IV-15 and IV-16, which fit well to the peaks of the observed Doppler-free spectra. The Doppler-free resonances L2 and C2, and L5 and C5 could not be well resolved owing to the power broadening and the spectral width of the GaAlAs laser. The resonance L6 could not be observed. The reason may be due to the fact that the atomic transitions associated with this resonance do not cause the hyperfine pumping. It must be emphasized that, in the improved optical system, these signals were scarcely affected by external

viblation even when no particular isolations of vibration was performed.

IV-5 Conclusion and Discussions

The oscillation frequency of the GaAlAs laser was stabilized by locking the laser frequency to one of the Doppler-free spectra of the Cs-D_2 line. The frequency locking was carried out after stabilizing the diode temperature. When the frequency stabilization was made by the the temperature stabilization, the fluctuation of the laser frequency could be reduced to less than 5 MHz, which was sustained against few degree drift of the room temperature. Under the control of the diode temperature, the laser frequency was locked to the crossover resonance by feeding back its first derivative to the injection current of the GaAlAs laser. We could obtain the short-term frequency-stability about 10 kHz and the minimum Allan variance 3.0×10^{-12} at the averaging time τ_{av}= 1.3 s. The long-term fluctuation observed was less than 37 kHz over the time interval of 3000 s, and the Allan variance was below 1.0×10^{-11} between τ_{av}= 0.1 s and 1000 s.

Since the proportional servocontrol was adopted in the feedback loop of the injection current, the frequency stability became slightly worse with longer averaging time, which was mainly due to the drift of room temperature. To improve this, we constructed a system with double control-loops of the diode temperature, where the P-I-D servocontrol was used to control the

temperature. A preliminary result showed that the fluctuation of the diode temperature was reduced to less than 1×10^{-4} °C which was maintained at least for an hour. This temperature fluctuation corresponds to the fluctuation of the laser frequency within 1 MHz. It should be noted that, the temperature stabilized GaAlAs laser can be used in the high resolution laser spectroscopy as a light whose frequency is stable and tunable over a wide frequency range.

In the case of alkali-metal atoms, the saturation effect is strongly enhanced owing to the hyperfine pumping in the atomic ground state. Even for a relatively weak laser power $\sim$2 mW/cm^2, the saturation broadening becomes about 10 $\sim$ 30 MHz (HWHM). From the point of view of achieving higher frequency-stability, it is apparently necessary to optimize the intensities and diameters of the pump and probe beams. These parameters have not, however, been changed largely in the present experiment in order to get the Doppler-free spectrum with sufficiently high signal-to-noise ratio. The strong saturation deformed the shape of the Doppler-broadened absorption line. For this reason the Doppler-broadened background was not completely eliminated from the saturated absorption spectra by dividing the signals of the probe and pump beams. This resulted in the nonzero offset in the first derivative of the Doppler-free spectrum, which slightly deviated the locked laser frequency from the center of the Doppler-free spectrum.

In the present work, we constructed a compact optical system

with size 20 × 10 × 5 cm^3. We carried out some improvements of this compact system. The most important improvement was that, by using polarizing beam splitters, the misalignment of the pump and probe beams could be nearly zero, and the line broadening of the Doppler-free spectrum due to the misalignment was almost completely reduced. This also enable us to use weak laser beams, for which the power broadening of spectra becomes very small. In fact we could observe sharp Doppler-free spectra. In addition, because of less distortion of the shape of absorption line, we could subtract almost completely the Doppler-broadened background from the signal of the probe beam. The compact optical system was also stable against mechanical vibration and acoustic noise. Although we have not carried out the frequency stabilization, it is expected from above preliminary results that considerablly high frequency-stability is obtained using this optical system. Such a compact and highly frequency-stabilized GaAlAs laser must be very useful as a convenient standard of wavelength or optical frequency for many fields such as optical telecommunications and precision measurements of length and velocity. This can also be applied to the Cs beam atomic clock as a stable light source for the hyperfine pumping.

Finally, it must be pointed out that, since the commercially available semiconductor lasers cover the wavelength range down to 750 nm, it is now possible to stabilize the laser frequency at D lines of Potassium (766.5 nm ; 769.9 nm) and Rubidium (780.0 nm ; 794.8 nm) and to absorption lines of molecules such

as water vapor, by using the similar techniques as mentioned in this thesis.

CHAPTER V

SUMMARY AND CONCLUDING REMARKS

In this thesis, we have studied theoretically and experimentally on the Doppler-free saturated absorption spectroscopy of the Cs-D_2 line using a GaAlAs semiconductor laser (in Chapter II - III), and the frequency stabilization of the GaAlAs laser using one of the Doppler-free spectra (in Chapter IV).

In Chapter II, we have studied theoretically on the saturated absorption spectroscopy, using the semiclassical theory of atom-light interaction. We have firstly analyzed the behavior of atoms subjected to the action of monochromatic light, using simplified atomic systems (two-level and three-level systems). We have shown here that the behavior can be discussed by classical rate equations. We have secondly discussed on the absorption spectrum of atomic vapor and on the saturation of absorption for two- and three-level systems. In these discussions, we have shown that the optical pumping in the atomic ground state enhances the saturation effect strongly, which makes it possible to use a semiconductor laser with small output power ($\sim$1 mW) for the saturated absorption spectroscopy. Under these foundations, the intensities and shapes of the saturated

absorption spectra were theoretically calculated for both cases of the Lamb dip and crossover resonance. The results have been used in the analysis of the saturated absorption spectra of the Cs-D_2 line.

In Chapter III, we have experimentally observed the narrow Doppler-free spectra of the Cs-D_2 line at 852.1 nm by using a GaAlAs laser. In order to control the oscillation frequency of the GaAlAs laser precisely, we have constructed a system to stabilize the temperature of the laser diode. We have shown that the laser frequency is precisely tunable to one of the Doppler-free spectra with spectral width of about 20 $\sim$ 30 MHz (HWHM) by varying the injection current or the diode temperature. The widths of observed Doppler-free spectra were much larger than the natural linewidth of the D_2 line 2.6 MHz (HWHM), because it is subjected to broadenings due to nonlinearity in atom-light interaction (power broadening), misalignment of pump and probe beams, and the spectral width of laser light. The Lamb dips and crossover resonances have been observed clearly in absorption lines from the hyperfine levels with F = 3 and 4 in the ground state of Cs. The relative positions of observed Doppler-free spectra are in good agreement with these expected from the theoretical values of hyperfine separations in the $6^2P_{3/2}$ state. The power of the pump beam was 910 μW in this experiment. Even for such weak laser beam ($\sim$2 mW/cm^2), strong saturation of absorption has been observed because of the presence of the hyperfine pumping.

We have also shown an experimental evidence of the velocity-selective hyperfine pumping in the ground state of Cs. In this experiment, we have monitored the velocity distribution of atoms in both of two hyperfine levels in the ground state, using two GaAlAs lasers, and we have been able to confirm that atoms are pumped from one hyperfine level to the other, conserving their velocity. Furthermore, we have been able to observe the Doppler-free spectra completely free from the Doppler-broadened background, using two GaAlAs lasers simultaneously. From these results, we can say with no doubt that the semiconductor laser, and especially the temperature-controlled system developed in the present work, can be a powerful tool in the high resolution laser spectroscopy.

In Chapter IV, we have stabilized the oscillation frequency of the GaAlAs laser at the center of one of the Doppler-free spectra of the Cs-D_2 line. Before locking the laser frequency to the Doppler-free spectrum, we have stabilized the laser frequency only by stabilizing the temperature of laser diode, and obtained the frequency fluctuation less than 5 MHz. Under stabilizing the diode temperature, the laser frequency was locked to the crossover resonance by feeding back the error signal (the first derivative of the Doppler-free spectrum) to the injection current. The obtained short-term frequency-stability was less than 10 kHz and the minimum Allan variance was 3.0×10^{-12} at the averaging time τ_{av}= 1.3 s, which is the highest frequency-stability of semiconductor lasers reported so far. The long term

fluctuation observed was 37 kHz or less for the time interval of 3000 s, and the Allan variance was less than 1.0×10^{-11} for the averaging time between τ_{av}= 0.1 s and 1000 s.

Since the injection current was controlled only by the proportional servocontrol in above experiment, the frequency stability became slightly worse with longer averaging time, which was mainly due to drift of room temperature. To improve the problem, we have constructed the system of the temperature stabilization, in which the double-loop temperature control and the P-I-D servocontrol were carried out. A preliminary result showed that the fluctuation of the diode temperature was reduced to be less than 1×10^{-4} °C, which was maintained at least for an hour at room temperature. Comparing this result with the experiment of the frequency-locking, we expect that the laser frequency is stabilized within 1 MHz if the improved temperature-control system is used.

Using the scheme similar to that described above, it is possible to make a compact and portable laser system whose frequency is highly stabilized. Actually, we have constructed a compact optical system using small optical components which are mounted on a platform with size of 20 × 10 × 5 cm^3. In this system, some improvements have been done, and the misalignment of pump and probe beams could be reduced to be almost zero. By making the beams overlapped in whole length of the cell, we can use weak laser beams without sacrificing the intensities of observed Doppler-free spectra. We have obtained the saturated

absorption spectra of the Cs-D_2 line, which are much sharper than those obtained in Chap. III. It has been found that this optical system is quite stable against mechanical vibrations and acoustic noise. We have not performed the frequency stabilization using this system, but it can be said with no doubt from our preliminary experiments, that the frequency stability becomes much higher than that obtained by the previous system. Further improvement of the frequency stability may be achieved by optimizing the powers and diameters of the laser beams and the time constants and gains of the servocontrol, and by using the P-I-D servocontrol of the injection current. The experiments to this direction is now under way in our laboratory. Such a compact frequency-stabilized GaAlAs laser is expected to be very useful as a convenient wavelength or optical frequency standard and for many applications such as optical telecommunications and precision measurements of length and velocity. It is also interesting to use this system as a stable light source for the hyperfine pumping in the Cs beam atomic clock.

It must be pointed out that, since the semiconductor lasers cover the wavelength range down to about 700 nm, it is now possible to stabilize the laser frequency at D lines of Potassium (766.5 nm ; 769.9 nm) and Rubidium (780.0 nm ; 794.8 nm) and to absorption lines of molecules such as water vapor, by using the techniques developed in this thesis. Furthermore, the highly stabilized GaAlAs laser can be applicated to stabilization of resonance frequencies of a Fabry-Perot resonator. It is not so

difficult to stabilize another laser, such as dye laser, at any frequency by locking its oscillation frequency to a transmission fringe of the stabilized Fabry-Perot resonator.

REFERENCES

1) T. Yabuzaki, A. Ibaragi, H. Hori, M. Kitano, and T. Ogawa, Jpn. J. Appl. Phys. 20, L451 (1981).

2) H. Hori, Y. Kitayama, M. Kitano, T. Yabuzaki, and T. Ogawa, IEEE J. Quantum Electron. QE-19, 169 (1983).

3) R. N. Hall, IEEE Trans. ED-23, 700 (1976).

4) I. Hayashi, M. B. Panish, P. W. Foy, and S. Sumski, Appl. Phys. Lett. 17, 109 (1970).

5) M. Wada, K. Itoh, H. Shimizu, T. Sugino, and I. Teramoto, IEEE J. Quantum Electron. QE-17, 776 (1981).

6) S. Araki, Y. Suematsu, and Y. Itoya, IEEE J. Quantum Electron. QE-16, 197 (1980).

7) G. A. Antcliff and S. G. Parker, J. Appl. Phys. 44, 4145 (1973).

8) J. N. Walpole, A. R. Calawa, R. W. Ralston, and T. C. Herman, J. Appl. Phys. 44, 2905 (1973).

9) T. Sugino, K. Itoh, H, Shimizu, M Wada, and I. Teramoto, IEEE J. Quantum Electron. QE-17, 745 (1981).

10) T. Hayakawa, s. Yamamoto, S. Matsui, T. Sakurai, and T. Hijikata, Jpn. J. Appl. Phys. 21, 725 (1982).

11) M. Nakamura, K. Aiki, N. Chinons, R. Ito, and J. Umeda, J. Appl. Phys. 49, 4644 (1978).

12) A. Dandridge, A. B. Tveten, R. O. Miles, and T. G. Giallorenzi, Appl. Phys. Lett. 37, 526 (1980).

13) T. L. Paoli, Appl. Phys. Lett. 24, 187 (1974).

14) A. Dandridge, A. B. Tveten, R. O. Miles, D. A. Jackson, and T. G. Giallorenzi, Appl. Phys. Lett. 38, 77 (1981).

15) M. Fleming and A. Mooradian, Appl. Phys. Lett. 38, 511 (1981).

16) C. H. Henry, IEEE J. Quantum Electron. QE-18, 259 (1982).

17) S. M. Sze, Physics of Semiconductor Devices (Wiley-Interscience, New York, 1969).

18) L. Goldberg, H. F. Taylor, and J. F. Waller, Electron. Lett. 17, 497 (1981).

19) S. Kobayashi, Y. Yamamoto, M. Ito, and T. Kimura, IEEE J. Quantum Electron. QE-18, 582 (1982).

20) M. Ito and T. Kimura, IEEE J. Quantum Electron. QE-16, 910 (1980).

21) H. Tsuchida, S. Sanpei, M. Ohtsu, and T. Tako, Jpn. J. Appl. Phys. 19, L721 (1980).

22) F. Favre, L. Jeunhomme, I. Joindot, M. Monerie, and J. C. Simon, IEEE J. Quantum Electron. QE-17, 897 (1981).

23) Y. A. Bykovskii, V. L. Velichanskii, I. G. Goncharov, and V. A. Maslov, Sov. Phys.-JETP 30, 605 (1970).

24) J. L. Picqué and S. Roizen, Appl. Phys. Lett. 27, 340 (1975).

25) F. Favre and D. L. Guen, Electron. Lett. 16, 709 (1980).

26) K. Kikuchi and S. Kawanishi, Electron. Lett. 17, 515 (1981).

27) H. Tsuchida, M. Ohtsu, and T. Tako, Jpn. J. Appl. Phys. 20, L403 (1981).

28) H. Tsuchida, M. Ohtsu, and T. Tako, Trans. Inst. Electron. and Commun. Eng. Jpn. E65, 65 (1982).

29) A. Dandridge and A. B. Tveten, Electron. Lett. 17, 937 (1981).

30) K. W. Cobb and B. Clushaw, Electron. Lett. 18, 336 (1982).

31) M. Ohi, Jpn. J. Appl. Phys. 20, L541 (1981).

32) H. Tsuchida, M. Ohtsu, and T. Tako, Jpn. J. Appl. Phys. 21, L1 (1982).

33) H. Tsuchida, M. Ohtsu, T. Tako, M. Kuramochi, and N. Oura, Jpn. J. Appl. Phys. 21, L561 (1982).

34) S. Yamaguchi and M. Suzuki, Appl. Phys. Lett. 47, 597 (1982).

35) S. Yamaguchi and M. Suzuki, Appl. Phys. Lett. 41, 1034 (1982).

36) R. L. Barger and J. L. Hall, Phys. Rev. Lett. 22, 4 (1969).

37) S. J. Bennett and P. Cerez, Opt. Commun. 25, 343 (1978).

38) L. Goldberg, H. F. Taylor, A. Danridge, J. F. Weller, and R. O. Miles, IEEE J. Quantum Electron. QE-18, 555 (1982).

39) F. Favre, D. L. Guen, and J. C. Simon, IEEE J. Quantum Electron. QE-18, 1712 (1982).

40) J. L. Hall, L. Hollberg, T. Bear, and H. G. Robinson, Appl. Phys. Lett. 39, 680 (1981).

41) H. Walther and K. W. Rothe, Laser Spectroscopy IV (Springer, New York, 1979).

42) T. W. Hänsch, K. C. Harvey, G. Meisel, and A. L. Schawlow,

Opt. Commun. 11, 50 (1974).

43) M. Arditi and J. L. Picqué, J. Phys. B. Atom. Molec. Phys. 8, L331 (1975).

44) L. N. Novikov, V. G. Pakazanev, and G. V. Strotskii, Sov. Phys.-JETP 101, 273 (1970).

45) W. E. Lamb, Jr., Phys. Rev. 134, A1429 (1964).

46) P. G. Pappas, M. M. Burns, D. D. Hinshelwood, M. S. Feld, and D. E. Murnik, Phys. Rev. A 21, 1955 (1980).

47) H. R. Schlossberg and A. Javan, Phys. Rev. 150, 267 (1966).

48) M. S. Feld, M. M. Burns, T. U. Kuhl, and P.,G. Pappas, Optics Lett. 5, 79 (1980).

49) J. H. Van Vleck and D. L. Huber, Rev. Mod. Phys. 49, 939 (1977).

50) C. Cohen-Tannoudji and F. Lalöe, J. Phys. (Paris) 28, 505 (1967).

51) C. Wieman and T. W. Hänsch, Phys. Rev. Lett. 36, 1170 (1976).

52) A. Kastler, J. Phys. Radium 11, 255 (1950).

53) W. Happer, Rev. Mod. Phys. 44, 169 (1972).

54) T. Yabuzaki and T. Ogawa, Oyo Buturi 46, 856 (1977).

55) M. Pinard, C. G. Aminoff, and F. Lalöe, Phys. Rev. A 19, 2366 (1979).

56) T. Yabuzaki, T. Endo, M. Kitano, and T. Ogawa, Opt. Commun. 22, 181 (1977).

57) T. Yabuzaki, H. Hori, and M. Kitano, Jpn. J. Appl. Phys.

21, 504 (1982).

58) U. Hochuli, P. Haldemann, and S. Siahatgar, J. Appl. Phys. 40, 3374 (1969).

59) M. Arditi and T. R. Carver, Proc. IEEE 51, 1 (1963).

60) M. Ariditi and J. L. Picqué, Opt. Commun. 15, 317 (1975).

61) J. L. Picque, IEEE J. Quantum Electron. QE-10, 392 (1974).

62) M Arditi, J. Phys. 42 Suppl. 12 C8 (1981).

63) L. Lewis, M. Feldman, and J. C. Bergquist, J. Phys. 42 Suppl. 12 C8 (1981).

64) T. Yabuzaki and T. Ogawa, J. Appl. Phys. 45, 1342 (1974).

65) C. Chen-Tannoudji, J. Dupont-Roc, S. Haroche, and F. Laloë, Phys. Rev. Lett. 22, 758 (1969).

66) R. L. Barger and J. L. Hall, Appl. Phys. Lett. 22, 196 (1973).

67) P. Cerez and S. J. Bennet, IEEE Trans. Instrum. Meas. IM-27, 396 (1978).

68) K. Dschaó, M. Gläser, and J. Helmcke, IEEE Trans. Instrum. Meas. IM-29, 354 (1980).

69) P. Cerez, A. Brillet, C. N. Man-Pichot, and R. Felder, IEEE Trans. Instrum. Meas. IM-29, 352 (1980).

70) G. R. Hanes and C. E. Dahlstrom, Appl. Phys. Lett. 14, 362 (1969).

71) A. J. Wallard, IEEE Trans. Instrum. Meas. IM-23, 532 (1974).

74) J. M. Chartier, J. Helmche, and A. J. Wallard, IEEE Trans. Instrum. Meas. IM-25, 450 (1976).

73) K. M. Evenson, J. S. Wells, F. R. Perterson, B. L. Danielson, G. W. Day, R. L. Barger, and J. L. Hall, Phys. Rev. Lett. 29, 1346 (1972).

74) A. Brillet and J. L. Hall, Phys. Rev. Lett. 42, 549 (1979).

75) T. Tako, Oyo Buturi 51, 465 (1982).

76) F. Spieweck, IEEE Trans. Instrum. Meas. IM-27, 398 (1978).

77) M. Ohtsu, S. Katsuragi, and T. Tako, IEEE J. Quantum Electron. QE-17, 1100 (1981).

78) M. Ohtsu, S. Ohta, and T. Tako, Jpn. J. Appl. Phys. 20, 1701 (1981).

79) I. Siio, M. Ohtsu, and T. Tako, Jpn. J. Appl. Phys. 20, L508 (1981).

80) T. Bear, F. V. Kowalski, and J. L. Hall, Appl. Opt. 19, 3173 (1980).

81) J. Helmcke, S. A. Lee, and J. L. Hall, Appl. Opt. 21, 1686 (1982).

82) R. L. Barger, M. S. Sorem, and J. L. Hall, Appl. Phys. Lett. 22, 573 (1973).

83) J. C. Bergquist, R. L. Barger, and D. J. Glaze, in Laser Spectroscopy IV, op. cit., 120.

84) J. C. Bergquist, S. A. Lee, and J. L. Hall, Phys. Rev. Lett. 38, 159 (1977).

85) C. V. Shank and M. B. Klein, Appl. Phys. Lett. 23, 156 (1973).

86) A. Yamagishi and H. Inaba, Opt. Commun. 16, 223 (1976).

87) P. P. Sorokin, J. R. Lankard, V. L. Moruzzi, and A. Lurio, Appl. Phys. Lett. 15, 179 (1969).

88) T. Endo, T. Yabuzaki, M. Kitano, T. Sato, and T. Ogawa, IEEE J. Quantum Electron. QE-13, 866 (1977).

89) T. Endo, T. Yabuzaki, M. Kitano, T. Sato, and T. Ogawa, IEEE J. Quantum Electron. QE-14, 977 (1978).

90) M. Sargent III, M. O. Scully, and W. E. Lamb, Jr., Laser Physics (Addison-Wesley, Reding, Mass., 1974).

91) E. U. Condon and G. H. Shortley, The Theory of Atomic Spectra (Cambridge Univ., London, 1963).

92) P. A. M. Dirac, The Principles of Quantum Mechanics (4TH ed., Clarendon Press, Oxford, 1958).

93) U. Fano, Rev. Mod. Phys. 29, 74 (1957).

94) R. P. Feynman, Statistical Mechanics (Benjamin, Reading, Mass., 1972).

95) W. Happer and B. S. Mathur, Phys. Rev. 163, 12 (1967).

96) R. Loudon, The Quantum Theory of Light (Clarendon Press, Oxford, 1973).

97) L. D. Landau and E. M. Lifshitz, Classical Theory of Fields (Addison-Wesley, Reading, Mass., 1951).

98) B. D. Fried and S. D. Conte, The Plasma Dispersion Function (Academic Press, New York, 1961).

99) F. Abramowitz and J. A. Stegun, Handbook of Mathematical Functions (Dover, New York, 1968).

100) D. H. Close, Phys. Rev. 153, 360 (1967).

101) G. Singh, P. DiLavore, and C. O. Alley, IEEE J. Quantum

Electron. QE-7, 196 (1971).

102) U. L. Bykovskii, V. L. Velichanskii, V. K. Egrov, A. L. Irshinskii, A. V. Makovkin, and V. A. Masrov, Sov. Phys.-JETP 17, 216 (1973).

103) J. L. Picqué, IEEE J. Quantum Electron. QE-10, 892 (1974).

104) T. Yabuzaki and T. Ogawa, J. Appl. Phys. 45, 1342 (1974).

105) P. Kartaschoff, Frequency and Time (Academic Press, London, 1978).

106) E. Arimond, M. Inguscio, and P. Violino, Rev. Mod. Phys. 49, 31 (1977).

107) P. Violino, Can. J. Phys. 47, 2095 (1969).

108) J. K. Link, J. Opt. Soc. Am. 56, 1195 (1966).

109) M. Rozwadowski and E. Lipworth, J. Chem. Phys. 43, 2347 (1965).

110) C. J. Borde, J. L. Hall, C. V. Kunasz, and D. G. Hummer, Phys. Rev. A 14, 236 (1976).

111) J. E. Thomas and W. W. Quivers, Jr., Phys. Rev. A 22, 2115 (1980).

112) T. Kaneda and K. Nawata, IEEE J. Quantum Electron. QE-15, 559 (1979).

113) N. Chinone, K. Aiki, and R. Ito, Appl. Phys. Lett. 33, 990 (1979).

114) D. W. Allan, Proc. IEEE 54, 221 (1966).

115) J. A. Barnes, A. R. Chi, L. S. Cutler, D. J. Healey, D. B. Leeson, T. E. McGunigal, J. A. Mullen, Jr., W. L. Smith, R. L. Sydnor, R. F. C. Vessot, and G. M. R. Winkler, IEEE

Trans. Instrum. Meas. IM-20, 105 (1971).

116) P. Lesage and C. Audoin, IEEE Trans. Instrum. Meas. IM-22, 157 (1973).

117) J. Rutman, IEEE Trans. Instrum. Meas. IM-23, 40 (1974).

118) W. C. Lindsey and C. M. Chie, Proc. IEEE 64, 1652 (1976).

119) R. B. Blackman and J. W. Tukey, The Measurement of Power Spectra (Dover, New York, 1958).

120) R. C. Tausworthe, IEEE Trans. Comm. COM-20, 214 (1972).

121) J. A. Barnes, Proc. IEEE 54, 199 (1966).

122) R. F. C. Vessot, L. Mueller, and J. Vanier, Proc. IEEE 54, 199 (1966).

123) P. Lesage and C. Audoin, IEEE Trans. Instrum. Meas. IM-24, 86 (1975).